CHEMICAL REVIEWS

pubs.acs.org/CR

Review

Bioinspired and Bioderived Aqueous Electrocatalysis

Jesús Barrio, Angus Pedersen, Silvia Favero, Hui Luo, Mengnan Wang, Saurav Ch. Sarma, Jingyu Feng, Linh Tran Thi Ngoc, Simon Kellner, Alain You Li, Ana Belén Jorge Sobrido, and Maria-Magdalena Titirici*

Cite This: *Chem. Rev.* 2023, 123, 2311−2348

Read Online

ACCESS | Metrics & More | Article Recommendations

ABSTRACT: The development of efficient and sustainable electrochemical systems able to provide clean-energy fuels and chemicals is one of the main current challenges of materials science and engineering. Over the last decades, significant advances have been made in the development of robust electrocatalysts for different reactions, with fundamental insights from both computational and experimental work. Some of the most promising systems in the literature are based on expensive and scarce platinum-group metals; however, natural enzymes show the highest per-site catalytic activities, while their active sites are based exclusively on earth-abundant metals. Additionally, natural biomass provides a valuable feedstock for producing advanced carbonaceous materials with porous hierarchical structures. Utilizing resources and design inspiration from nature can help create more sustainable and cost-effective strategies for manufacturing cost-effective, sustainable, and robust electrochemical materials and devices. This review spans from materials to device engineering; we initially discuss the design of carbon-based materials with bioinspired features (such as enzyme active sites), the utilization of biomass resources to construct tailored carbon materials, and their activity in aqueous electrocatalysis for water splitting, oxygen reduction, and CO_2 reduction. We then delve in the applicability of bioinspired features in electrochemical devices, such as the engineering of bioinspired mass transport and electrode interfaces. Finally, we address remaining challenges, such as the stability of bioinspired active sites or the activity of metal-free carbon materials, and discuss new potential research directions that can open the gates to the implementation of bioinspired sustainable materials in electrochemical devices.

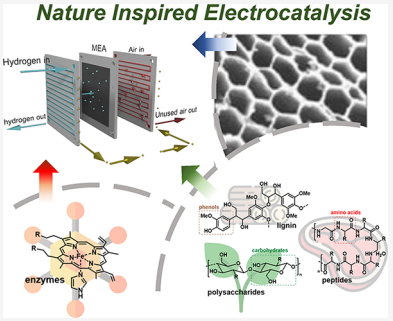

CONTENTS

Special Issue: Sustainable Materials

Received: June 28, 2022
Published: November 10, 2022

https://doi.org/10.1021/acs.chemrev.2c00429
Chem. Rev. 2023, 123, 2311−2348

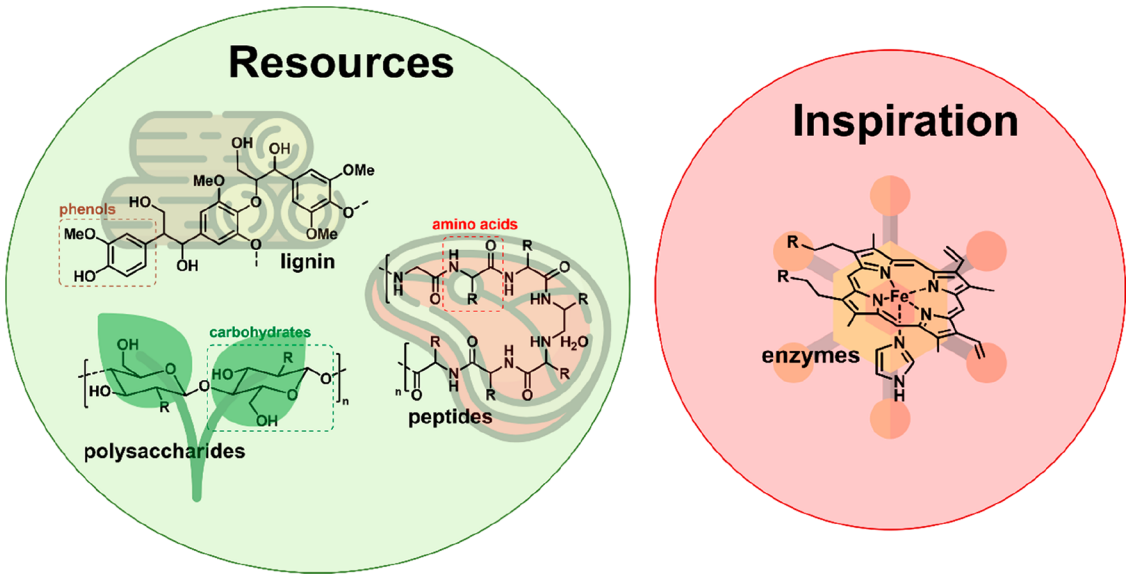

Figure 1. Schematic representation of the different sources of biomass and bioinspiration present in nature.

1. INTRODUCTION

Our CO_2 emissions are on a constant rise, reaching a monthly average of 419 ppm in 2021, a record high in the last 2 million years.[1] In response, many countries have committed to net-zero emissions by 2050 (The EU Green Deal[2] and the UK 2019 pledge to net zero[3]) or by the latest 2060 (i.e., China).[4] Consequently, decarbonizing the global economy via the implementation of sustainable and environmentally benign technologies across all sectors has become a main priority for the benefit of future generations. The energy sector contributes to around three-quarters of global greenhouse gas emissions today and will play a pivotal role in averting climate change.[5] Decarbonizing the energy sector calls for a complete transformation of energy production, transport, and consumption, where shifting away from fossil fuels is key. The development of renewable energy plants, such as solar power, wind power , and hydropower, could deliver a sustainable and carbon neutral electricity system, bring opportunities for decarbonization by electrification.[6] However, although sectors such as light-duty transportation can potentially be entirely electrified, in other hard-to-abate sectors, such as steel and chemical production, the electrification shares are predicted to remain below 70% by 2050.[7] For example, processes such as the anthraquinone process for H_2O_2,[8] the Haber−Bosch process for NH_3,[9] or methane steam reforming for H_2[10] rely on heavily centralized carbon-intensive infrastructures. The Haber−Bosch process alone accounts for 1.3% of the global CO_2 emissions, contributed to 2% of the world's total energy consumption,[11] and requires transportation to the consumption point. An electrochemical approach, however, could help solve these issues by allowing on-site production such as either electrified power-to-X (X = fuels, chemicals) or on-site electricity generation through energy carriers (e.g., H_2). Commonly explored electrocatalysis for decarbonized energy conversion technologies include green H_2 production via water electrolysis,[12,13] power generation from fuel cells,[14] chemical manufacturing through CO_2 reduction,[15,16] H_2O_2 production from the oxygen reduction reaction (ORR),[17] and NH_3 synthesis by N_2 reduction.[18,19] All of these technologies require efficient electrocatalysts to decrease the activation energy barrier and efficiently drive the reactions. Although research in these fields has made significant progress in terms of improving their energy efficiency,[20−22] so far, many of these electrocatalysts (particularly those involved in water splitting, the hydrogen oxidation reaction (HOR), and ORR) require critical precious metals. For instance, Pt/C is the benchmark catalyst for both ORR in a fuel cell[23] and the hydrogen evolution reaction (HER),[24] and Ir-based catalysts are currently irreplaceable for the oxygen evolution reaction (OER) in proton-exchange membrane (PEM) water electrolyzers.[25,26] These precious metals have been included in the EU's latest report on critical raw materials,[27] meaning their natural reserves are depleting and will not sustain the demand in the long term.[28,29] These uncertainties have largely increased the risk in the catalyst material supply chain, inducing volatility in the commodity prices of Pt and Ir that can significantly impede the large-scale PEM electrolyzer deployment rate. In an analysis performed by Jaramillo and co-workers, they pointed out that current Pt production will limit the PEM electrolyzer capacity to 100 GW/year, and that of Ir will be limited to 2 GW/year, far from the Terawatt (TW) target we need to reach by 2050.[29] It is also very energy-intensive to source and manufacture these raw materials; 10% of the total global energy-related greenhouse gas (GHG) emissions in 2018 came from the primary production of minerals and metals, with Pt standing out as one of the most GHG-intense metals (more than 10 tons of CO_2 emitted per kg).[30] To secure a sustainable future, one has to look for synergy with nature to find environmentally friendly solutions. Nature can potentially provide solutions to energy conversion technologies (including water splitting, ORR, and CO_2 reduction) in different ways, such as providing both a natural feedstock (biomass) that can be employed for the preparation of advanced carbonaceous catalysts[31] and models of highly efficient electrochemical systems (enzymes) (Figure 1).

1.1. Bioinspired and Bioderived Catalysts

Biomass is a renewable and abundant natural resource that includes agricultural and forestry residues and municipal food waste. Biomass has been recognized as an ideal renewable resource substitute to fossil fuels,[32] with an estimated worldwide production of approximately 100 billion metric tons per year.[33]

https://doi.org/10.1021/acs.chemrev.2c00429
Chem. Rev. 2023, 123, 2311−2348

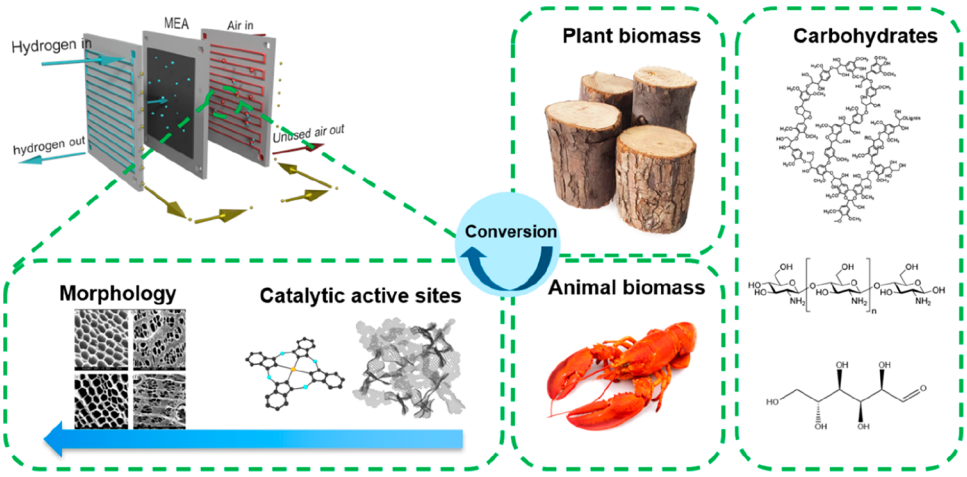

Figure 2. Schematic of biomass types and the active sites in the cathode side of the fuel cell. Figures reproduced with permission from ref 86. Copyright 2010 Hosowaka Powder Technology Foundation.

Exploiting biomass can help address concerns related to the availability of raw materials for advanced materials manufacturing and reduce CO_2 emissions resulting from the mining and manufacturing of materials.[30,34] For instance, we performed a life cycle assessment that compared the hard carbon anode for a Na-ion battery synthesized from a biomass precursor to commercial graphite (used in Li-ion batteries).[35] The results show that the former displays significant savings up to 31% in terms of the potential global warming impact.[35] It can also create important economic revenues due to the wide availability of biomass worldwide, helping farmers and bridging agriculture, waste, and forestry with the materials and chemical industries.

The production of advanced materials and chemicals from raw biomass has been widely investigated, and several relevant review articles have been published on the topic.[36−40] The complexity of raw biomass can be exploited to prepare carbonaceous materials with aligned channels, fractal structures, and tunable properties, as well as polymers and other nanomaterials.[41−44] Two types of biomass precursors have been employed for the synthesis of carbon-based materials: plant biomass (such as lignin from wood and carbohydrates) and animal biomass (such as chitin from shrimps, Figures 1 and 2).[45] Carbohydrates are comprised of monosaccharides (C_6 such as glucose, fructose, and galactose or C_5 such as xylose, arabinose, etc.), disaccharides (maltose, sucrose, lactose, etc.), and polysaccharides (starch, chitin, chitosan, cellulose, etc.), and can be used as carbon-support precursors. Using hydrothermal carbonization or direct pyrolysis, they can be transformed into different types of carbons (amorphous or graphitized)[46] through complex cascades of dehydration and condensation reactions.[36] Both the precursor and the heat treatment conditions will influence the chemical composition, surface chemistry, surface area, and pore structure of the resulting carbon.[47] Additionally, the diversity of raw biomass makes it very compositionally variable depending on where it is extracted from, affecting the composition and reproducibility of the final material. For instance, the chemical composition of lignin and cellulose varies greatly depending on their sources (hard wood or soft wood) and the extraction method.[48,49] Plant biomass is easier to use when separated in its constituent components, namely, cellulose, hemicellulose, and lignin, by employing biomass fractionation techniques such as the lignoboost process or different organosolv and ionosolv processes.[50−54]

Nevertheless, biomass precursors with natural hierarchical structures can be exploited to optimize electrolyte transport to active sites,[55] maximizing current density. For instance, employing a wood or bone precursor with a natural hierarchical structure leads to well-defined morphologies and also provides nitrogen moieties derived from the organic collagens.[56−63] These nitrogen-containing biomass-derived species can form complexes with transition metals and generate carbon-embedded MN_x (M = metal) catalytic sites resembling those of heme (Figure 1) and part of the enzymatic active site in cytochrome c oxidase (CcO).[64−66]

Nature's enzymes, such as CcO, have evolved over millions of years into highly efficient mechanisms and pathways that convert abundant atmospheric molecules such as CO_2 and N_2 using abundant metal active sites (Fe, Mn, Ni, and Cu) to produce essential chemicals for life, such hydrocarbons and ammonia.[67,68] Enzymes display remarkable selectivity and turnover numbers toward certain chemical reactions, and no heterogeneous electrochemical catalyst is currently able to compete with enzyme activity and selectivity.[69−71] Their remarkable efficiency lies primarily in their well-defined active sites and finely tuned surrounding structure, which allows high activity and selectivity by controlling the reactivity of the active site. Additionally, their outer coordination sphere often consists of a peptide matrix with defined channels that allows the efficient and selective transport of reactants (such as H^+ and electrons) to the active site.[72] Unsurprisingly, both the active sites and secondary structures of enzymes have been of inspiration for the development of electrocatalysts with a rationally designed interface and enhanced catalytic performance.[73−76] However, enzymes cannot tolerate harsh pressure or temperature conditions or highly acidic or alkaline pH levels.[77] Emulating similar structures on more robust materials would benefit the design of new electrocatalysts, improving their selectivity for electrochemical reactions. Biomass-derived materials could potentially resemble the active sites of enzymatic systems while exhibiting conductivity. For example, hemoglobin, which is derived from animal biomass, was recently employed to construct ORR catalysts, as it contains FeN_5 sites, and has been used as either a catalyst after pyrolysis,[78] or a doping agent[79] to hybridize FeN_x sites into other conductive carbon frameworks. In terms of the transport of reactants, nature also displays unique hierarchical structures that combine different pore sizes across

https://doi.org/10.1021/acs.chemrev.2c00429
Chem. Rev. 2023, 123, 2311−2348

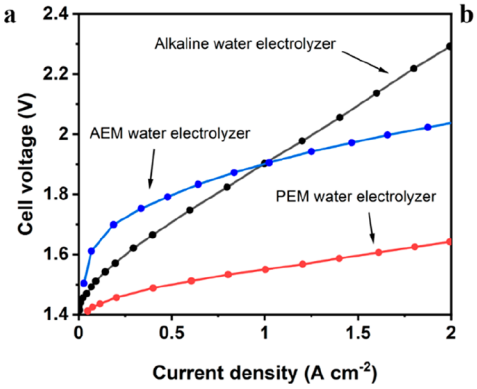

	Alkaline	PEM	AEM
Anode	NiAl (56% - 44%) alloy on Ni plates	2 mg cm^{-2} of IrO_x nanoparticles	2 mg cm^{-2} $NiFe_2O_4$
Cathode	NiAlMo (39% - 44% - 17%) alloy on Ni plates	0.1 mg cm^{-2} of Pt/C nanoparticles (HiSpec9100)	2 mg cm^{-2} NiFeCo
Electrolyte	30 wt% KOH	Nafion N117 membrane	1 M KOH
Separator	460 μm diaphragm	Solid electrolyte (above)	Sustainion 37-50 membrane
Operating temperature	80°C	80 °C	60°C

Figure 3. (a) Comparison of typical voltage−current characteristics of the alkaline (black), PEM (red), and AEM (blue) water electrolyzers in a two-electrode configuration. (b) Summary of the cell components and testing conditions. Adapted from refs 93 and 94.

the length scale, which is highly desirable to enable a higher active-site density.[80] The branching of plants, the vascular networks of animals, the lungs of mammals, and the spiracles of insects are some examples of hierarchal structures.[81,82] Imitating such structures for the fabrication of electrocatalysts for different reactions has consequently garnered plenty of attention within the last few years.[83−85]

As highlighted above, nature provides a wide set of tools for fabricating the next generation of catalysts for use in energy-conversion technologies (Figure 2). Biomass is a precursor for advanced carbonaceous materials, enzymes are an inspiration for active sites, and hierarchical structures are an inspiration for efficient mass transport. In this review, we discuss in-depth the benefits of nature-inspired aqueous electrocatalysis, focusing on water splitting, ORR, and CO_2 reduction reactions. We cover the state of the art of biomass-derived carbon materials and bioinspired electrochemical systems and how can we emulate nature employing its own resources. The article will be divided into different electrocatalytic processes: water splitting (HER and OER), the hydrogen oxidation reaction (HOR), the ORR, and CO_2 reduction. We then delve into the solid−liquid interface control in electrochemical systems resembling the secondary structures of enzymes, and we summarize how nature has aided the development on proton-exchange membranes and flow fields, which are essential components of electrochemical cells. Finally, we provide perspectives for the future of nature-inspired electrocatalysis.

2. BIOMASS-DERIVED AND BIOINSPIRED WATER SPLITTING

Green hydrogen production, defined as hydrogen produced via electrochemical water splitting, is one of the most important energy vectors in our transition to net-zero emissions. There are three major technologies for low-temperature water electrolysis: (1) industrial alkaline water electrolyzers, which use Ni-based alloy electrodes separated by a diaphragm working in highly basic media; (2) PEM water electrolyzers (also known as polymer−electrolyte membrane water electrolyzers) with a Pt-based cathode and an Ir/Ru-based anode separated by a perfluorated sulfonic membrane; and (3) anion exchange membrane (AEM) water electrolyzers, which employ a hydroxide-conducting membrane sandwiched by two Ni-based electrodes.[87,88]

Chemical reactions taking place in acid media are written below, where * represents an available active site for the reactant or intermediate to be adsorbed.[89]

Anode:

$$H_2O(l) + * \rightarrow HO^* + H^+ + e^-$$
$$HO^* \rightarrow O^* + H^+ + e^-$$
$$O^* + H_2O(l) \rightarrow HOO^* + H^+ + e^-$$
$$HOO^* \rightarrow * + O_2(g) + H^+ + e^-$$

Cathode:

$$* + H^+ + e^- \rightarrow {}^*H$$
$${}^*H + H^+ + e^- \rightarrow H_2 + *$$
$$\text{Or} \quad {}^*H + {}^*H \rightarrow H_2 + 2^*$$

Under alkaline conditions, the chemical reactions are written as shown below.[90]

Anode:

$$* + OH^- \rightarrow {}^*OH + e^-$$
$${}^*OH + OH^- \rightarrow {}^*O + H_2O(l) + e^-$$
$${}^*O + OH^- \rightarrow {}^*OOH + e^-$$
$${}^*OOH + OH^- \rightarrow * + O_2(g) + H_2O(l) + e^-$$

Cathode:

$$H_2O + e^- + * \rightarrow {}^*H + OH^-$$
$${}^*H + H_2O + e^- \rightarrow H_2 + * + OH^-$$
$$\text{Or} \quad {}^*H + {}^*H \rightarrow H_2 + 2^*$$

Although a conventional alkaline system can utilize transition-metal catalysts, its current densities still fall below those of a PEM system due to the considerable Ohmic loss caused by the large gap between the two electrodes and the thickness of the diaphragm. However, only Ru- or Ir-based catalysts can sustain the highly acidic working environment of PEM water electrolyzers, as carbon-based supports are not suitable due to carbon oxidation,[91] making it difficult to widely deploy this technology. The recently developed AEM water electrolyzers that use nonprecious metals have exhibited comparable performance,[92] demonstrating the great potential for upscaling. Nonetheless, further research is required to develop sufficient membranes and enhance the durability of such systems.[92] Figure 3 shows

https://doi.org/10.1021/acs.chemrev.2c00429
Chem. Rev. 2023, 123, 2311−2348

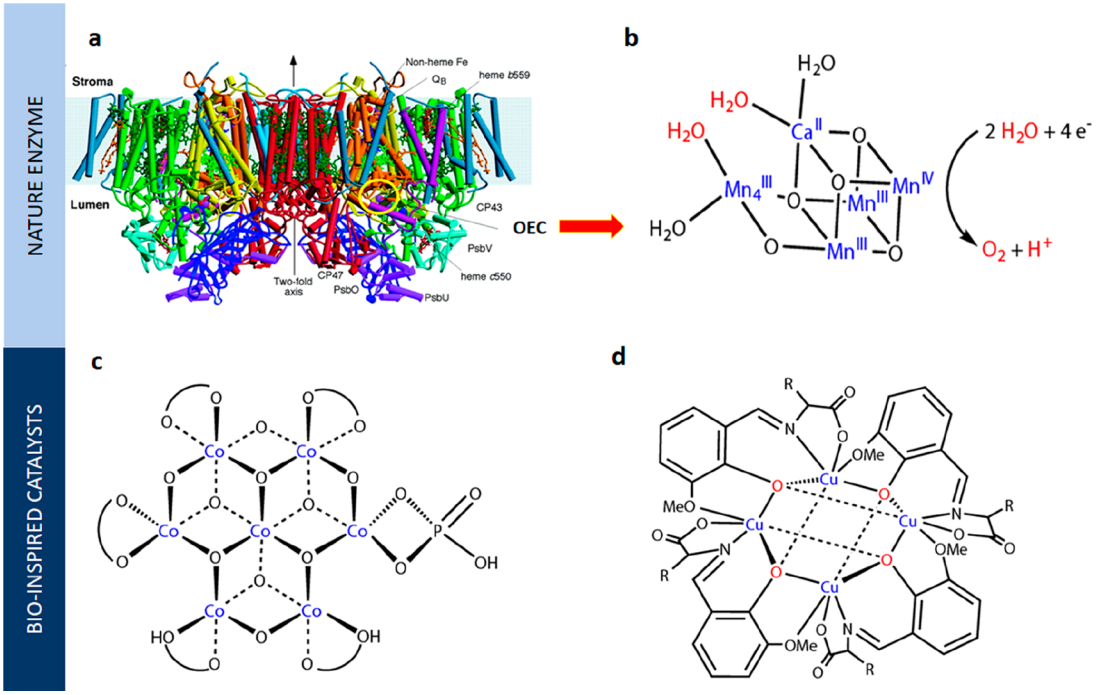

Figure 4. (a) Overall structure of photosystem II. Reprinted with permission from ref 151. Copyright 2004 American Association for the Advancement of Science. (b) Molecular structure of the Mn_4CaO_5 OEC. Adapted with permission from ref 136. Copyright Springer Nature 2011. (c) 45°-Rotated view of Co-OEC. Adapted with permission from ref 142. Copyright 2021 American Chemical Society. (d) Cu_4O_4 cubane. Adapted with permission from ref 145. Copyright 2018 Wiley-VCH.

polarization curves of these three cells, where the PEM system exhibits the highest efficiency.

In PEM water splitting systems, while HER can occur at minimum overpotentials with low Pt loadings, OER requires much higher overpotentials. With a Pt loading of 0.05 mg cm^{-2} in PEM electrolyzer, it is possible to achieve an HER overpotential below 2 mV,[95] but more than 0.3 mg cm^{-2} IrO_x is required to sustain an overpotential below 440 mV on the OER side.[96] The overall performance is mainly suppressed by the sluggish anodic OER as the limiting factor. OER is thus one of the most researched reactions in decades due to its critical roles in electrocatalytic energy storage and fuel production. Several models have been developed for OER mechanistic descriptors, representatives of which are scaling relations (Sabatier principle) and the lattice oxygen mechanism (associated with structural stability).[89,97] The Sabatier principle focuses on the free energy of adsorption of an intermediate at the catalyst's metal surface, while lattice oxygen evolution suggests the participation of lattice oxygen as another important descriptor besides metal-site adsorption on a dynamic surface.[98] The lattice oxygen mechanism features direct O−O coupling achieved by the evolution of lattice oxygen when the oxide catalyst is destabilized, hence having the potential to bypass the theoretical overpotential set by the scaling relation and being closely linked to thermodynamic instability.[98−101]

2.1. Bioderived Catalysts for OER

Metal-doped carbon-based materials have primarily been investigated as hydrogen evolution catalysts, with only a few reports focusing on oxygen evolution in alkaline conditions.[102−104] Due to their chemical diversity and the inherent presence of heteroatoms, biomass precursors can be utilized to synthesize heteroatom-doped (metallic or nonmetallic) carbons,[105−107] which is one of the most widespread approaches to introduce active sites via charge redistribution.[108−115] Their OER performances have been summarized in detail in other reviews.[116,117] A uniform distribution of transition-metal atoms (Fe, Co, and Ni) in the carbon matrix enhances interfacial charge transfer while also promoting hydroxide accessibility and electronic conductivity, leading to enhanced activity.[107,115,118−121] This is reflected in previous work, where egg-derived carbon microspheres exhibited low onset potentials (~1.5 V_{RHE}, RHE = reversible hydrogen electrode), a high current density (74.6 $mAcm^{-2}$ at −1.6 V_{RHE}), and excellent stability for 20 h with 95% current retention due to a large specific surface area, a high pore volume, and the innate presence of nitrogen, phosphorus, and iron.[107]

It has also been observed that a small percentage of doped N in the carbon matrix can considerably reduce the OER overpotential due to the decreased kinetic barriers and the assisted binding of *OH, *O, and *OOH intermediates.[122] The introduction of electron donors (P and S), electron acceptors (B), or oxygen defects with different degree of oxidation can also be used to engineer the valence band orbitals of a carbon matrix or facilitate electrolyte infiltration and oxygen desorption.[123−125]

At this stage, it is also important to mention that carbon-based feed stocks (graphite, carbon nanotube, bioderived carbon, etc.), chemical precursors, and common electrolytes (NaOH, KOH, and $HClO_4$) might contain metallic impurities, conceivably causing artifacts or completely misleading conclusions for metal-free materials.[126,127] Purification should be conducted consistently and throughout the whole process from synthesis to control experiments to eliminate the effect of trace metals. Carbon-based materials are also prone to oxidation due to the high oxidation potential applied during catalyst testing. Furthermore, the bubbles produced during the OER process might cause the carbon morphology to collapse. Therefore, the

https://doi.org/10.1021/acs.chemrev.2c00429
Chem. Rev. 2023, 123, 2311−2348

application of carbon-based materials as catalysts for OER remains in its infancy, and the role of carbon-based materials is reduced to acting as hosts for their metallic counterparts.[128] Consequently, we believe that a fair comparison of their performance with the state-of-the-art catalysts is inaccurate and challenging to achieve. For a more focused comparison of OER performances among different catalysts, we would like to refer the reader to previously published reviews.[116,117]

2.2. Bioinspired Catalysts for OER

In nature, oxygen is produced in plants and algae via the photosynthetic process, which employs the enzyme photosystem II (PSII). This enzyme is constructed by a large homodimer protein complex comprised of many polypeptide subunits and cofactors (Figure 4a).[129] Upon receiving photons, an electron−hole pair is generated within the enzyme that oxidizes a chlorophyll molecule (P680 → $P680^+$) and reduces a pheophytin acceptor. The oxidized molecule subsequently activates the Mn-based oxygen-evolving complex (OEC),[129] which is the active site for water oxidation (Figure 4b), before returning to its most reduced state.[129,130] The produced oxygen species are highly toxic to organisms and can cause the removal of the protein within the photosystem and the disassembly of the Mn-based cluster. Upon the incorporation of the newly synthesized protein into the membrane-bound complex,[131] the OEC is also reassembled. This continual self-healing catalytic process allows precise control of active sites for water oxidation, yields high selectivity, and resembles the dynamic cycle associated with dissolution−redeposition process in the lattice oxygen mechanism.[132] High-resolution crystallographic analysis of the photosystem revealed the structure of the cubane-like $Mn-Mn_3CaO_5$ cluster (the OEC),[130,133−136] and density function theory (DFT) models described its reconstruction.[136−138]

As the molecular structure was elucidated, initial efforts were made to synthesize an artificial photosynthesis II system or OECs, but the outcomes have shown limited success.[139−141] Nevertheless, such inspiration from nature resulted into the discovery of many transition μ-oxo-bridged metal oxide clusters and complexes. In the pioneer work on an artificial leaf,[142] Nocera prepared a cobalt−phosphate cluster through electrodeposition with edge-sharing octahedral CoO_6, a structural analog to the OEC in the photosystem II that can split water at neutral and near-neutral conditions. Other cubane-like complexes with similar molecular motifs have been explored for water oxidation, including mixed-metal manganese oxide,[143] layered organic cobalt phosphonate,[144] copper oxide,[145] and octanuclear Cu(II) clusters (Figure 4 c and d).[146] Since oxygen evolution in nature involves not only the core catalyst but also assistance from the protein backbone, supporting mediators can be added as part of the biomimetic strategy. Li et al. synthesized a carboxylate-incorporated Ni−Fe coordination polymer in which the negatively charged carboxylate ligands not only stabilized the high valence states of metal centers but also served as proton-transfer relays, efficiently reducing the redox potential.[147] Similarly, introducing an electron-transfer mediator is another viable approach for controlling oxidation-reaction kinetics.[148] Electron-transport assemblies imitating the charge-transfer function of the tyrosine−histidine pair were found to suppress undesirable recombination and consequently increase the quantum efficiency.[149,150]

2.3. Bioderived Catalysts for HER

HER involves a series of elementary steps that take place at the electrode−electrolyte interface. Depending on the pH of the electrolyte, H_2 is generated via the reduction of either a proton (H^+ in acidic media) or H_2O (in alkaline media), as shown in the equations at the beginning of section 2. Since the HER kinetics strongly correlate with the hydrogen adsorption energy (ΔG_H°), this factor constitutes a good descriptor of materials that can catalyze HER. Therefore, in 2004, Nørskov's group calculated the corresponding ΔG_H° on various metals using DFT, which features the volcano plot, and the results perfectly explained the superior HER activity of Pt.[152] In alkaline media, the kinetics of HER on most metal catalysts is more sluggish compared to that in acidic electrolytes due to a distinct pathway. Due to higher pH, H_2O must first be dissociated into H^+, which requires additional energy to drive the overall reaction.[153] So far, a Pt-based catalyst is still the state-of-the-art HER catalyst in both acidic and alkaline conditions.[95,154] Nonprecious-metal-based HER catalyst research has also made significant achievements, with several metal sulfides, phosphides,[155,156] and selenides such as MoS_2,[157] CoP,[158] and WSe_2 active in acidic conditions and Ni-based catalysts functional in alkaline conditions.[159,160]

Like OER, bioderived materials can be used to facilitate electron transfer and proton diffusion for HER. Since the best-performing metal-based HER catalysts were extensively researched previously, engineering bioderived materials as the carbon support to these active sites constitutes a more suitable strategy. In a previous review, Zhao et al. listed the state-of-the-art HER catalysts in acid and alkaline conditions, with a detailed description of their morphologies and electrochemical performance.[153] On one hand, the excellent conductivity of the carbon matrix can lead to a higher proton or electron transport rate. On the other hand, templated mesoporous carbon can provide sufficient electrolyte transport channels and promote mass transport, the bubble release of carbon sites, and H* adsorption, improving HER activities.[161,162] Catalysts formed via in situ templating, such as the 3D coral-like carbon support for Ni_3S_2 and the cube-on-sheet matrix for $Co(OH)_2$, possess intrinsic hierarchical structures[163,164] that not only promote gas diffusion but also provide more accessible active sites. In addition, heteroatom-doped carbon can help stabilize metal catalytic sites against leaching or aggregation by coordinating interactions between the heteroatoms and the metals.[165] Wang et al. made a N−P-doped hierarchically porous carbon matrix from phytic acid and chitosan that can stabilize $FeCoP_2$ sites, protecting the active metal sites from acidic corrosion and thus exposing abundant catalytic sites.

2.4. Bioinspired Catalysts for HER

Besides the state-of-the art Pt- and several nonprecious-metal-based alterative catalysts described above, nature has also provided inspiration for the design of highly active HER catalysts. Interestingly, proton reduction is a typical reaction of bioenergetic metabolism in many living organisms.[166] The metalloenzymes responsible for catalyzing such a reaction are called hydrogenases, which work with remarkably high catalytic rates close to the thermodynamic reaction equilibrium.[167] The nature of the active sites in such hydrogenases and their ability perform a catalytic HER function could be judiciously transposed to artificial nonprecious-metal-centered catalysts to rival Pt. Since these enzymes can also catalyze the reverse reaction, namely, proton oxidation, the inspiration from these

https://doi.org/10.1021/acs.chemrev.2c00429
Chem. Rev. 2023, 123, 2311−2348

enzyme materials can also apply to the HOR, as shown in the following section.

Hydrogenase-inspired molecular electrocatalysts use only relatively inexpensive and highly abundant transition metals, such as Fe, Ni, Mn, and Mo, coordinated to different donor ligands containing basic N or S atoms.[169] Various coordination spheres can be defined on the catalysts (Figure 5). With Ni-based catalysts, the metal center is reduced prior to protonation, forming a Ni hydride complex. The whole ligand contributes to reducing the activation energy, with the phosphines affecting the reducibility of the Ni center and the dangling hydroxyl group on the ligand helping heterolytic H_2 formation by promoting intramolecular proton transfer.[168] This metal−ligand synergy greatly helps reduce the overpotential of the process.[166,170−172] When these molecular catalysts are loaded onto electrodes, typically carbon nanotubes, they can serve as active HER catalysts in the half-cell reaction.[173] Pioneering work from the DuBois group has shown the potential of a Ni-based molecular catalyst mimicking hydrogenase for HER, with a high turnover frequency (TOF) of 500 s^{-1}.[148,174,175]

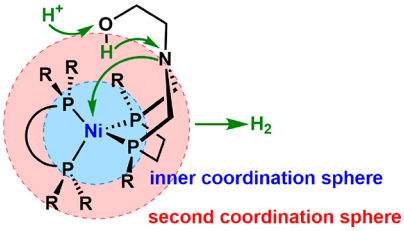

Figure 5. Coordination sphere illustration of a Ni-based molecular catalyst and catalytic reaction diagram for HER. Adapted with permission from ref 168. Copyright 2014 American Chemical Society.

Similar to OER, the proton-transfer relay process that happens in the portion backbone in natural hydrogenases can also be imitated by engineering the supporting mediator of the molecular catalysts. Dubois et al. introduced an amine-containing diphosphine ligand for Ni. They showed that the incorporated nitrogen assisted proton transport and resulted in a significant decrease in the activation barrier for dihydrogen bond formation.[148]

Although the above-mentioned molecular catalysts have shown good activity, their low resistance to oxidative or other harsh conditions results in low stability. Catalyst synthesis and electrode fabrication also remain large challenges.[166] Besides, the large coordination sphere structure (Figure 5) required to drive the catalytic reaction and proton or electron transport has also restricted the active site density per geometric electrode, resulting in low performance in real devices. For instance, Artero and co-workers prepared the same gas diffusion electrode (GDE) with a Ni-centered molecular catalyst and Pt/C for water electrolysis. The former loading can be achieved at 2.5×10^{-8} mol_{Ni} cm^{-2}, an order of magnitude lower than that of Pt/C (2.5×10^{-7} mol_{Pt} cm^{-2}). As a consequence, the current density for the Ni catalyst at an overpotential of 100 mV at 25 °C is only 7.1 mA cm^{-2} compared to that of 18.4 mA cm^{-2} for Pt/C.[175] A strategy to overcome these issues is to design supported single or dual catalysts, where the metal center coordinated by base atoms (i.e., N, S, and P) replicates the active sites in the enzymatic catalysts and can optimize the binding strength of *H and the supporting materials are engineered to enable fast proton and electron transfer. For the synthesis strategy and recent advances, readers may refer to previous reported reviews.[177−184] By developing a universal design principle to evaluate the activity of graphene-based single-atom catalysts, Xu et al. indicated that the catalytic activity of single-atom catalysts is highly correlated with the local environment of the metal center. The electronic structures of these metal centers are controlled by the coordination number and the nearest-neighbor atoms, affecting the HER performance through the *H binding energy.[185] Dual-atom catalysts can further modulate the interaction with *H through the synergetic effect between the two metal centers, leading to superior HER activities (Figure 6).[176,183]

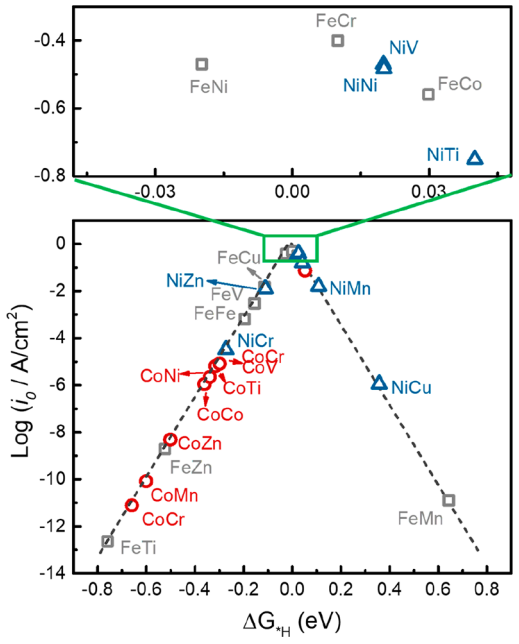

Figure 6. HER volcano curve of the exchange current density (i_0) as a function of MM′-NPG (in-plane dual-metal atom in nitrogen-doped porous graphene). Reproduced with permission from ref 176. Copyright 2021 Elsevier.

Besides these molecular and single-atom catalysts, MoS_2 has also shown exceptional HER performance. MoS_2 has a low activation energy requirement due to its resemblance to the FeCo cofactor active site found in nitrogenase (Figure 7a), which has a hydrogen binding energy close to that of Pt.[186] Jaramillo et al. combined experimental analysis with computational methods to identify the active sites in nanoparticulate MoS_2. They discovered a linear correlation of the HER performance with the number of edge sites on the MoS_2 catalyst, which were later proved to be the active sites.[187] They summarized in a review the general synthesis strategies and performance figures of metrics, based on which further development toward increasing the number of accessible active sites per the geometric electrode area has been pointed out (Figure 7b).[157]

Overall, inspiration from nature via photosynthesis led to the successful design of various transition μ-oxo-bridged metal oxide clusters and complexes for OER. Similarly, molecular catalysts and carbon-supported single- or dual-atom catalysts inspired by the active sites in hydrogenases, as well as the MoS_2 catalyst structure inspired by nitrogenase, have also lead to breakthroughs in HER research.[147−150] Electrocatalytic active centers can work in conjunction with charge mediators in their coordination sphere to assist proton an electron transfer, akin

https://doi.org/10.1021/acs.chemrev.2c00429
Chem. Rev. 2023, 123, 2311−2348

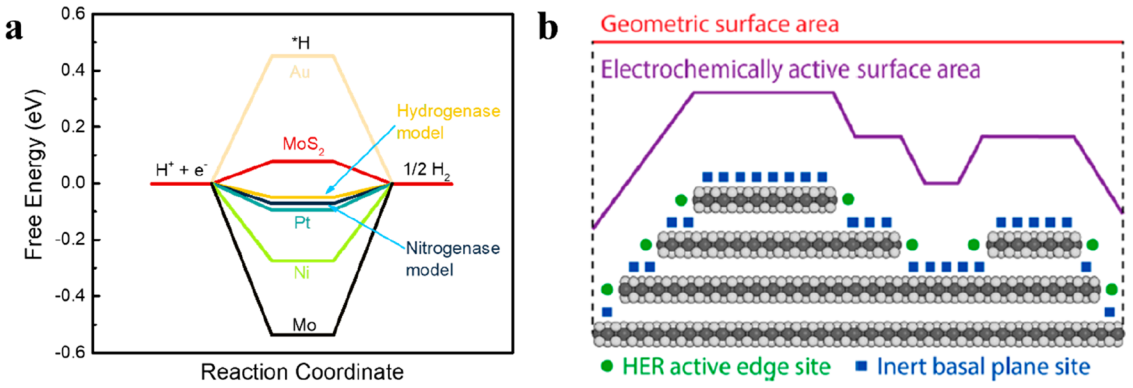

Figure 7. (a) Calculated free-energy diagram for HER for the hydrogenase model, the nitrogenase model, MoS_2, and metal-surface (Au, Pt, Ni, and Mo) catalysts at a potential $U = 0$ relative to the standard hydrogen electrode (SHE) at pH 0. Reproduced with permission from ref 186. Copyright 2005 American Chemical Society. (B) Two-dimensional representation of MoS_2 catalyst electrocatalytic active surface area and projected geometric surface area. Reproduced with permission from ref 157. Copyright 2014 American Chemical Society

to natural enzymes. At a macroscopic level, the catalyst scaffold is important for the effective dispersion of active sites and gas diffusion. This can be achieved through a carbon network or by self-construction. Finally, the combination of metal complexes, charge-transfer relays, and hierarchical structures will bring about unprecedented catalytic performance for which a new class of metal−arbon hybrids has been foreseen to emerge in the future.

3. BIODERIVED AND BIOINSPIRED CATALYSTS FOR ORR AND HOR

Both the switch from gray (steam methane reforming) to green hydrogen (in electrolyzers) and its utilization in fuel cells could bring significant environmental benefits through low carbon emissions and highly efficient energy conversion. In a typical PEM fuel cell, H_2 gas is supplied to the anode side where it is oxidized into protons, with electrons generated (i.e., HOR) following either Tafel/Volmer or Heyrovsky/Volmer steps as follows:

$$H_2 + 2^* \rightarrow 2H^* \quad \text{(Tafel)}$$

$$H_2 + {}^* \rightarrow H^* + H^+ + e^- \quad \text{(Heyrovsky)}$$

$$H^* \rightarrow H^+ + e^- + {}^* \quad \text{(Volmer)}$$

$$\text{Overall: } H_2 \rightarrow 2H^+ + 2e^-$$

The produced electrons in a PEMFC travel through an external circuit to dispense electrical power, while the protons cross the membrane to the cathode side, where they react with the oxygen stream to produce water (i.e., ORR) in a multistep four-electron-transfer process via the following mechanism:

$$O_2 + {}^* \rightarrow O_2^*$$

$$O_2^* + H^+ + 4e^- \rightarrow OOH^* + 3e^-$$

$$OOH^* + H^+ + 3e^- \rightarrow O^* + H_2O + 2e^-$$

$$O^* + H^+ + 2e^- \rightarrow OH^* + e^-$$

$$OH^* + H^+ + e^- \rightarrow H_2O + {}^*$$

$$\text{Overall: } O_2 + 4H^+ + 4e^- \rightarrow 2H_2O$$

In the case of an alkaline anion-exchange-membrane fuel cell (AEMFC), H_2 is still oxidized at the anode, although OH^- instead of the H^+ passes through the membrane to react with H_2. The Tafel/Volmer or Heyrovsky/Volmer mechanisms are as follows:

$$H_2 + 2^* \rightarrow 2H^* \quad \text{(Tafel)}$$

$$H_2 + OH^- + {}^* \rightarrow H^* + H_2O + e^- \quad \text{(Heyrovsky)}$$

$$H^* + OH^- \rightarrow H_2O + e^- + {}^* \quad \text{(Volmer)}$$

$$\text{Overall: } H_2 + 2OH^- \rightarrow 2H_2O + 2e^-$$

Consequently, at the cathode of an AEMFC, the ORR produces OH^-:

$$O_2 + {}^* \rightarrow O_2^*$$

$$O_2^* + 2H_2O + 4e^- \rightarrow OOH^* + OH^- + H_2O + 3e^-$$

$$OOH^* + OH^- + H_2O + 3e^- \rightarrow O^* + 2OH^- + H_2O + 2e^-$$

$$O^* + 2OH^- + H_2O + 2e^- \rightarrow OH^* + 3OH^- + e^-$$

$$OH^* + 3OH^- + e^- \rightarrow 4OH^- + {}^*$$

$$\text{Overall: } O_2 + 2H_2O + 4e^- \rightarrow 4OH^-$$

ORR is highly sluggish in its kinetics and can also proceed by a "two-electron" process, generating H_2O_2.[188] An efficient fuel cell ORR electrocatalyst should drive the reaction toward four-electron pathways to provide a high current and high operating potential, since the H_2O_2 pathway reduces the achievable current and degrades the membrane.[189,190] The binding energies in the four-electron ORR process have adsorbed intermediates of the first and third electron or proton transfer step (OOH* and OH*) that are strongly correlated to each other, obeying a linear scaling relationship.[191] The difference in energy of these intermediates follows a constant of ca. 3.2 eV.[192] Therefore, at least ca. 1.6 eV (3.2 eV/2) is the minimum energy for each of the two electron or proton transfer steps. As the energy difference between each of the four intermediates ideally amounts to 1.23 eV, a minimum overpotential of ca. 0.3 V can be expected for ORR catalysts with one active site, such as the active sites present in Pt(111) and $PtNi_3$ (Figure 8)[193], the most active ORR catalyst in an aqueous environment to date.[194] Increasing the number of oxygen binding sites to two via dual-

https://doi.org/10.1021/acs.chemrev.2c00429
Chem. Rev. 2023, 123, 2311−2348

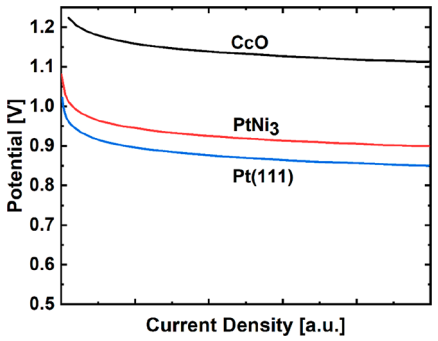

Figure 8. Theoretical polarization curves of the cathode potential versus current density of CcO (black), $PtNi_3$ (red), and Pt(111) (blue). Reproduced with permission from ref 195. Copyright 2010 American Chemical Society. Original data of CcO were calculated from ref 196.

metal atoms in atomic proximity, present in CcO, can enable the optimization of the electronic structures of each binding site such that the binding energy is modified in accordance with the scaling relation, allowing a reduced minimum overpotential (Figure 8).[195] The possible benefits of bioinspired dual-metal atom sites are further discussed in section 3.3.

In terms of catalysts for fuel cells, Pt nanoparticles supported on carbon (Pt/C) are commonly used commercially, but the high Pt requirement in fuel cells could lead to global supply issues. For instance, assuming an annual production of 1.25 million PEMFC-based vehicles (10 million deployed globally by 2030),[197] current Pt loadings (0.125 $mg_{pt,cathode}$ cm^{-2} and 0.05 $mg_{pt,anode}$ cm^{-2}, 1165 mW cm^{-2}, 87.9 kW gross power)[198] require ∼12.4 tons of Pt annually (assuming 25% Pt recycling), therefore alone consuming ∼7% of the global Pt produced annually (180 tons of Pt produced in 2021).[199] Combined with other developing fuel cell applications (buses, trains, boats, aviation, back-up power, and electrolyzers), this would exceed the reasonable annual consumption of 10% of an element for a new technology.[200] Moreover, as mentioned, the high loading of Pt-group catalysts is identified as the one significant barrier to reducing cost, accounting for 40−50% of the cost of a fuel cell (at 500,000 units yr^{-1}).[201] Pt is also prone to cost fluctuations and limited accessibility, further hindering its commercialization in fuel cells. Besides, Pt also suffers from CO poisoning and methanol crossover.[202] To address these issues, significant progress has been made to lower the Pt loading, including designing non-Pt metal and nonmetal heteroatom-doped carbon catalysts.[64,203] Strategies such as increasing the density and intrinsic activity of active sites,[204] constructing hierarchical structures, and enlarging triple-phase boundaries have improved both electrocatalytic activity and stability.[203] In the sections below, we will discuss how catalysts have so far been inspired or derived from nature along with how nature can continue to direct future research directions toward active and stable electrocatalysts.

3.1. Bioderived Metal-Free Catalysts for ORR

Biomass in electrocatalysis is often used as a precursor for the formation of conductive carbon supports with high surface areas and ORR activities in alkaline conditions.[203] Bioderived catalysts have been successfully prepared from numerous materials, including wood,[56−59] sisal leaves,[205] pine needles,[206] rice husks,[207] bamboo,[208] loofahs,[209] watermelon,[210] pomelo peels,[211] hemp,[212,213] clover,[214] peanut skin,[215] fern fiber,[216] bones,[60−63205] leather,[217] shrimp shells,[218] and even butterfly wings.[219] Clearly some of these sources are not practically suitable due to limited supplies (an example is discussed further in section 3.2) and environment destruction. Biomass-derived carbon sources with heteroatoms have been employed to help with the formation of active sites or to form the active site itself. B- or N-doped carbons have shown better activity as active sites for ORR compared to oxygen, sulfur, and carbon edges, as shown by volcano plots (Figure 9). In addition, B- and N-doped carbons share similar free-energy diagrams, while carbon edge sites require a much larger driving force to complete their four-electron pathway (Figure 9b). Via a simple heat treatment under inert gas, the heteroatoms originating from biomass could hybridize into the carbon framework. Meanwhile, NH_3 activation and the addition of melamine, urea, or dicyandiamide have become common methods to introduce or further add nitrogen and improve activity.[220] The type of a particular dopant element introduced will affect the performance,[220] although the true active sites in metal-free catalysts are often debated, as defects in the carbon framework have experimentally been shown to provide greater catalytic activity than nitrogenated sites.[221] An understanding of the most active and stable heteroatoms or defects would help form the criteria for the targeted synthesis of active sites used in metal-free carbon-based electrocatalysts.

Despite the many publications on this topic,[222223] the performance of heteroatom-doped carbons is still too kinetically

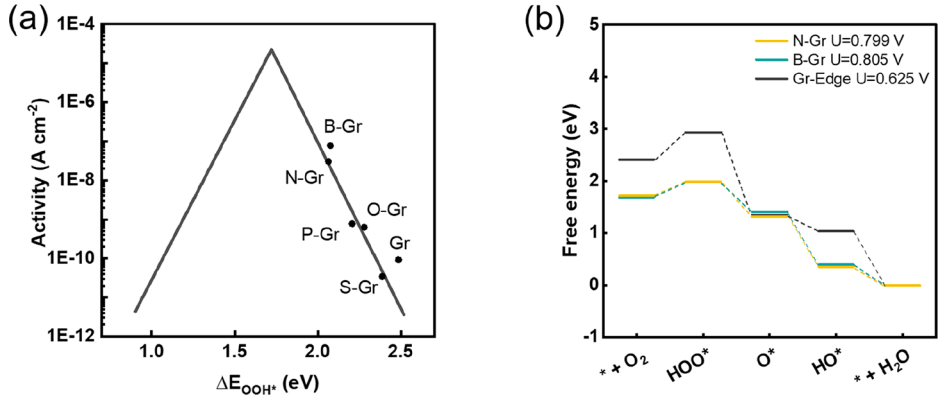

Figure 9. (a) Volcano plot of activity versus OOH* binding free energy (G_{OOH*}) for heteroatom-doped graphene. (b) Free-energy diagrams for graphitic N-doped graphene (N-Gr, U (limiting potential) = 0.799 V), graphitic boron-doped graphene (B-Gr, U = 0.805 V), and carbon on graphene edge (Gr-Edge, U = 0.625 V). Panels a and b were adapted from ref 203.

https://doi.org/10.1021/acs.chemrev.2c00429
Chem. Rev. 2023, 123, 2311−2348

hindered in the four-electron ORR pathway to produce electricity in practical fuel cell devices. However, they have demonstrated the selective two-electron pathway to H_2O_2 production through heteroatom doping such as nitrogen[224] and phosphorus.[225,226] The H_2O_2 production market is estimated to be worth 6 billion dollars by 2023,[227] opening opportunities for the production of metal-free carbon electrocatalysts from biomass. However, the heteroatom amount and species vary depending on the source, significantly reducing the reproducibility of biomass-derived catalysts.[228] Using purified bioderived precursors to prepare catalysts can help tackle this irreproducibility issue.[229] However, extracting raw pure precursors from biomass such as carbohydrates and lignin adds an additional synthetic step, thus increasing the price of the catalyst while decreasing its overall sustainability because of the harsh conditions required for biomass fractionation (KOH, sulphites, or organic solvents).[229] Therefore, if cheap and reproducible biomass-derived catalysts can be obtained, they can be practically implemented in H_2O_2 production devices.

3.2. Bioderived Non-PGM-Based Catalysts for ORR

Although to date Pt and platinum-group metal (PGM) alloys work best in both acid and alkaline conditions, the design of PGM-free catalysts is a promising method to replace the scarce and expensive PGM materials. So far, the most widespread PGM-free catalysts are transition-metal nanoparticles and single sites loaded on carbon substrates with or without nitrogen (M−C and M−NC; M = Fe, Co, Ni, Mn).[230,231] While metal clusters aggregate easily during long-term operation, chelating nitrogen atoms around single metallic species leads to sites more resistant to alkaline and acid leaching.[232] Unfortunately, most biomass sources do not provide a sufficient amount of heteroatoms (nitrogen or others) for proper metal single-site chelation,.[228] However, chitosan from crustaceans, with its naturally high N content, has shown promise as a suitable nitrogen-doped carbon-biomass-derived precursor to host non-PGM ORR catalysts.[233] To understand if sufficient chitosan (and other potential biomass sources) could be supplied for electrocatalyst applications, we look at the cathode catalyst in PEMFC light-duty vehicles. We again use our previously calculated assumed global annual production of 1.25 million PEMFC light-duty vehicles,[197] each with an fuel cell active area of 9.9 m^2 (as estimated in the Toyota Mirai).[234] Assuming that state-of-the-art non-PGM cathode catalysts could provide the required fuel cell power and durability at 4 mg_{carbon} cm^{-2} (reasonable considering recent developments[235]), this results in 495 tonnes per annum of non-PGM catalyst required for the PEMFC cathode. Assuming a 20% process yield from precursor materials results in ∼2500 tonnes of catalyst precursors required annually. Chitosan-derived catalysts have not provided state-of-the-art non-PGM catalyst performance, so one can expect to require at least 10× more of the chitosan-derived catalyst to reach an equivalent performance. Chitosan comprises between 10% and 25% dry weight of crustaceans, with 8.4 million tonnes of crustacean shell estimated to be produced as waste in 2017;[236] this demonstrates the large production capability of chitosan, which could fulfill new applications such as electrocatalysis. However, real market production quantities of chitosan are much lower, with a projected market size of 21,400 tonnes for 2015, and there are no known industrial chitosan production facilities to date for pure chitosan, leading to high costs.[237,238] This highlights some issues with the use of biomass feedstocks for scalable synthesis methods.

Carbohydrates such as glucose and gelatin are cheap, abundant, and do not require complex synthesis processes and pretreatment, making them suitable precursors for single-atom M−NC catalysts on a large scale; however, they would require an additional dopant, such as N, to be introduced to assist the formation of chelating metal sites. Another issue in biomass-derived materials for ORR lies in the difficulty of achieving defined highly active catalytic sites such as single-metal-atom MN_x sites.[239,240] During synthesis, MN_x sites tend to aggregate into particles to form carbides or oxides with the carbon skeleton during typical pyrolysis, hence reducing the catalytic activity and stability.[241,242] To avoid this, efforts should be focused on first synthesizing pyrolyzed heteroatom-doped carbon from biomass and then subsequently incorporating metal ions to avoid the undesirable carbothermal reactions at high temperatures.[21,243−246]

Researchers have intensively studied the influence of the structure,[247] evolution pathways,[248] and degradation mechanism[249] and made comparisons between different single-atom M−NC sites,[249,250] which established a fundamental understanding of the active sites. Interestingly, highly active MN_x sites can be found in nature within CcO or hemoglobin.[195] Therefore, in the next section we expand on the design concept of an active site inspired by nature to create next-generation ORR catalysts.

3.3. Bioinspired Design of Active Sites in ORR Catalysts

Pt is highly efficient toward HOR in PEMFCs, requiring only ultralow loadings (<10 μg_{Pt} cm^{-2}) to proceed effectively.[251,252] However, at these ultralow loadings the catalyst becomes highly sensitive to fuel contaminants such as CO and H_2S, which irreversibly poison Pt.[253] Alternative hydrogenase-inspired Ni-based catalysts, previously discussed for HER in section 2.2 and illustrated in Figure 6, can display tolerance to these contaminants, thereby lowering fuel cell stack and H_2 purification costs. For instance, a molecular $[Ni(P_2^{Cy}N_2^{CH_2pyrene})_2](BF_4)_2$ complex attached to multiwalled carbon nanotubes (MWCNTs) on a gas diffusion layer electrode maintained a constant H_2 oxidation current (at 0.25 V vs normal hydrogen electrode (NHE)) in a 50 ppm CO atmosphere over 80 min, while a commercial Pt electrode (0.5 mg_{Pt} cm^{-2}) became completely poisoned within 40 min.[254] In terms of power output, a biomimetic Ni bisdiphosphine complex ($[Ni(P_2^{Cy}N_2^{Arg})_2]^{7+}$) immobilized on modified carbon nanotubes at the anode (and Pt at the cathode) reached 14 mW cm^{-2} (at 0.47 V and 60 °C) in a PEMFC, only six times less than a comparably constructed full-Pt-based PEMFC.[255] Further optimizing the testing of a similar Ni-based complex, Artero and co-workers recently achieved up to 83 ± 6 A mg_{Ni}^{-1} in a gas diffusion layer (at 55 °C and 0.4 V overpotential), a mass activity <1 order of magnitude lower than those of state-of-the-art ultralow-loading Pt-based anodes.[256] This signifies the possible practical application of these complexes, assuming that bubble accumulation can be overcome,[256] long-term stability can be demonstrated, and a scalable synthesis approach can be developed. Successful attempts at incorporating bioinspired catalysts at the anode in AEMFCs have not, to the best of our knowledge, been reported to date, likely due to the slow HOR kinetics in alkaline conditions. The difficultly of HOR in AEMFC was demonstrated Davydova et al., who found via simulations of a Pt/C anode (0.08 mg_{Pt} cm^{-2}) that the overpotential was non-negligible at 1 A cm^{-2}.[257] Conversely,

https://doi.org/10.1021/acs.chemrev.2c00429
Chem. Rev. 2023, 123, 2311−2348

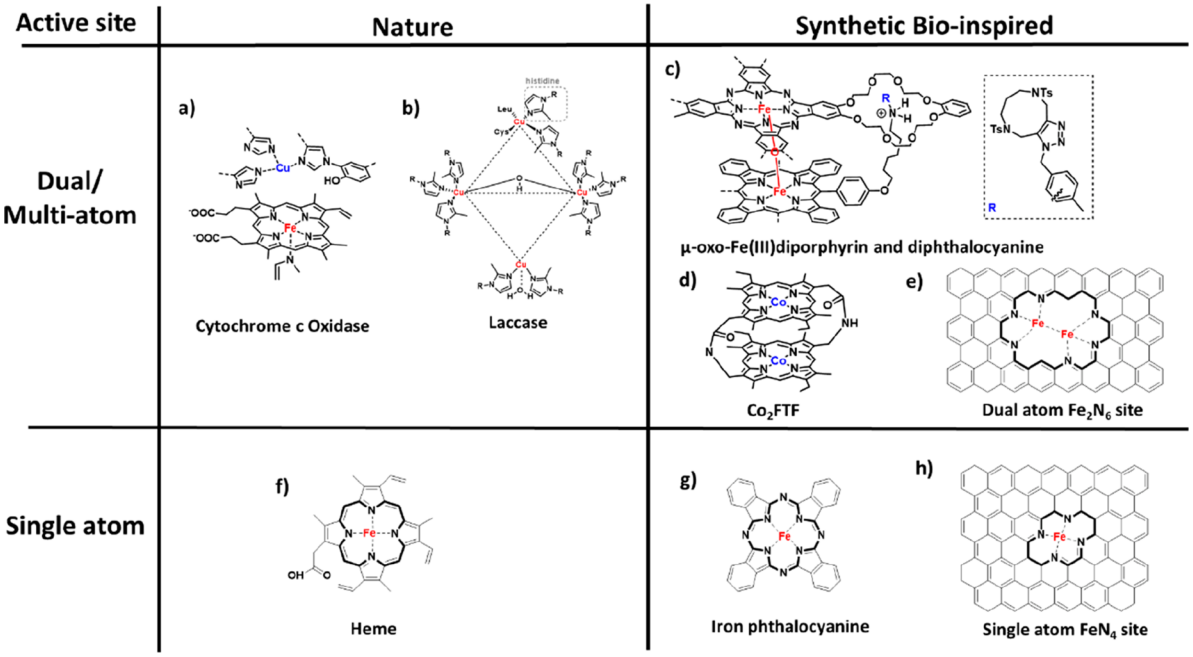

Figure 10. Key structural features of dual and multiatom active sites in naturally occurring (a) CcO and (b) laccase and nature-inspired M_xN_y active sites in (c) μ-oxo-Fe(III)diporphyrin and diphthalocyanine. Figure 10c was adapted from ref 265. (d) Co_2FTF. Adapted with permission from ref 266. Copyright 1980 American Chemical Society. (e) Dual-metal-atom Fe_2N_6 site in graphene. Key structural features of single-atom active sites in naturally occurring (f) heme and (g) iron phthalocyanine and the (h) single-atom FeN_4 site in graphene.

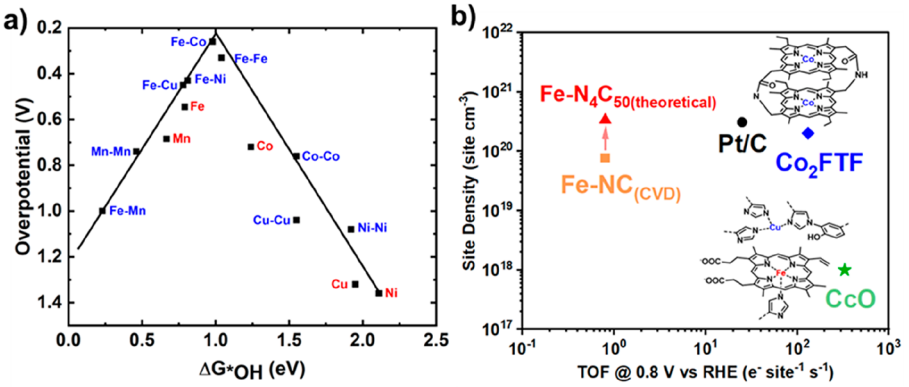

Figure 11. (a) Thermodynamic relations (volcano) of the overpotential for ORR calculated for single ($M-N_4$–graphene, M = metal) and dual-metal-atom (M_2-N_6–graphene) sites versus the DFT-calculated *OH binding free energy (G_{*OH}). Reproduced from ref 267. Copyright 2019 American Chemical Society. Reproduced from 276. Copyright 2019 American Chemical Society.. (b) Calculated TOF (0.8 V vs RHE) and measured (Fe-$NC_{(CVD)}$) or calculated (rest) site density for single atoms ($FeNC_{CVD}$ and $FeN_4C_{50(theoretical)}$), dual-metal atoms in molecular (Co_2FTF) and enzyme (CcO) structures, and Pt/C. Site densities of all catalysts (excluding CcO) were calculated based on an electrode volume of 0.4 g_{carbon} cm^{-3}, with $Fe-N_4C_{50}$ and Co_2FTF calculated based on their molecular mass. CcO (green star) is from A. ferrooxidans CcO with a ferrocenecarboxylic acid redox mediator,[184] with the TOF calculation provided in ref 184. The site density of CcO was calculated based on an occupied volume of ca. 1000 nm^3 (bovine heart CcO,[277] distances from XRD were analyzed using RCSB PDB[278]). Fe-NC_{CVD} tested in an O_2-saturated 0.5 M H_2SO_4 electrolyte at 900 rpm in RDE, with a site density based on nitrite stripping and the TOF from the kinetic current density.[21] $Fe-N_4C_{50(theoretical)}$ (red triangle) is based on a theoretical Fe-NC[279] with the same TOF as Fe-NC_{CVD}. The site density of Pt/C (Pt nanoparticle, black circle) was obtained from ref 253 (with Pt = 50 wt % with 25% site utilization), and the TOF was from PEM fuel-cell conditions (80 °C, 100 kPa_{abs} H_2 and O_2).[280,281] Co_2FTF (blue diamond) tested in O_2-satured 0.5 M CF_3CO_2H at 250 rpm.[266]

in PEMFCs, the anode operates similar to a nonpolarizable electrode.[257]

To improve the activity of an ORR catalyst, two design principles can be applied: either increasing the number of active sites or enhancing the intrinsic activity per active site.[258] Nature mastered the latter when evolving the active-site structures relevant for biochemical oxygen transport and conversion. The two main ORR enzymes are CcO, (Figure 10a),[259] where the electron transfer of ORR drives a transmembrane proton pump, and multicopper oxidase, an ORR catalyst that concomitantly oxidizes various organic molecules and metal ions.[260,261] The active-site structure of a multinuclear copper catalyst such as laccase is composed of four Cu atoms, which are integrated into the enzyme by a different number of amino acid ligands, mainly histidine (Figure 10b). The scientific community aims to mimic enzymes via dual atom catalysts (Figure 10c–e) or by replicating the simpler single-site catalysts derived from the heme structure (Figure 10f), the binding site for O_2 in CcO, hemoglobin, and

https://doi.org/10.1021/acs.chemrev.2c00429
Chem. Rev. 2023, 123, 2311–2348

myoglobin, which bind O_2 reversibly for transport.[262] The central FeN_4 in heme has been emulated by molecular model systems such as porphyrins, phthalocyanines, and Fe single-atom catalysts (Figure 10g and h).[263,264]

With nature utilizing a library of earth-abundant transition metals,[68] the choice of the active metal center for ORR has been explored both theoretically and experimentally.[264] Computational studies of a model system with $M-N_4$ sites in a graphene matrix concluded that stronger oxygen binding energies of the intermediates on Fe and Mn preferentially lead to the four-electron ORR mechanism and water as a product. In contrast, Co, Cu, and Ni, which feature weaker oxygen bonds, were found to favor the two-electron ORR toward the production of hydrogen peroxide (Figure 11a).[267] The Fe binding energy and hence the turnover frequency (TOF) are related to the Fe(III/II) redox potential in Fe macrocycle catalysts, which can be tuned by refining the electronic structure and the coordination environment to enhance *OH binding and reach the top of the volcano.[239,268] For instance, the electron-withdrawing ability of electronegative substituents favorably shifts the redox potential for the Fe(III/II) couple in the positive direction.[239,269,270] Additionally, penta-coordinated transition-metal macrocycles with a fifth nitrogen ligand, reflecting the real coordination environment in the enzymatic heme sites in CcO and vitamin B12, have shown enhanced ORR activity.[271] For instance, FePc has been anchored onto pyridine-functionalized carbon nanotubes.[272−274] Advances in penta-coordinated transition-metal macrocycle catalysts were summarized recently.[275]

Nevertheless, single-atom active sites coordinated with nitrogen atoms embedded in graphene obey the same scaling relationships as Pt(111), causing a minimum overpotential >0.4 V (Figure 11a).[193] Meanwhile, dual-metal-atom active sites can facilitate an optimized binding energy of each oxygen atom, allowing a reduced minimum overpotential (Figure 11a). Additionally, the 3D geometric arrangement of the active site could potentially introduce alternative reaction pathways or new types of interactions with the ORR intermediates, thereby breaking scaling relations. This 3D arrangement could be achieved with dual-metal-atom-site electrocatalysts with cofacial active sites, biomimicking CcO structures.[282,283] The experimental evidence for diporphyrinic Co structures leading to highly selective $4e^-$ pathways has been known since 1979, following instrumental work by Collman et al.[266,284] More recently, similar porphyrinic molecular catalysts with a cofacial binuclear active site were suggested to have the potential to circumvent the limitations of the scaling relation between G_{OH} and G_{OOH}.[285] Meanwhile, new generations of porphyrinic metal−organic frameworks (MOFs) with tailored spacing could provide another pathway to 3D dual-metal-atom sites,[286] with structurally similar designs predicted by DFT circumventing scaling relations for ORR.[287] What has yet to be demonstrated is a robust and conductive 3D dual-metal-atom catalyst able to withstand the harsh conditions of a fuel cell, which could potentially be provided by a new class materials termed "ordered carbonaceous frameworks".[288,289] Interestingly, Svane et al. modeled porphyrin-like cofacial dual-atom CoN_4C_{12} and in-plane Co_2N_6/graphene sites (with O bound on the opposing side) for ORR and found that only the in-plane site results in a significant deviation from scaling relations, which could be potentially further improved by substituting the Co atoms with other metals.[290] Compared to experimental results, synthesized in-plane dual-metal atoms of Co, determined as Co_2N_5 (derived from pyrolyzed Co-doped ZIF-8), have been reported to exhibit mass activity over an order of magnitude higher compared to their single-atom-site Co counterparts (at 0.75 V vs RHE).[291] As predicted by DFT, experimentally synthesized mixed-metal dual-metal-atom catalysts, most notably those containing Fe and Co, have achieved the highest ORR activities of dual-metal atom catalysts to date,[292,293] with some displaying stabilities of over 100 h in a fuel cell, as confirmed by postelectrochemical testing of the extended X-ray absorption fine edge structure (EXAFS) and X-ray absorption near-edge structure (XANES).[294] Additionally, mixed-metal biomass-derived ORR catalysts containing a portion of neighboring in-plane Zn−Co dual-metal=atom sites have been produced from chitosan due to the high concentration of naturally occurring amine groups, which stabilize the metal atoms.[233,295] However, whether biomass-derived catalysts can form dual-metal-atom sites exclusively and in a controlled manner remains to be seen. Increasing the number of reactant binding sites further to trimetal-atom[296,297] or even multimetal-atom sites, as inspired by Laccase,[298] can also favorably direct selective ORR to water, although controllably synthesizing mimics and stabilizing such sites for electrochemical reactions becomes even more challenging.

The theoretically predicted low overpotential of enzymes (Figure 11a) has even been demonstrated experimentally to surpass the ORR kinetics of Pt-based catalysts (and native enzymes) by modifying naturally occurring enzymes.[299] For instance, a laccase-based enzymatic fuel cell reached considerably low overpotentials as low as 0.1 V for ORR.[300] However, the power densities in enzymatic fuel cells fall into the 1−1000 $\mu W\ cm^{-2}$ range,[301] constricting their practical application.[302,303] This is caused by the bulky protein structure, which effectively limits the number of active sites per electrode volume.[299] As illustrated in Figure 11b, while the turnover frequency (TOF) of CcO is >300 $e^-\ site^{-1}\ s^{-1}$ (at 0.8 V vs RHE), the active-site density in CcO (and other enzymes) is orders of magnitude lower compared to those in metal nanoparticles or single-atom catalysts. An ideal catalyst would maximize both TOF and the site density.[304] Recent progress in state-of-the-art high-site-density heme-like FeN_4 sites produced via chemical vapor deposition methods (Figure 10c, denoted Fe-$NC_{(CVD)}$) means further possible site density improvements are limited, although possible beneficial synergistic effects could take place at the upper site-density limits. Other methods to improve the TOF may be still needed, possibly via dual-metal-atom sites. Interestingly, as shown in Figure 10c, if one could create accessible layers of enzyme-inspired active dual-metal-atom complexes, such as that of Co_2FTF by Collman et al. (Figure 10e),[266] it could lead to a step change in the fuel cell performance of non-PGM catalysts beyond that of PGM-based catalysts; however, these molecular complexes are typically unstable and would suffer conductivity issues.

Nevertheless, significant improvements have been made in M−NC testing and activity, the understanding of the active site, and methods of quantifying the site density, such as using probe molecules of either nitrite, carbon monoxide, or cyanide,[305−307] which are (unsurprisingly) known to inhibit enzyme and/or heme function. In particular, remarkable progress in the performance of the heme-like active sites of Fe−NC has been achieved through collaborative consortium research efforts (ElectroCat from the U.S. Department of energy[308,309] and PEGASUS and CRESCENDO from the EU Fuel Cells and Hydrogen Joint Undertaking[310,311]), although, like enzymes, they still possess stability over an order of magnitude below

https://doi.org/10.1021/acs.chemrev.2c00429
Chem. Rev. 2023, 123, 2311−2348

practical PEMFC stability (~100 h vs >5000 h target).[312] However, the commercialization of Fe−NC catalysts toward alkaline and direct methanol fuel cells is already underway.[313,314] Focus is moving toward improving durability by understanding the mechanisms of catalysts degradation (such as demetalation, radical attack such as H_2O_2, active-site protonation and anion binding, and micropore flooding).[315] Inspiration from nature's ability to repair could be used to extend the lifetime of degraded MN_x catalysts through active-site regeneration and reactivation.[316,317] Other bioinspired research efforts for ORR active sites should be directed toward maximizing the site density of heme-inspired FeN_x catalytic active sites and at creative ideas to break the scaling relations of ORR intermediates by engineering dual-metal-atom sites, such as those present in CcO. Future designs of catalysts could allow the local movement and flexibility of their active sites to enable optimal configurations for intermediate reaction steps. For instance, in multicopper oxidase, the Cu−Cu distance of two Cu ions decreases from ~5[318] to ~3.3 Å when moving from fully reduced to fully oxidized states.[319] In a rare example, Tanaka and co-workers have experimentally synthesized and tested for ORR a cofacial bridged μ-oxo-Fe(III) diporphyrin and diphthalocyanine connected by a flexible fourfold rotaxane dual atom catalyst (Figure 11d).[265] Upon achieving a highly efficient and stable nature-inspired active site, macroscale reactant transport to the active site could become the rate limiting factor, the importance of which is discussed in detail in section 5.

4. BIOINSPIRED AND BIOMASS-DERIVED CATALYSTS FOR CO_2 REDUCTION

Rising CO_2 levels in the atmosphere have prompted scientists to prioritize their research on CO_2 recycling through carbon capture, utilization, and sequestration processes.[320−322] Electrochemical CO_2 reduction (CO2RR) is one of these technologies, wherein waste CO_2 can be converted to value-added chemicals, such as carbon monoxide, formate, methane, methanol, ethane, ethylene, ethanol, propanol, etc.[320−322] Single-carbon products such as CO can be used for the synthesis of higher hydrocarbons with the formula C_nH_{2n+2}.[323−325] Currently, some of the most widely utilized electrocatalysts for CO2RR are noble metals, including Au or Ag nanoparticles, that display a high selectivity toward CO,[326,327] while others such as Ni, Fe, or Pt nanoparticles are much more selective to the competing HER. Carbon-based nanomaterials are potential alternatives to such noble-metal catalysts due to their easily available raw materials, tunable structure, chemical stability, and high electrical conductivity.[328,329] However, pristine carbon is not active for CO2RR due to the difficulty of the first activation step to form CO_2^- following the reaction

$$CO_2 + e^- \rightarrow CO_2^- \qquad E^0 = -1.9\,\text{V vs. SHE}$$

This is due to stable linear structure of CO_2, which translates into a large thermodynamic barrier of −1.9 V vs SHE. Thus, pristine carbon remains inert toward CO_2 activation due to its symmetric charge distribution.[329] Heteroatom (such as boron, nitrogen, oxygen, phosphorus, or sulfur) doping resolves this issue through redistributing the charge density of the carbon matrix.[330−332] Positively charged carbon atoms generated due to heteroatom doping can promote the adsorption of CO_2 and the stabilization of the intermediate, thereby lowering the CO_2 activation energy.[328] Furthermore, porous and tunable carbon nanostructures enhance the local concentration of CO_2, thus favoring CO_2 reduction. It was recently observed that nonmetal dopants such as nitrogen, sulfur, and oxygen have minimal contributions to hydrogen evolution, while metal dopants in amounts above 100 ppm promote hydrogen evolution.[333] Thus, the utmost care should be taken to prevent metal contamination from the electrolyte or the electrochemical cell. In addition to the doping, the morphology of the nanostructure also plays a crucial role. A nanoconfinement effect induced by the porous carbon nanostructures enhances the concentration of CO_2 near the electrode surface, thus promoting the adsorption of CO2RR intermediates and favoring C−C coupling.[334]

CO2RR to different products such as HCOOH, CH_3OH, and CH_4 involves a multiple proton−electron transfer process (as described in reactions below) and thus faces significant challenges such as (i) low current density, (ii) unsatisfactory product selectivity, (iii) low catalyst stability, and (iv) competing HER.

$$CO_2 + 2H^+ + 2e^- \rightarrow CO + H_2O \qquad E^0 = -0.53\,\text{V vs SHE}$$

$$CO_2 + 2H^+ + 2e^- \rightarrow HCOOH \qquad E^0 = -0.61\,\text{V vs SHE}$$

$$CO_2 + 6H^+ + 6e^- \rightarrow CH_3OH + H_2O \qquad E^0 = -0.38\,\text{V vs SHE}$$

$$CO_2 + 8H^+ + 8e^- \rightarrow CH_4 + 2H_2O \qquad E^0 = -0.24\,\text{V vs SHE}$$

$$2H^+ + 2e^- \rightarrow H_2 \qquad E_0 = -0.42\,\text{V vs SHE}$$

Most of these challenges can be resolved by means of bioinspired approaches through either mimicking the active sites of a known enzyme or replicating the features of the secondary enzyme that protects the active site. Therefore, in this section we delve into the recent developments of bioinspired catalysts for CO_2 reduction and how emulating natural enzymes in a solid heterogeneous catalyst can lead to the sustainable production of high-added-value chemicals from such electrochemical process.

The presence of diverse active sites (vacancies, defects, grain boundaries, undercoordinated edges, and step sites, among others) on a polycrystalline metal catalyst, such as Cu, is responsible for lower product selectivity.[335] Such sites have different intermediate adsorption energies and hence result in the formation of a wide array of products, such as CO, CH_4, C_2H_4, C_2H_5OH, etc.[336] It is thus imperative to design electrocatalysts with uniform active sites to improve product selectivity and circumvent expensive purification processes, such as reverse osmosis, electrodialysis, etc.[337] For instance, using technoeconomic analysis, Zhu et al. reported the production cost of formic acid to be ~0.2 USD kg^{-1}, which is significantly cheaper than the current market price of ~0.7 USD kg^{-1}.[338] When purification steps are considered, the cost increases to ~1 USD kg^{-1}, rendering the process commercially unviable. However, this issue can be resolved with enhanced catalytic performance and selectivity.

Enzyme-inspired catalytic materials with atomically dispersed metal sites can inspire us to foster the large-scale sustainable production of value-added products with better selectivity.[339] Natural metalloenzymes such as formate dehydrogenases (found in bacteria and yeast) use a Mo- or W-based mononuclear metal complex to reduce CO_2 and produce HCO_2H.[340] Molecular catalysts that imitate such active sites have been reported, though none were active toward CO2RR.[341] CO dehydrogenases (CODHs), found in aerobic and anaerobic bacteria, catalyze the reversible transformation of CO_2 to CO using either a Mo−S−Cu active site (Mo−Cu CODH)) or a Ni center bound to a unique Fe_4S_4 cluster (Ni−Fe

https://doi.org/10.1021/acs.chemrev.2c00429
Chem. Rev. 2023, 123, 2311−2348

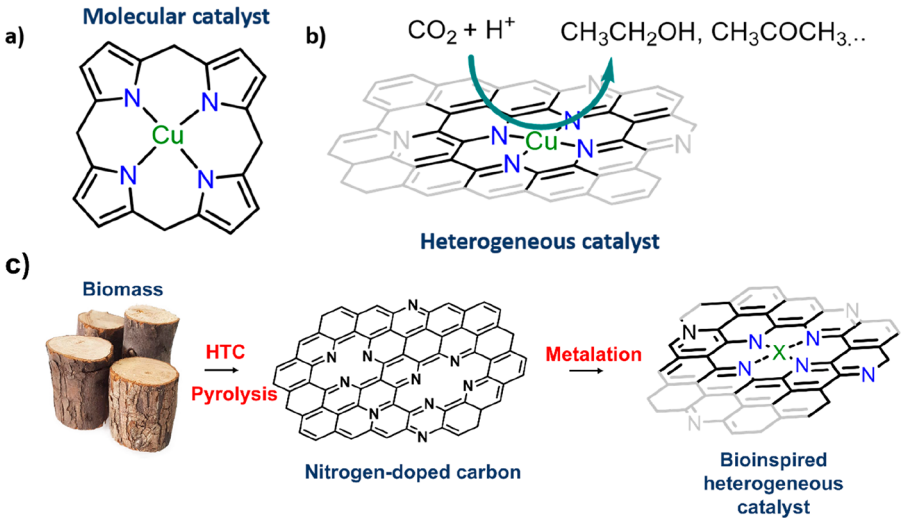

Figure 12. (a) Cu−porphyrin, (b) CO_2 reduction over CuN_4 sites embedded in a carbon matrix, and (c) schematic representation of the synthesis of bioinspired heterogeneous catalysts from biomass.

CODH) polynuclear complex.[342,343] Mougel et al. synthesized a $[(bdt)Mo^{VI}(O)S_2Cu^{I}CN]^{2-}$ (bdt = benzenedithiolate) bimetallic molecular complex, inspired by Mo−Cu−CODH, that successfully catalyzed CO_2 reduction to formate with a FE of 74% at −2.37 V vs Fc/Fc^+.[344] However, CO_2 was instead reduced to CH_4 (FE_{CH4} = 12%) on the surface of another Ni−Fe-based molecular catalyst inspired by Ni−Fe−CODH active sites.[344] This difference in the selectivity pattern of molecular complexes could be attributed to the lack of secondary features compared to their enzymatic counterparts. Such features, mostly peptide matrices,[345] are critical for stabilizing reaction intermediates, shuttling reactants between active sites, introducing hydrophobicity, and removing products from the active sites in order to enhance efficiency and selectivity (as discussed in section 5).[346] Molecular catalysts are indeed advantageous in terms of mimicking the active sites of enzymes. Owing to their well-defined active sites, mechanistic studies and structure−activity correlations can be monitored easily.[347,348] However, such catalysts possess low electronic conductivity and stability; hence, it is desirable to either support them on a conducting substrate prior to electrocatalysis or subject them to high-temperature pyrolysis to enhance the conductivity, although this leads to the aggregation of metal centers, the degradation of the well-defined active sites and undesirable side reactions such as carbothermal reduction.

Porphyrins and phthalocyanines are another group of heterocyclic organic compounds that are found in a wide range of enzymes and can activate small molecules. The implementation of their active site embedded within carbon matrixes has been widely explored in electrocatalysis such as ORR (as discussed in section 3). In CO2RR, these materials are typically selective toward the formation of CO.[349−352] Another major challenge in CO2RR is the lower selectivity for the formation of C_{2+} products, which are commercially more valuable than C_1 products. Competition between C−C, H−H, and C−H bond formation makes it difficult to produce multicarbon products during CO2RR in an aqueous environment.[353] Metallic Cu and oxides favor the formation of large-chain hydrocarbons due to the strong CO adsorption, allowing subsequent C−C coupling.[335] Nevertheless, they do not allow maximum atom utilization, and it is still a challenge to modulate C−C coupling and obtain high faradaic efficiencies for long-chain hydrocarbons.[335] Therefore, while supporting Cu nanoparticles in N-doped supports can lead to the production of C_2 products in a moderate yield ($FE_{ethanol}$ = 63% at −1.2 V vs RHE),[354,355] achieving maximum atom-utilization efficiency through the formation of $Cu−N_4$ sites within a carbon matrix has emerged as a very effective alternative to achieve C_{2+} products with high faradaic efficiencies (Figure 12a and b). Fontecave and co-workers recently showed the production of ethanol with a 55% faradaic efficiency over CuN_4 single sites in 0.1 M $CsHCO_3$, although the strong reducing potential of −1.2 V degraded them into Cu nanoparticles, which are undetectable using the ex-situ techniques.[356] Utilizing similar materials, Zhao et al. reduced CO_2 to acetone with a faradaic efficiency of 36.7% in 0.1 M $KHCO_3$ at −0.36 V, with the Cu−pyrrolic N_4 sites acting as the active centers for C−C coupling.[357] While these results are encouraging, no report has successfully replicated monoxide dehydrogenase-type Cu dual-atom catalytic sites, which would promote bridge-type adsorption and break the scaling relationship.[358] There have been a number of recent reports of the computational screenings of dual-atom catalysts for CO2RR. Wan et al. modeled a cofacial diporphyrin-based 3D electrocatalyst with a dual-metal-atom center (Co−Co) that was computationally predicted to produce hydrocarbon products from CO_2. Such a site can stabilize reaction intermediates such as $*CH_2O$, $*OCH_3$, and *OCCHOH, resulting in the production of multicarbon products; however, the stability of such catalysts would be a large challenge.[359] Zhao et al. studied the CO2RR performance of Cu dual-atom catalysts supported on C_2N materials and observed that CH_4 and C_2H_4 were the main obtained products due to the moderate binding energies for the reaction intermediates HCOO* and HCOOH*.[360] Unlike $Cu−N_4$ materials, which tend to degrade into Cu NPs at negative potentials, Fe-NC catalysts have been proven to be more robust under CO2RR conditions. Gu et al. showed the performance of an Fe^{3+}−NC material with pyrrolic coordination for the reduction of CO_2 to CO.[361] Besides the remarkable performance (>90% faradaic efficiency at −0.45 V vs RHE), these catalysts were shown to remain stable at potentials up to −0.5 V vs RHE, where Fe^{3+} started to be reduced to Fe^{2+} and the pyrrolic coordination started to degrade. Achieving such stability in an Fe-based dual-atom catalyst, which provides bridge-mode adsorption,[362] could potentially lead to the

https://doi.org/10.1021/acs.chemrev.2c00429
Chem. Rev. 2023, 123, 2311−2348

bioinspired large-scale production of C_{2+} chemicals.[363] Indeed, Chan and co-workers computationally screened a wide variety of Fe−M combinations supported in nitrogen-doped carbons using a potential-dependent microkinetic model based on CO_2* and COOH* binding energies as activity descriptors. Such dimers exhibit a two-site bidentate binding mode to the reaction intermediates that results in surface dipoles, promoting the CO_2-to-CO activity (comparable to that of Au (211)) and decreasing the selectivity for HER.[364]

Several reports of biomass-derived nitrogen-doped carbons being used as CO2RR catalysts have also been published; however this approach is still at its infancy. Huang and co-workers demonstrated the synthesis of defective N-doped carbon derived from a silk cocoon, but the absence of a metal resulted in moderate currents (<5 mA cm^{-2}) and selectivity toward CO (FE_{CO} = 89%).[365] Combining biomass-derived nitrogen-doped carbons with an appropriate method of controlled metalation can potentially lead to the formation of a new generation of sustainable, highly active materials to produce value-added chemicals (Figure 12c).[244]

5. BIOINSPIRED INTERFACES AND MASS TRANSPORT

As discussed above, the active sites of enzymes have been mimicked in molecular catalysts for the carbon dioxide reduction reaction, oxygen evolution, and ORR. However, chemical reactions carried out by enzymes are typically much more efficient and selective than their manmade counterparts. This suggests that the complex protein matrix surrounding the active sites in enzymes has a significant impact on the activity, specificity, and even durability of the enzyme.[366] One of the most essential roles of this outer coordination sphere is the spatial and temporal control of reactants and products delivered to the active site.[366] For example, CcO offers a defined path for the transport of oxygen, water, protons, and electrons. At the same time, the environment around the active site is finely tuned to control the reactivity and specificity of the active site itself.[259] On the other side, the reaction in electrochemical cells happens at the triple-point interface between the liquid electrolyte, the gaseous reactant or product, and the solid catalyst, with no defined pathways for the reactants and products. This causes significant mass-transport limitations, particularly for the case of nonprecious metal and bioderived catalysts, which require higher loadings compared to their precious-metal counterparts.

To improve transport and accessibility to catalyst sites, researchers have once again taken inspiration from nature, creating bioinspired 3D supports with hierarchical pore size distributions by designing dedicated proton channels similar to those present in enzymes. Finally, they have optimized water and bubble management, taking inspiration from natural hydrophobic and hydrophilic surfaces.

5.1. Catalyst Nanostructures

Catalyst structure development has long benefited from bioinspiration in terms of surface area and site density, for instance, by directly employing biomass in catalysts synthesis with the aim to retain the structural features in the resulting materials. Nevertheless, catalysts derived directly from biomass could suffer from inconsistencies across samples, limited supply, and competition with food resources. Therefore, attempts have also been made to mimic the natural structure with other scalable and accessible materials. In terms of OER electrocatalysts, there have been various bioderived carbon allotropes featuring three-dimensional and hierarchical structures reported to facilitate charge and mass transport; for example, a 3D cotton-derived N-doped carbon microtube[113] possesses interconnected hollow graphitized fibers, and plant-derived porous carbon inherits a tubular array structure with a wide range of macro- to mesoporosities,[367] building multilevel transporting channels. Carbon networks delivering effective conductivity and physical sturdiness can excellently accommodate metallic compounds or nanoparticles for synergetic catalytic effects.[121,368−373] In such cases, although metallic compounds are the main OER catalysts, the carbon support plays a critical role in dispersing and stabilizing metal-based nanoparticles within its skeleton, affording accessible active sites, ensuring rapid charge transfer at the interface, and facilitating gas diffusion throughout the bulk. For example, Guan et al. observed the superior catalytic activity of Co_3O_4 nanoparticles anchored on cattle-bone-derived nitrogen-doped carbon. The activity was attributed to the uniform distribution of Co_3O_4 on the carbon matrix, the large specific surface area (1070 m^2 g^{-1}), and the well-defined porous network of the carbon framework.[61]

When looking at improving mass transport in ORR, Liu et al., inspired by the shape of a grape cluster, integrated 1-D nanofibers with isolated carbon spheres to obtain a 3D framework with enhanced electron and mass transfer by combining the electrospinning strategy with the in situ growth of polydopamine.[374] Similarly, unique structures such s honeycomb or pomegranate have inspired many works on the development of semblable catalyst structures. In particular, the honeycomb structure features mechanical stability from the hexagonal channels along with highly ordered pores. Wang et al. prepared N,P-codoped honeycomb-shaped carbon nanoarchitectures via the hydrothermal treatment of melamine, phytic acid ,and glucose, followed by freeze-drying and pyrolysis carbonization. The porous structure featured highly aligned and interconnected open macrochannels, which provided multiple diffusion paths for the electrolyte and facilitated mass transportation within the catalyst material.[211] Meanwhile, inspired by the stomata structure, Han et al. fabricated 2D Cu−N−C nanodisks with an interconnected hierarchical porous topology from Cu-containing MOFs. The stomata-like hierarchical porous structure possessed more exposed Cu single-atom sites exhibiting ORR performance comparable to that of commercial Pt/C catalysts, which was much higher than the Cu−N−C structures without this structural feature.[375]

Indeed, many works have reported enhanced ORR performance as a result of the hierarchical structure, and some of them have focused on understanding the different roles of micro-, meso-, and macropores in ORR.[376,377] Nevertheless one of the main remaining challenges is to control the pore distribution of biomass-derived materials by the predictive design of a hierarchical structure. Back in 1926, Murray reported the secret of the vascular network in terms of minimizing transport costs (Murray's Law), which can serve as a powerful biomimetics design tool.[378] This principle is based on the hierarchical porous structures of different organisms, where the pore dimensions decreased steadily across multiscale to achieve a maximized transport ability. This is done in different ways in nature depending on whether the organisms require liquid transportation or gas diffusion. For instance, in leaf veins where one parent branch splits into n child branches (Figure 13a and b), the law states that

$$r^3 = r_1^3 + r_2^3 + r_3^3 + ... + r_n^3$$

https://doi.org/10.1021/acs.chemrev.2c00429
Chem. Rev. 2023, 123, 2311−2348

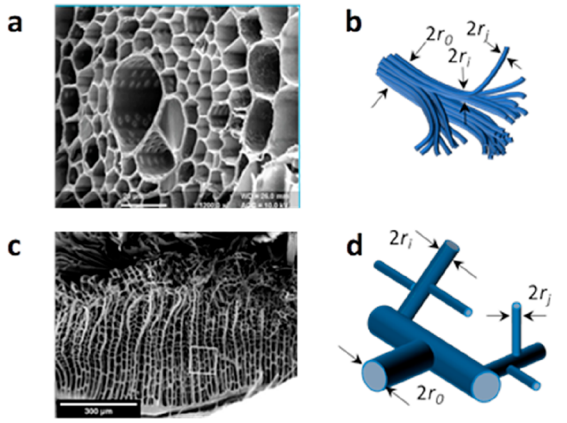

Figure 13. Hierarchically porous structures of living Murray networks in a leaf.[380] (b) Schematic illustration of the branch network in a leaf. (c) Hierarchically porous structures of living Murray networks an insect.[381] (d) Schematic illustration of the branch network in an insert. Panel (a) reproduced from ref 380. Copyright 2017 Wiley publishing group. Panel (b) and (d) adapted from ref 382. Copyright 2017 Springer Nature. Panel (c) reproduced from ref 381. Copyright 2001 The Company of Biologists Limited.

where r is the radius of the parent branch and r_1, r_2, ..., r_n are the radii of child branches. The constant pore volumes at different scales guarantees optimized flow. In contrast, insects rely on surface gas exchange for breathing. here, the sums of the surface area remain the same rather than the volume to maximize the delivery of gas components (Figure 14c and d),[379] and the law states that[379]

$$r^2 = r_1^2 + r_2^2 + r_3^2 + ... + r_n^2$$

$$r^2 = \sum_n r_n^2$$

However, Murray's law was completely overlooked in chemistry and materials science until 2017 when Su et al. revisited it and both provided a generalized equation to correlate the micro-, meso-, and macropores and successfully developed a series of "Murray materials" based on it.[382] A microporous ZnO nanocrystal was used as the primary building block to construct a hierarchically porous network layer-by-layer through evaporation-driven self-assembly. The resulting Murray materials revealed excellent interconnected channels ranging from micro- to meso- to macr-scale and demonstrated significantly improved mass transfer in a three-phase electrochemical reaction. Nevertheless, the tedious synthesis process hindered its industrial application to general material preparation and resulted in very limited following up work.[383,384] Following this work, several attempts have been made to prepare Murray-type assemblies via less demanding synthesis processes, for example, through a simple pyrolysis method leading to a Murray-type assembly of Co−NC nanoparticles with a multi-scale intraparticle porous network.[385] These materials demonstrated activity for ORR comparable to that of commercial Pt/C in alkaline conditions, but further insights are required to confirm whether the exhibited hierarchical structure truly follows Murray's Law.

In summary, the advancement of the development of fuel cell catalysts has long benefited from nature on aspects ranging from active sites imitating CcO and heme to electrocatalyst structures replicating hierarchical natural networks. Researchers have

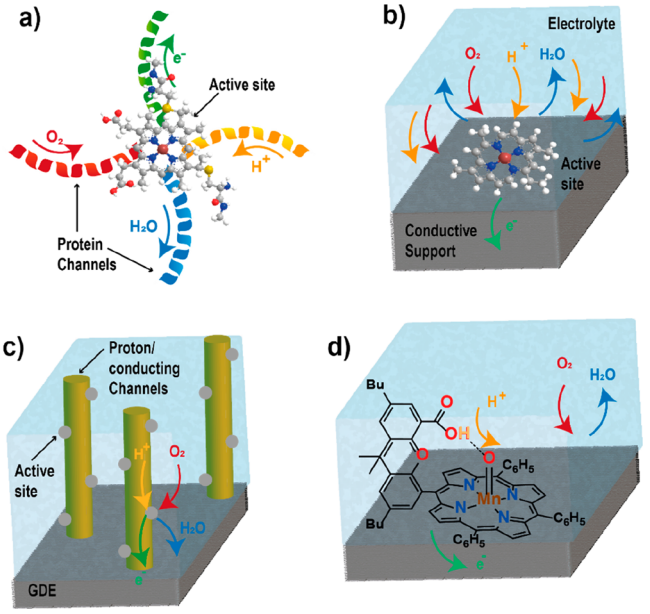

Figure 14. (a) Schematic of the enzyme CcO showing the FeN_4 active site surrounded by the outer coordination sphere, which features defined channels for the transport of oxygen, water, protons, and electrons. (b) Schematic of molecular catalysts showing the active site deposited on a conductive support. In this configuration, the reaction happens at the triple-point interface between the aqueous electrolyte, the solid catalyst, and the gaseous reactant, with water, oxygen, and protons transported through the electrolyte together. (c) Schematic of the enzyme-inspired architecture proposed by Xia et al.,[76] where protons and electrons are transported to the active site via ordered proton-conducting and electron-transporting channels on which the active site (Pt nanoparticles) has been deposited. (d) Schematic of a "Hangman" porphyrin featuring an acid−base group above the porphyrin macrocycle, which imitates the structure and functionality of the amino residues in the distal cavities of heme hydroperoxidase and offers a defined pathway for proton transport.

learned a lot from nature in terms of structure engineering to increase accessible, high-site-density catalysts. This can be done via (1) directly employing existing three-dimensional biomass to prepare the catalysts, (2) imitating the specific structure or properties of a given biosystem, or (3) developing a hierarchical structure inspired by nature. However, significant challenges remain in two main aspects: (1) theoretically understanding the ideal pore features for ORR to clarify the requirements for catalyst structures with predictive design and rational synthesis and (2) developing more sustainable and effective catalyst preparation methods to avoid the complex and costly template-involved process. Overcoming these two challenges will help maximize the utilized site density for high-performance bioinspired ORR catalysts. Nature offers much ahead of our current technology, especially in terms of the capability of systematically fulfilling all objectives at different scales. Therefore, one can expect that fuel cell catalysts of the future will feature many aspects taken from nature.

5.2. Proton Conduction

Fuel cells and electrolyzers necessitate either proton or hydroxide conduction, depending on the pH. Since acidic conditions are the most common and well-developed for both technologies, this section will focus solely on bioinspired proton conduction, which is also a common requirement for CO_2 and N_2 reduction cells. Lack of access to protons can reduce catalyst

https://doi.org/10.1021/acs.chemrev.2c00429
Chem. Rev. 2023, 123, 2311−2348

utilization for all the above-mentioned reactions, and limited proton conduction in the catalyst layer can become rate-determining, limiting the overall performance of the catalyst. Proton transport is usually achieved by physically mixing the electrocatalysts with the polymer electrolyte Nafion, which also acts as a binder for the catalyst layer. Despite its outstanding proton conductivity and excellent chemical stability, Nafion suffers from high costs and limited performance at high temperatures. Additionally, the random proton carrier distribution obtained by drop-casting the catalyst ink with physically mixed Nafion rarely matches that of the catalytic sites, leading to an inefficient proton -transfer network. The high molecular weight of Nafion also precludes it from accessing the smallest pores, exacerbating the initial problem and further reducing catalyst utilization. Furthermore, in fuel cells, the transport of protons competes with that of water and oxygen, which all diffuse in the liquid electrolyte (Figure 14b). This is a very different scenario from what happens in enzymes, which rely on specific pathways for the spatial and temporal control of reactant and product delivery. In the case of cytochrome-c, this consists of separate channels for the transport of oxygen, water, protons, and electrons (Figure 14a). Nonpolar oxygen is delivered to the active site through a hydrophobic channel, while produced water is transported away to the Mg site within milliseconds of the reaction with oxygen.[259] Electrons are transported long-range via buried metal centers bound to the polymer matrix, while protons move in dedicated proton channels wherein the proton is free and moves by hopping from an oxygen ion to another, breaking and reforming covalent and hydrogen bonds via the so-called by means of the Grotthuss mechanism. Mimicking these structures, researchers have proposed engineered catalyst layer designs with dedicated pathways for the transport of protons.

Taking a bioinspired approach, Pillai and co-workers mixed Nafion with plant hormones as low-molecular-weight proton conductors. They reported that indole-3-acetic acid significantly increased the electrocatalytic surface area of the Pt catalyst used (from 30% to 60%) and improved the fuel cell performance by 150 mW cm^{-2}.[386] Even though it was demonstrated for Pt-catalyzed ORR, this approach could be beneficial for all the electrocatalytic reactions that rely on access to protons. In an attempt to mimic the outer coordination spheres of enzymes, Xia et al. synthesized a hierarchically ordered structure with rationally designed channels for proton transport (Figure 14c).[76] This architecture was obtained by electrochemically polymerizing pyrrole decorated with Nafion ionomers directly on a gas diffusion layer, thus obtaining ordered proton-conducting channels. Consequently, platinum Pt nanoparticles were decorated on the so-obtained arrays. Using this enzyme-mimicking, the authors obtained a specific power density of 5.23 W mg^{-1}_{Pt}, 3.7× that obtained with a commercial catalyst coating.[76]

An additional approach to mimic proton transport in enzymes consists of the use of Hangman prophyrins, which provide a distinct pathway for protons to reach the metal center and the active site of the single-atom catalyst. These molecules poise an acid−base group above the porphyrin macrocycles, capturing the structure and functionality of the amino residues in the distal cavities of heme hydroperoxidase (Figure 14d).[387] In the case of electrocatalysis, this architecture defines a pathway for the transport of proton to the metal center present on the porphyrin, and in the case of ORR it promotes selectivity toward the $4e^-$ pathway.[388,389] In addition, other distal residues, which can form hydrogen bonds to bound oxygen species at the active Fe site of the porphyrin, have been shown to affect the ORR rate by a pH-dependent "push" and "pull" effect.[390,391] At low pH, the pendant residues are protonated, stabilizing the Fe^{III}−OOH species and facilitating the cleavage of the O−O bond in a "pull" effect similar to that observed in peroxidase. In contrast, at higher pH, a "push" effect characteristic of cytochrome P450 is observed by which the trans-axial water is deprotonated to a hydroxide, increasing the pK_a of Fe^{III}−OOH.

Proton transport, and more specifically ionomer distribution and utilization, in the catalyst is still a much-overlooked problem. Despite the growing interest regarding Nafion replacement in proton-exchange membranes, very little research has been directed toward alternative ionomers for the catalyst layer. Nevertheless, the limited examples reported above show how enzyme-mimicking could pave the way for the synthesis of improved catalysts, for example, by developing defined channels for the transport of protons similar to those present in enzymes or by mimicking the "push" effect characteristic of cytochrome P450 with distal residues.

5.3. Water and Bubble Management

As discussed above, enzymes benefit from a defined pathway for water and gas transport. These structures are currently too complex to be reproduced in an electrocatalyst, but the electrode surface can be modified to tune the hydrophobicity at the triple-point interface, hence controlling gas and water access at the surface (Figure 15).

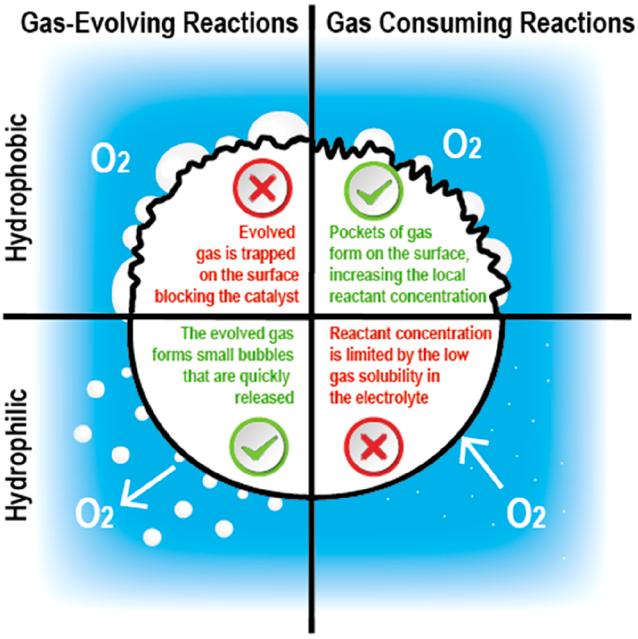

Figure 15. Schematic showing the effects of hydrophobic and hydrophilic surfaces on reactions evolving gases (such as OER and HER) and consuming gases (such as ORR, HOR, and CO_2RR).

Nature offers several examples of how chemical composition and hierarchical structures can be employed to effectively manipulate hydrophobicity and gas bubble behavior, and several comprehensive reviews have been published on the topic[74,392−395] without discussing the application of these modifications to electrocatalysis, which will be the focus of this section. For example, lotus leaves feature micropapillae and nanobranch-like hydrophobic wax crystals that lead to a superhydrophobic surface with excellent bubble-bursting

https://doi.org/10.1021/acs.chemrev.2c00429
Chem. Rev. 2023, 123, 2311−2348

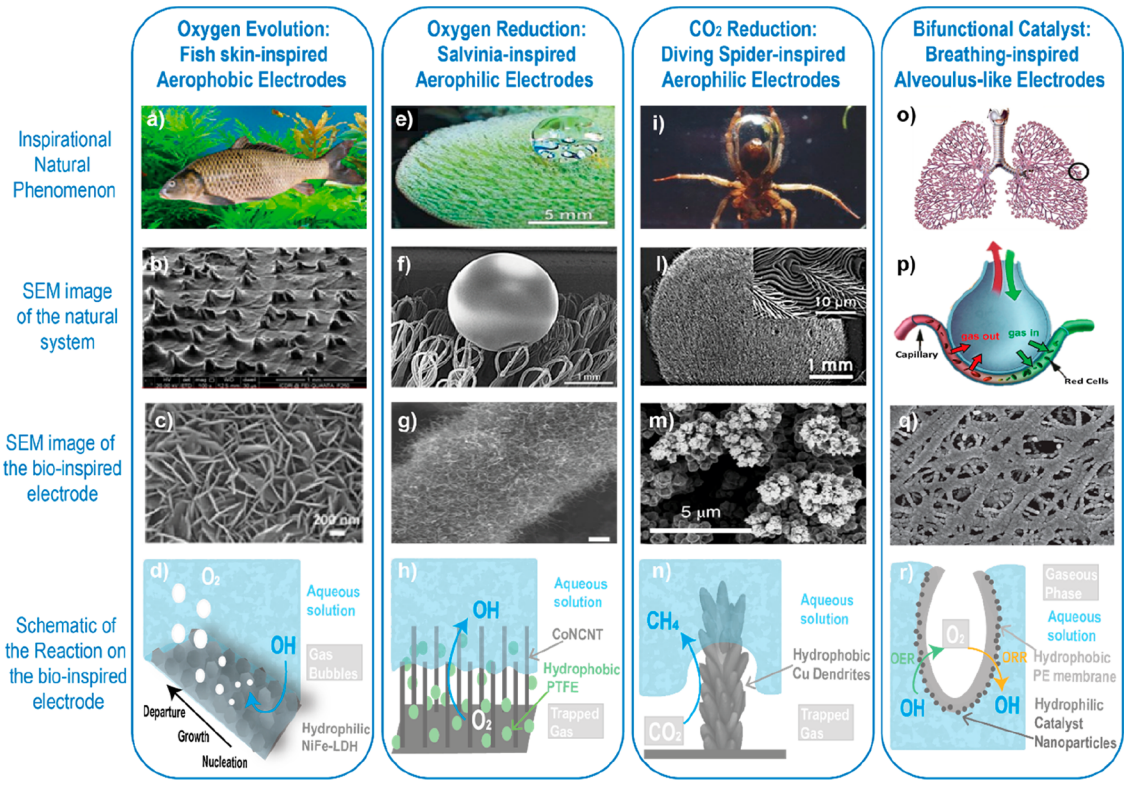

Figure 16. Aerophobicity for oxygen evolution: (a) Picture of a carp and (b) scanning electron microscopy (SEM) image of a fish scale skin showing underwater superaerophobicity. Reproduced with permission from ref 398. Copyright 2017 American Chemical Society. (c) SEM image of a fish-scale-like aerophobic NiFe-LDH electrode. Reproduced with permission from ref 399. Copyright 2016 WILEY-VCH Verlag GmbH & Co. KGaA. (d) Schematic of oxygen evolution on a fish-scale-like aerophobic electrode, which helps the release of evolved gas bubbles. Aerophilicity for ORR: (e) picture and (f) SEM image of floating water fern *Salvinia*. The egg-beater-shaped hair array on the salvinia surface consists of hydrophilic pins and hydrophobic pedestals that allow it to trap air. Reproduced with permission from ref 397. Copyright 2010 WILEY-VCH Verlag GmbH & Co. KGaA, Weinheim. (g) SEM image of Co nitrogen-doped carbon nanotubes on carbon fiber paper. Reproduced with permission from ref 400 Copyright 2016 WILEY-VCH Verlag GmbH & Co. KGaA. (h) Schematic of CoNCNT with hydrophobic PTFE nanoparticles.[397] This aerophilic electrode creates a layer of trapped oxygen, increasing the catalytic activity. Aerophilicity for CO_2 reduction: (i) Picture of a water spider and (l) SEM image of its skin. The feather-like hair on its abdomen allows the water spider to efficiently trap air bubbles underwater. (i) reproduced with permission from ref 402. Copyright 2013 Neumann and Woermann; licensee Springer. (l) reproduced with permission from ref 401. Copyright 2011 The Company of Biologists. (m) SEM image of the water spider-inspired hydrophobic Cu dendrite. Reproduced with permission from ref 73. Copyright 2019 Springer Nature. (n) Schematic of CO_2 reduction on the hydrophobic Cu dendrite. The formation of a layer of trapped gas increases the local CO_2 concentration, improving the selectivity toward CO_2 reduction rather than hydrogen evolution. Bifunctional OER and ORR catalysts: (o and p) Schematics of the breathing process in alveoli. Reproduced with permission from ref 75. Copyright 2018 Elsevier Inc. (q) SEM image of a PE membrane modified with a Ag/Pt catalyst. Reproduced with permission form ref 75 Copyright 2018 Elsevier Inc. (r) Schematic of the alveolus-like structure of the catalyst-modified PE membrane, presenting a hydrophilic side in contact with the electrolyte and a hydrophobic side in contact with the gas.

performance.[396] On the contrary, *Salvinia* offers long-term air retention thanks to its hydrophilic pins and hydrophobic pedestals.[397] Electrochemical reactions have a wide range of requirements in terms of aerophilicity, which is mainly dependent on whether the gas is evolved or reacted. The required properties have been achieved by bioinspired electrodes with tuned chemical compositions and microstructures.

For all the gas evolution reactions, such as HER and OER, hydrophilic surfaces are preferred (Figure 16). Gas products can adhere on hydrophobic catalysts, forming a continuous film and blocking the electrolyte's access to the active site. In contrast, hydrophilic surfaces reduce the size of gas bubbles and their time of residence on the catalyst, leading to stable electrochemical behavior and higher catalyst utilization.[403]

Kim et al. synthesized nickel phosphorus films with identical chemical compositions and tuned their contact angles with different complexing agents. The so-synthesized electrodes were used as HER catalysts, demonstrating that increasingly hydrophilic surfaces provide superior performance; specifically, the contact angle reduction from 77° to 40° caused a 134 mV reduction in overpotential at 100 $mAcm^{-2}$ current density.[398] Similar beneficial effects of hydrophilic electrodes have been reported for hydrogen[399,404−406] and oxygen evolution.[399,406−408]

A further increase in hydrophilicity can be obtained via bioinspiration. Fish skin displays superaerophobic properties that reduce gas bubbles on their bodies, thus improving their balance and resistance to swimming. The skin of most fish is composed of fan-like scales, coated in hydrophilic mucus, and covered in ordered micropapillae (Figure 16 a and b). A similar structure was obtained by Xu et al., who used a one-step hydrothermal process to synthesize NiFe-layered double hydroxide nanoplates offering a gas contact angle of 150° (Figure 16c).[399] The as-synthesized superhydrophilic material offered exceptional oxygen evolution performance and fast gas product release with an average bubble size of 39 μm, compared

https://doi.org/10.1021/acs.chemrev.2c00429
Chem. Rev. 2023, 123, 2311−2348

to the impeded release of 220 μm gas bubbles observed for IrO_2/C (Figure 16d).[399]

Meanwhile, ORR relies on access to the gaseous reactant and rather benefits from hydrophobic surfaces (Figure 16e).[400,409−411] This was demonstrated by Sun and co-workers, who obtained a superhydrophobic surface by modifying a carbon paper with poly(tetrafluoroethylene) nanoparticles to yield a stable oxygen gas layer underneath the cobalt-incorporated NCNT catalyst, which displayed superior performance in both acidic and alkaline media (Figure 16 g and h).[400] This architecture resembles that of floating water fern *Salvinia molesta* which, thanks to its eggbeater-shaped structure, can hold air underwater for several weeks (Figure 16e and f).[397] Another approach recently introduced to control the presence of water and gas at the electrochemical interface is the use of ionic liquid layers. Oxygenophilic and hydrophobic ionic liquids, such as those used as coatings on the surface of electrocatalysts, can modify the triple-point interface, improving oxygen concentration and water expulsion. A recent review by our group has summarized the unexplored potential of ionic liquid layers.[412]

Hydrophobicity also has a positive, and perhaps an even more drastic, effect on CO_2 reduction due to (1) the low solubility of CO_2 (33 mM) in aqueous electrolytes causing a mass-diffusion limitation for CO_2 to the electrode surface[413] and (2) the competition with the more thermodynamically favorable HER. In nature, hydrophobicity is utilized to solve these issues; for example, active sites in enzymes such as CODHs/acetyl-CoA synthase are protected by the presence of a hydrophobic protein framework.[413] Hydrophobic secondary features close to the active sites create CO_2 gas pockets, thus suppressing the competing hydrogen evolution and enhancing the conversion rate of CO_2 to glucose. Thus, a bioinspired cathode can be designed with a catalyst on one side and a hydrophobic polymer on its opposite side, imitating the role of a metalloenzyme.[414]

Mougel and co-workers have taken inspiration from another natural example, namely, diving spiders, which make use of the plastron effect to breath underwater. The plastrons are composed of hydrophobic feather-like hairs, which present both nanoscale and microscale surface structures able to trap air underwater (Figure 16I and j). They achieved a similar multiscale surface by modifying a hierarchically structured Cu dendrite, with a monolayer of waxy alkanethiol (Figure 16m and n). As a result, the hydrophobic electrode can trap a thin film of CO_2, increasing its local concentration at the electrochemical surface and ultimately improving the selectivity toward CO_2 reduction.[73] After the hydrophobic modification, the faradaic efficiency toward undesired HER decreased from 71% to 10%.[65] Xing et al. used a very similar strategy consisting of mixing polytetrafluoroethylene with the active material to create a triple-phase boundary of solid−liquid−gas around the active site, suppressing hydrogen evolution.[415]

The dichotomy in hydrophilicity requirements for gas evolution and gas reaction introduces a new challenge in the development of bifunctional OER and ORR catalysts, for integrated fuel cells and electrolyzers. Once again, a possible solution can be found in nature by imitating the breathing process. Alveoli in lungs are covered on the inner side by a layer of lecithin-type hydrophobic molecules to reduce surface tension at the gas interface, while the outer side is hydrophilic to maintain contact with the bloodstream (Figure 16o and p). This asymmetric hydrophobic/hydrophilic membrane ensures efficient gas transport in both directions.[416] Inspired by this mechanism, Li et al. produced an alveolar structure with a hydrophilic and a hydrophobic side by rolling and sealing a catalyst-coated polyethylene membrane (Figure 16 q and r). This alveolus structure was found to improve both ORR and OER performance compared to that of the same flat electrode.[75]

In conclusion, nature has successfully inspired the development of electrodes with rational and optimized transport of reactants and products, improving the catalytic activity of various electrochemical reactions. However, bioinspiration has guided not only the engineering of active sites and electrodes but also the design of other critical components of electrochemical cells, such as membranes and flow-field plates, which will be discussed below.

6. BIOINSPIRED DEVICES

Bioinspiration does not stop at the catalyst layer but can be advantageous for several parts of an electrochemical device. In this section, we will focus on two fundamental aspects of most electrochemical devices, the flow field and the membrane. The type of membrane depends on the electrochemical device and on the pH at which it operates, but this review will solely focus on proton-exchange membranes, which are the most developed and common to PEM fuel cells, PEM electrolyzers, and CO_2 reduction electrochemical cells. Section 6.1 will present an overview of both bioinspired and bioderived proton-exchange membranes. Section 6.2 will focus on the flow field, which is common to all electrochemical devices involving gaseous reactants and is responsible for the uniform distribution of gas on the catalyst surface. For its design, researchers have taken inspiration from complex 3D structures that require a similar homogeneous distribution of materials, such as that of sap in leaves or blood in human bodies. Finally, we will discuss flexible electrochemical devices as an example of how bioinspiration can also play a role in the design of electrochemical devices at a macroscale.

6.1. Proton-Exchange Membranes

Another critical component of electrochemical devices is the membrane. Depending on the pH, the membrane has the role of transporting hydroxide ions (AEM) or protons (PEM). Recently, research efforts have been focusing on AEMs thanks to the activity of noble-metal-free catalysts for ORR in alkaline conditions. Nevertheless, the ion conductivity and durability of these membranes are still much lower compared to those of PEMs, limiting their widespread adoption. In this section, we will be focusing on proton-exchange membranes, which are common to PEM fuel cells, CO_2 reduction, and N_2 reduction cells.

Perfluorosulfonic acid (PFSA) membranes are the most used in low-temperature PEMFC, and the most commercially available options are Nafion (Dupont) and Gore-Select (W. L. Gore & Associates). Nafion owes its popularity to its exceptionally high ionic conductivity ($6.2 10^{-2}$ S cm^{-1} at 100% relative humidity) and durability.[417] However, PFSA membranes with this membrane have several drawbacks, including high costs, negative environmental impact, toxicity, and low performance at high temperatures or low humidity.[418] These limitations have driven increased interest in the development of suitable alternatives and, once again, nature has guided this research, both as an inspiration and as a starting material (Figure 17).

One of the most studied natural materials for proton-exchange membranes is chitin, a natural polymer abundantly present in shrimp shells, which are often discarded as waste.

https://doi.org/10.1021/acs.chemrev.2c00429
Chem. Rev. 2023, 123, 2311−2348

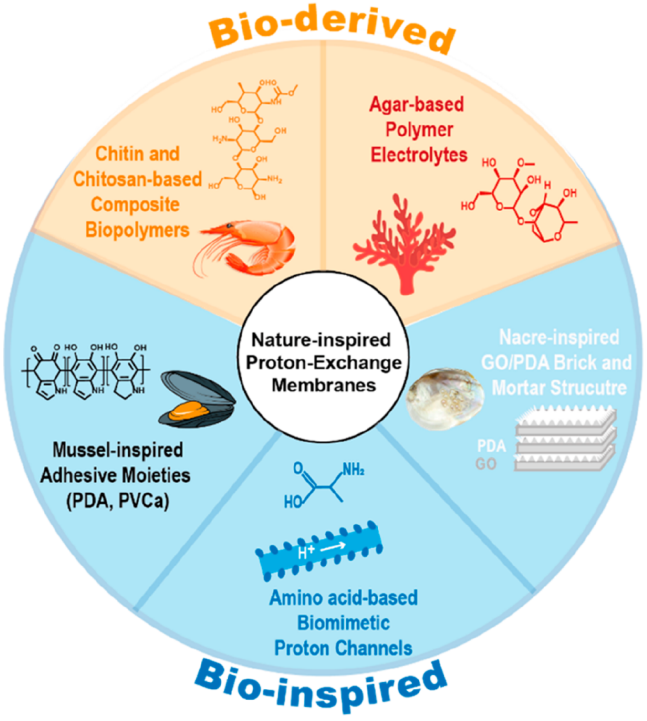

Figure 17. Selection of bioinspired and bioderived materials for PEMs.

Furthermore, chitin is biodegradable, nontoxic, and low-cost.[419] Yamada and co-workers have used two derivatives of this polymer, chitin phosphate and chitosan, to produce acid−base composite biopolymers as anhydrous proton-conducting membranes. Despite showing lower conductivity compared to Nafion, the so-obtained membranes retained a reasonable conductivity of up to 10^{-2} S cm^{-1} even in absence of water and at temperatures up to 180 °C.[420] Lupatini et al. reported a conductivity of 1.9×10^{-2} S cm^{-1} at 100% relative humidity and 80 °C by cross-linking chitosan with sulfuric acid.[421] Several other chitosan composites have been reported as polymer electrolytes, such as chitosan and polysulfone,[422] sulfonated polysulfone,[422] phosphotungstic acid,[423,424] phosphomolybdic acid,[425] zeolites,[426] sulfonated graphene oxide,[427] and silicotungstic acid.[428,429] Finally, Alves and co-workers linked the individual properties of chitosan, such as deacetylation and molar mass, to the proton conductivity of the resulting membrane. They concluded that lower deacetylation and higher molar mass were favorable, with different thicknesses resulting in an order of magnitude increase in proton conductivity.[430]

Another common bioprecursor for the development of membranes is agar-agar, a biodegradable, cheap, and nontoxic polysaccharide derived from red seaweed. Agar-based polymer electrolytes have been developed for applications in several electrochemical devices,[431,432] including supercapacitors,[433] dye-sensitized solar cells,[434] and fuel cells.[435−437] However, the reported ionic conductivity is around an order of magnitude lower than that of Nafion. Bioinspiration has also led the way to the development of new membranes. The most reported nature-mimicking membranes utilize mussel-inspired adhesive moieties, such as polydopamine and poly(vinyl) catechol. Nagao and co-workers reported the synthesis of nanocomposite films of poly(vinyl) catechol and polystyrene block copolymers, obtaining well-aligned lamellae structures.[438]

Mussel-inspired polydopamine has also been investigated as a universal interfacial cross-linking agent, as it contains bearing abundant $-NH_2$ and $-NH-$ groups that can lead to high proton conductivity. This concept has been applied to the synthesis of PEMs with graphene oxide,[439] SiO_2,[440] and CeO_2.[441] By modifying the metal−organic framework DHZIF-8 with polydopamine, Rao et al. very recently reported a proton conductivity under anhydrous conditions (120 °C) of 3.66 mS cm^{-1}, which is 2.2× higher than that of Nafion.[442] Taking further inspiration from nature, Cai et al. synthesized a layered proton-exchange membrane based on polydopamine, graphene oxide, and sulfonated poly(vinyl alcohol).[443] This assembly mimics the brick-and-mortar structure of nacre, with graphene oxide as the brick and the polymers as the mortar. The optimized structure is endowed with a high tensile strength (216.5 MPa, 2.7× higher than that of natural nacre) and excellent proton conductivity (0.303 S.cm^{-1} at 80 °C) and offers higher fuel cell power output and a lower weight compared to Nafion.[443]

Finally, protein-based biomimetic channels were used as inspiration for highly efficient proton transfer.[444] Most recently, Li and co-workers obtained bioproton channels by incorporating metal−organic frameworks with attached amino acids into a sulfonated polysulfonic matrix. Among the amino acids tested, the glutamate-functionalized MOF demonstrated the highest proton conductivity of 0.212 S cm^{-1} at 80 °C.[445] Amino acids have also been tested in proton-exchange membranes in conjunction with cellulose whiskers,[446] chitosan nanofibers,[447] and cellulose nanofibers.[448] Finally, protein-based biomimetic channels were used as inspiration for highly efficient proton transfer.[444]

PFSA membranes, in the form of Nafion first and Gore-Select more recently, have been the gold-standard since the 1960s. However, their high cost, toxicity, and limited performance at low humidity have driven research into alternative PEMs. Nafion modification has been extensively used to improve the proton conductivity and stability of the PFSA membrane; however, price and toxicity remain the main drawbacks of this approach. In that sense, bioderived membranes are ideal candidates, as they utilize biodegradable, cheap, and often waste products as starting materials. However, membranes obtained from the popularly studied chitosan and agar display modest proton conductivity. On the other had, bioinspiration has been extremely useful for overcoming some of Nafion's limitations, such as proton conduction in anhydrous conditions, and offers high tensile strength. Even though significant challenges remain and more research is needed in this area, there are very bright prospects for the commercialization of cost-effective nontoxic proton-exchange membranes, and we are convinced that bioinspiration will play a key role in the development of such materials.

6.2. Flow Fields

As discussed in section 3, H_2 and O_2 need to be distributed sufficiently and uniformly onto the catalysts surface, thus calling for careful design of the flow field. Bioinspiration can greatly benefit the design of the flow field in electrochemical devices by mimicking apparent characteristic of certain biological structures (leaves, blood vessels, etc.).[449,450] In 2009, Guessous et al. presented two flow channel designs by imitating the structures of both a leaf and a lung for the first time,[451] and these findings led to more reports by different groups.[452,453] However, the lack of a theoretical foundation in these systems led to certain concerns about the scalability or the inhibition of fuel cell performance. Nevertheless several mathematical models have emerged that support such these theories, such as Murray's Law, fractal

https://doi.org/10.1021/acs.chemrev.2c00429
Chem. Rev. 2023, 123, 2311−2348

theory, and bionic similarity theory.[451,454−456] Before the designed flow fields were manufactured, computational fluid dynamics modeling was usually performed to simulate the performance of the bioinspired bipolar plate. Some common characteristics of the performance can be the distribution of reactants, the current density, water management, pressure drop, and energy dissipation, among others. Currently, the unique structure of leaves still serves as the most common inspiration source for the flow field design because of its superior ability to uniformly distribute nutrients on a 2D surface. For instance, in 2018, Ouellette et al. reported the effect on direct methanol fuel cells of bioinspired interdigitated and noninterdigitated flow fields compared to a standard serpentine flow field, following their earlier work on Murray's Law-inspired flow field design.[457,458] A 3D steady-state, isothermal, and single-phase model was developed to help understand the experimental results obtained under different anode and cathode flow rate combinations. The conventional serpentine design and the interdigitated bioinspired design exhibited the best performance for the anode and the cathode, respectively, due to the enhanced under-rib convection of both flow fields. Ouellette et al. also noted the importance of having an interdigitated design to prevent the reactants from traveling directly from the inlet to the outlet.[419] Other than the common symmetrical design, asymmetric leaf-shaped flow channels have also been studied. Liu et al. investigated the difference of these two using both a numerical simulation and an experimental study, concluding that an asymmetric bionic flow channel works better when placed perpendicularly with a relatively flat pressure variation.[459]

Another powerful inspiration from nature for flow field design is mammal lungs.[451,455,458] Recently, Coppens et al.[451,455,458] developed a model based on the fractal geometry of a lung, with the primary role of distributing reactants homogeneously.[82] To have diffusion-driven flow equal to the convection-driven flow for even reactant distribution, the optimal generations of branching were found to be four. A 3D-printed large-scale prototype (25 cm^2) of the design revealed outstanding performance compared to the conventional flow field design, with a 30% improvement of the max power density at 75% RH and the lowest voltage decay (5 mV h^{-1}). Following this initial report, neutron radiography was employed to visualize the liquid water distribution of the bioinspired design for the first time.[460] The results addressed the flooding problem in the interdigitated outlet channels, which leads to performance decay at high humidity conditions and calls for water removal strategies.[460] More examples have been well documented in reviews focusing specifically on bioinspired flow field design and development.[449,450,461,462]

In summary, despite the manufacturing challenges and the cost, device flow field designs inspired by nature show huge potential to become the new standard. These designs benefit from more efficient water management, enhanced reactant distribution, and reduced pressure drop, resulting in better cell performance comparing to the conventional design.

6.3. Flexible Electrochemical Devices

The evolving trend toward wearable electronics has increased the demand for flexible energy devices that can offer a reliable power supply upon bending, stretching, and twisting. To date, research has focused on supercapacitors and Li-ion batteries, which will not be covered in this review; readers may refer to relevant review articles.[463−467] Most recently, flexible fuel cells have received increased attention thanks to their high energy density and fast recharging times compared to Li-ion batteries. Several types of flexible fuel cells have been reported, including biofuel, proton-exchange membrane, and photocatalytic fuel cells.[468]

Once again, bioderived precursors have proven advantageous for the manufacture of such materials. For wearable devices, the flexibility of all components, such as the electrode, the separator, and the current collector, is essential. The electrodes are especially important to the flexibility of the device and complex to produce. Fiber-based materials are among the most promising catalyst supports thanks to their high flexibility and deformability. Paper has been widely investigated as an electrode support,[469,470] particularly for microfluidic fuel cells, as the natural capillary structure of paper can drive the flow, removing the need for an external pump.[471−474] For example, Chan and co-workers fabricated a flexible, membrane-less hydrogen peroxide microfuel cell on paper. Exploiting paper's unique features such as flexibility, porosity, and capillarity, they obtained a power density of 0.81 mW cm^{-2} at 0.26 V even after the distortion of the cell. Additionally, cellulosic paper is abundant, low-cost, and biocompatible, making it an ideal candidate for flexible and sustainable fuel cells.[472] Similarly, Wang et al. reported 75−87% performance retention upon bending a paper-based hydrogen fuel cell from 45° to 135°, reaching a peak power density of 4 mW cm^{-2}.[470] Paper-based fuel cells have also been reported using formate as a fuel, achieving a maximum power density of 2.5 mW mg_{Pd}^{-1}.[474] Besides paper, Zhang et al. reported the use of cotton in the production of a flexible nanocomposite membrane for application in microbial fuel cells. Once again, the use of a natural fiber, such as cotton, offers low costs and low toxicity but also allows high proton conductivity and a higher current density, compared to Nafion, in microbial fuel cells, demonstrating a peak power of 400 mWm^{-2}.[475]

Silk fibroin, the main protein constituent of silk fibers of *Bombyx mori* silkworms, is another example of bioderived materials for flexible fuel cells. In a recent report, Tseng et al. successfully utilized silk fibroin−carbon nanotube composites in the production of biocatalytic fuel cells.[476] In this assembly, silk fibroins act as binders by mechanically trapping enzymes and improving the electrical connection between the enzymes' active sites and the carbon nanotubes, enabling the formation of flexible electrodes with enhanced durability. Even though they have not yet been applied to fuel cells, transparent and flexible microstructured surfaces have also been synthesized from chitin. As mentioned before in this review, chitin is a natural, abundant, and biodegradable amino-polysaccharide that can be extracted from the exoskeletons of shrimps and crabs, which are often discarded as waste.

Despite recent interest and improvement, at present, flexible fuel cells suffer from low durability, particularly upon bending and twisting, which can decrease the adhesion of the catalyst to the electrode and change its mechanical structure. We believe that nature can help the design of bendable fuel cells the same way it helped the design of flexible energy storage and conversion devices. For example, flexible Li-ion batteries have been synthesized by mimicking the structure of an animal spine, with alternating thick stacks of the electrode and an unwound part corresponding to vertebrae and soft marrow, respectively.[477] Taking inspiration from snake skin, where rigid keratin scales are interconnected with flexible hinges, shape-forming batteries consisting of hexagonal, rigid unit cells with flexible electrical interconnections have also been reported .[478] Flexible

https://doi.org/10.1021/acs.chemrev.2c00429
Chem. Rev. 2023, 123, 2311−2348

phototermo-supercapacitors have also benefited from looking at natural structures, for example, that of nacre, where mechanical robustness is achieved by a mortar-and-brick structure.[479]

Other examples include leaf-skeleton-inspired supercapacitors and HER photocatalysts,[480,481] vertebral- and nacre-inspired brick-and-mortar design for solar cells,[482,483] and biomimetic interlocking structures for interfacially strengthened flexible supercapacitors.[484] Flexible pressure sensors with improved sensitivity have also been reported using a range of biotemplates, such as aureum leaves,[485] rose petals,[486] banana,[487] mimosa,[488] and lotus leaves.[489] These examples demonstrate how nature can offer valuable insights and pave the way for the development of flexible energy devices.

7. CONCLUSIONS AND OUTLOOK

In this review, we summarized how nature can inspire solutions to energy conversion technologies by providing natural feedstock and inspiration. Biomass can be employed for the preparation of advanced carbonaceous materials, and enzymes serve as models of highly efficient electrochemical systems in scenarios ranging from water splitting or oxygen reduction to CO_2 conversion. Despite the recent advancement in the field in terms of bioinspired catalyst preparation or the implementation of bioinspired devices, there is still a long way to go before nature can make a tangible impact in modern energy conversion devices. Based on the current state-of-the-art, and with the aim of advancing toward nature-inspired and derived devices, we believe that upcoming research should tackle the following challenges:

1. Rigorous electrochemical testing protocols. When testing any electrocatalyst, one should make sure standardized tests take place and that the reported data are compared to a rigorously benchmarked common reference catalyst (Pt/C in ORR, IrOx in OER, etc.) with sufficient provided experimental details. We would like to refer the reader to previously published reviews that address best practices and the growing concern for the proper assessment of electrocatalytic measurements.[490−493]

2. Reliable synthetic protocols for the preparation of bioinspired catalysts from biomass. Biomass-derived carbon materials display, in general, high overpotentials for water splitting half-reactions, CO_2 reduction, and $4e^-$ ORR owing to their metal-free character. Additionally, biomass-derived catalysts can be obtained in many different complex nanostructures, making it difficult to screen for standardized structure−activity relationships, as recently highlighted.[494] Through the rational selection of heteroatom-containing biomass precursors and reaction conditions, such as using active site templates,[21,243,244] a biomass-derived carbon-based material could be engineered in terms of chemical composition and porosity, leading to a suitable substrate for the coordination of atomic metallic species to form electrochemically active sites such as single-atom $M-N_x$, which resembles heme. Meanwhile, the next generation of nature-inspired heterogeneous electrocatalysts should incorporate 3D dual-metal-atom active sites resembling enzymes, such as CcO for ORR, which can achieve high TOFs with lower reaction overpotentials than Pt and PGM alloys. Directly employing enzymes in practical devices is not feasible due to their orders of magnitude lower site densities and limited stability in harsh but practical device environments. Emulating their 3D active-site structure would require a well-controlled synthetic pathway, which is likely not possible with biomass. Instead, new classes of materials are required that can withstand practical device conditions with sufficient porosity and conductivity while maintaining a 3D structure; this can possibly be achieved using ordered carbonaceous frameworks[288,289] or carbon materials derived from tailored metal organic frameworks.[286,495]

3. Assessment of the bioinspired active site structure and degradation. The structure of bioinspired active sites that contain single- or dual-metal atoms is highly challenging and often leads to controversy in the field. For advanced characterization techniques suitable for differentiating between these kind of active sites, we would like to refer the reader to our previously published review.[184] Recent advances include work by Mitchell et al., who reported a deep-learning method for the automated detection of single atoms in a TEM that overcomes the poor statistical significance and reproducibility inherent of manual operation.[496] Meanwhile, the stability and degradation of atomic active sites remain relatively unexplored to date; therefore, emphasis should be placed on developing in situ techniques. The importance of applying known techniques in novel ways was recently highlighted by Elbaz and co-workers, who for the first-time applied Fourier-transform alternatin- current voltammetry to probe the active site density and degradation of a Fe-NC ORR catalyst in situ in a PEMFC.[497] Additionally, thorough post-mortem characterization (for example, XPS, identical location microscopy, XAS, etc.) of the catalyst should be provided to confirm active-site stability.

4. Self-healing. In OER, the catalytic self-repairing PSII is firmly established via cluster reassembly of the core active sites. While this complex structural process has not been successfully mimicked to date, continually regenerating metal oxide OER systems have been established, where activities of the species are restored through dynamic equilibrium dissolution−redeposition cycles under specific operational conditions.[498] By increasing the understanding of this process, an ideal self-healing catalyst could be achieved via instantaneous redeposition coupled with structural stabilization. Meanwhile, for ORR, nature's ability to regenerate has some similarities to the ability of single-atom M−NC catalysts to become reactivated following thermal pyrolysis or electrochemical reduction.[316,317] Further understanding the mechanism of this process could help extend of the life of these catalysts and move from current lifetimes (∼100 h) toward practical device lifetimes (>5000 h).

5. Improvement of electron, mass, and proton transport in electrochemical devices. In contrast to enzymes, where every molecule involved in the reaction has a separate and well-defined pathway, in most electrochemical devices the products and reactants diffuse through the same electrolyte in opposite directions. This lack of order for mass, electron, and proton transport limits the overall performance of these devices and should be tackled starting from nature. One way to approach this problem is to tailor the hydrophobicity of the catalytic surface. This has been successfully achieved for both gas-evolving and gas-consuming reactions, inspired by, among others, the hydrophilic scales of fishes[399] and the hydrophobic skin of

https://doi.org/10.1021/acs.chemrev.2c00429
Chem. Rev. 2023, 123, 2311−2348

diving spiders.[73] Proton transport can also be rationally improved by mimicking the outer coordination spheres of enzymes.[76] We believe that the imitation of proteins channels in enzymes still holds a great potential for the rational control of product and reactant transport to the active site.

6. Development of low-cost, nontoxic, and high-performing proton-exchange membranes. The benchmark perfluorosulfonic acid proton-exchange membranes offer great proton conductivity but are expensive, toxic, and low-performing at low humidity. Regarding the first two limitations, bioderived membranes are excellent replacements, as they can offer cheap and biodegradable starting materials. On the other hand, bioinspiration can improve proton conductivity in a wider range of temperatures and humidity, as shown by the recent development of nature-inspired anhydrous proton-conducting membranes.[420]
7. Evaluation of the sustainability and scalability of bioderived catalysts. Despite the vast amount of literature on developing bioderived and bioinspired catalysts, currently very few systematic evaluation methods have been developed to assess the impact of transforming biomass into catalysts across all life stages. In addition, although biomass is a renewable resource, the impact of excessive sourcing presents a point of important consideration in regard to ecosystem damage. This will in turn affect the scale-up of systems for catalyst manufacturing. Therefore, sustainable, and socioeconomic frameworks need to be established to benefit the development of relevant technoeconomic analysis and life cycle assessment models. Based on such frameworks, robust analysis needs to be performed and benchmarked to the utilization of conventional raw materials, considering biomass sourcing, extraction, pretreatment, and synthesis steps.
8. Rational design and applicability of the hierarchical catalyst structure. Despite the vast research carried out on developing catalyst architectures via either directly employing the hierarchical biomaterials or fabricating structures inspired by the nature, remarkable challenges remain. First, there is a lack of rationale behind the designs of the structures. The ideal porosity or architecture required by the reaction systems is still undetermined and unable to guide the construction of catalysts. Computational modeling should be combined with careful material synthesis to clarify the requirements. Moreover, current catalyst development often results in difficult application in real devices due to various reason,s including tedious synthesis processes, fragile products, and impracticable scale-up procedures. All these factors need to be tackled thoroughly to fully utilize bioinspired hierarchical catalysts.

AUTHOR INFORMATION

Corresponding Author

Maria-Magdalena Titirici − *Department of Chemical Engineering, Imperial College London, London SW7 2AZ England, U.K.; Advanced Institute for Materials Research (WPI-AIMR), Tohoku University, Sendai, Miyagi 980-8577, Japan;* orcid.org/0000-0003-0773-2100; Email: m.titirici@imperial.ac.uk

Authors

Jesús Barrio − *Department of Materials, Royal School of Mines and Department of Chemical Engineering, Imperial College London, London SW7 2AZ England, U.K.;* orcid.org/0000-0002-4147-2667

Angus Pedersen − *Department of Materials, Royal School of Mines and Department of Chemical Engineering, Imperial College London, London SW7 2AZ England, U.K.*

Silvia Favero − *Department of Chemical Engineering, Imperial College London, London SW7 2AZ England, U.K.*

Hui Luo − *Department of Chemical Engineering, Imperial College London, London SW7 2AZ England, U.K.*

Mengnan Wang − *Department of Materials, Royal School of Mines and Department of Chemical Engineering, Imperial College London, London SW7 2AZ England, U.K.*

Saurav Ch. Sarma − *Department of Chemical Engineering, Imperial College London, London SW7 2AZ England, U.K.*

Jingyu Feng − *Department of Chemical Engineering, Imperial College London, London SW7 2AZ England, U.K.; School of Engineering and Materials Science, Queen Mary University of London, London E1 4NS England, U.K.*

Linh Tran Thi Ngoc − *Department of Chemical Engineering, Imperial College London, London SW7 2AZ England, U.K.; School of Engineering and Materials Science, Queen Mary University of London, London E1 4NS England, U.K.*

Simon Kellner − *Department of Chemical Engineering, Imperial College London, London SW7 2AZ England, U.K.*

Alain You Li − *Department of Chemical Engineering, Imperial College London, London SW7 2AZ England, U.K.*

Ana Belén Jorge Sobrido − *School of Engineering and Materials Science, Queen Mary University of London, London E1 4NS England, U.K.;* orcid.org/0000-0002-8798-4991

Complete contact information is available at: https://pubs.acs.org/10.1021/acs.chemrev.2c00429

Author Contributions

The manuscript was written through contributions of all authors. All authors have given approval to the final version of the manuscript. CRediT: **Jesús Barrio** conceptualization, data curation, supervision, writing-original draft, writing-review & editing; **Angus Pedersen** conceptualization, data curation, formal analysis, visualization, writing-original draft; **Silvia Favero** conceptualization, writing-original draft; **Hui Luo** conceptualization, data curation, formal analysis, validation, visualization, writing-original draft; **Mengnan Wang** conceptualization, writing-original draft; **Saurav Ch Sarma** conceptualization, writing-original draft; **Linh Tran Thi Ngoc** conceptualization, writing-original draft; **Simon Kellner** writing-original draft; **Alain You Li** conceptualization, supervision, visualization, writing-original draft; **Ana Belén Jorge Sobrido** resources, supervision, writing-original draft, writing-review & editing; **Maria-Magdalena Titirici** conceptualization, funding acquisition, supervision, validation, writing-original draft, writing-review & editing.

Notes

The authors declare no competing financial interest.

Biographies

Jesús Barrio graduated with a degree in Chemistry and received his M.Sc. in Nanoscience and Molecular Nanotechnology at Universidad Autónoma de Madrid. He then obtained his Ph.D. from Ben Gurion University of the Negev, where he studied the design of metal-free

https://doi.org/10.1021/acs.chemrev.2c00429
Chem. Rev. 2023, 123, 2311−2348

carbon nitride materials for photoelectrocatalytic applications in Prof. Menny Shalom's group. Since June 2020 he has been a Research Associate in the Materials Department at Imperial College London working on the synthesis of hybrid metal−carbon composites for different electrochemical applications alongside Dr. Ifan Stephens and Prof. Magda Titirici.

Angus Pedersen received his M.Eng. in Chemical Engineering with industrial placement from the University of Bath in 2019. He is currently pursuing a Ph.D. under the supervision of Prof. Maria-Magdalena Titirici and Dr. Ifan E. L. Stephens at Imperial College London and Prof. Dan J. L. Brett and Dr. Rhodri Jervis at University College London. Angus' research focuses on synthesizing and characterizing single- and dual-metal-atom electrocatalysts for oxygen reduction in low-temperature hydrogen fuel cells.

Silvia Favero received her M.Eng. in chemical engineering from Imperial College London in 2019. She is currently pursuing Ph.D. under the supervision of Maria-Magdalena Titirici and Ifan E. L. Stephens at Imperial College London. Her research focuses on engineering the triple-point interface of oxygen reduction electrocatalysts, with ionic liquids and poly(ionic liquid)s.

Hui Luo received her Ph.D. in Materials Science from Queen Mary University of London in 2019, where she worked on photo(electro)-catalytic water splitting. She is currently a research associate at the Department of Chemical Engineering in Imperial College London, where she works with Prof. Maria-Magdalena Titirici. Her research focuses on biomass electrolysis, which investigates the possibility of transforming abundant biomass platform molecules into H_2 and high-value biobased compounds with low energy consumption and minimal carbon footprints.

Mengnan Wang received her B.Eng. in Chemical Engineering (2014) and her M.Sc in Chemistry (2015) from the National University of Singapore. She then worked on technology transfer and consultancy connecting academia and industry in both Singapore (2015−2018) and the United Kingdom (2018−2019). She is currently pursuing a Ph.D. under the supervision of Prof. Maria-Magdalena Titirici and Dr. Ifan E. L. Stephens at Imperial College London and Dr. Rhodri Jervis at University College London. Mengnan's research focuses on developing high-performance low-Pt-loaded proton-exchange membrane fuel cells, focusing on the micro- or nanostructure engineering of the cathode catalyst layer.

Saurav Chandra Sarma received his Ph.D. in Chemical Science from Jawaharlal Nehru Centre for Advanced Scientific Research, Bengaluru, India, in 2020. He then received Marie Skłodowska-Curie Research Fellowship to pursue his postdoc at the Department of Chemical Engineering, Imperial College London (2020−2022). His research interests include designing materials for electrocatalytic water-splitting, oxygen electrocatalysis, and electrochemical CO_2 reduction.

Jingyu Feng received his Ph.D. in Chemical Engineering from Imperial College London in 2022, where he worked on nanocarbon-based critical materials free electrocatalysts for the oxygen reduction reaction. He is currently a research assistant at the School of Engineering and Materials Science at Queen Mary University of London. Jingyu's research focuses on alkali graphite intercalation compounds, free-standing carbon electrodes for lithium-ion battery anode and electrocatalysis applications.

Linh Tran received her Master's of Science from Pohang University of Science and Technology (POSTECH, Korea) under the supervision of Prof. Jae Sung Lee in 2014. Her Master's work focused on the development of heteroatom-doped copper tungsten oxide for photocatalytic water splitting. Soon afterward, she joined the semiconductor industry and took a role in the failure analysis of electronic devices. In 2018, she started her Ph.D. under the supervision of Dr. Ana Sobrido (Queen Mary University of London) and Prof. Magdalena Titirici (Imperial College London) researching the syntheses of transition-metal compounds and lignin-derived carbon fiber hybrids for oxygen electrocatalysis, novel testing configurations, and mechanistic studies.

Simon Kellner graduated with a Master of Science degree in Molecular Nano Science from Friedrich-Alexander-University Erlangen-Nuremberg in 2019. As a Ph.D. student, he moved to the department of Chemical Engineering at Imperial College, London, where he is developing and testing flexible freestanding mesoporous carbon film electrodes based on abundant carbon resources for applications in electrocatalysis.

Alain Li received his MSc. in organic chemistry from l'Ecole Nationale Supérieure de Chimie of Montpellier, France, in 2013. He then obtained his Ph.D. in 2019 from McGill university in Montréal, Canada, where he worked under the cosupervision of Prof. Audrey Moores and Prof. Chao-Jun Li on sustainable catalysis applied to carbonyl reduction.

Ana Jorge Sobrido graduated with a degree in Chemistry in Canary Islands in 2004. She obtained her Ph.D. in Materials Science from the Instituto de Ciencia de Materiales and the Universidad Autonoma de Barcelona in 2009. After some time in industry, she returned to academia in 2011, taking up a postdoctoral position at University College London to investigate new graphitic carbon nitrides for energy applications. In 2016, she was offered an Academic Fellow position at QMUL that led to a Lecturer position in 2019. Since 2021, Ana has been a reader in Sustainable Energy Materials and a UKRI Future Leaders Fellow at Queen Mary University of London. Her research focuses on designing the next generation of energy materials using sustainable resources and processes for application in redox flow batteries, oxygen electrocatalysts, and supercapacitors.

Maria Magdalena Titirici received her Ph.D. from the University of Dortmund. She then completed a postdoc and later became a group leader at the Max-Planck Institute of Colloids and Interface. She held positions at Queen Mary University of London between 2013 and 2019, first as a reader and then full professor. She is currently a chair in Sustainable Energy Materials at Imperial College London and RAEng Chair in Emerging Technologies. Her research is in the field of sustainable materials for energy storage and conversion.

ACKNOWLEDGMENTS

The authors acknowledge the financial support from the Engineering and Physical Sciences Research Council (EPSRC) (EP/M0138/1, EP/M013812/1 and EP/S023259/1), and the National Research Council of Canada through the Materials for Clean Fuels Challenge Program. A. P. thanks the EPSRC Centre for Doctoral Training in the Advanced Characterisation of Materials (grant number EP/L015277/1). A. Y. L. acknowledges Marie Skłodowska-Curie Fellowship H2020-MSCA-IF-2019 (892614) through the project HAEMOGLOBIN. S. F. thanks EPSRC for the award of the DPT scholarship (EP/R513052/1). S. K. acknowledges the Department of Chemical Engineering for providing a departmental scholarship. H. L. acknowledges the donation from Mr Mark Richardson to the Department of Chemical Engineering at Imperial College London. S. C. S. acknowledges Marie Skłodowska Curie—Individual Fellowship H2020-MSCA-IF-2019 scheme (Grant Agreement No. 896637).

https://doi.org/10.1021/acs.chemrev.2c00429
Chem. Rev. 2023, 123, 2311−2348

LIST OF ABBREVIATIONS

ORR	oxygen reduction reaction
HER	hydrogen evolution reaction
GHG	greenhouse gases
PEM	proton-exchange membrane
OER	oxygen evolution reaction
PCET	proton-coupled electron transfer
OEC	oxygen-evolving complex
TOF	turnover frequency
MWCNT	multiwalled carbon nanotubes
GDE	gas diffusion electrode
MEA	membrane−electrode assembly
DFT	density functional theory
EXAFS	extended X-ray absorption fine-edge structure
XANES	X-ray absorption near-edge structure
SD	site density
PGM	platinum-group metal
CO2RR	CO_2 reduction reaction
CODH	CO dehydrogenase
SEM	scanning electron microscopy
AEM	anion exchange membrane
MOF	metal−organic framework
PFSA	perfluorosulfonic acid
RH	relative humidity

REFERENCES

(1) Lindsey, R.*Climate Change: Atmospheric Carbon Dioxide*. Climate.gov. https://www.climate.gov/news-features/understanding-climate/climate-change-atmospheric-carbon-dioxide (accessed 2021).

(2) European Commission. *The Green New Deal*; European Commission: Brussels, Belgium: 2019.

(3) Stott, R.; Arulkumaran, S.; Gilmore, I.; Godlee, F.; Page, L. Legislate for Carbon Net Zero by 2030. *Lancet* **2019**, *393*, 981.

(4) Mallapaty, S. How China Could Be Carbon Neutral by Mid-Century. *Nature* **2020**, *586*, 482−484.

(5) IEA. *Net Zero by 2050: A Roadmap for the Global Energy Sector*; International Energy Agency: Paris, France, 2021.

(6) Bogdanov, D.; Farfan, J.; Sadovskaia, K.; Aghahosseini, A.; Child, M.; Gulagi, A.; Oyewo, A. S.; de Souza Noel Simas Barbosa, L.; Breyer, C. Radical Transformation Pathway towards Sustainable Electricity via Evolutionary Steps. *Nat. Commun.* **2019**, *10*, 1077.

(7) Luderer, G.; Madeddu, S.; Merfort, L.; Ueckerdt, F.; Pehl, M.; Pietzcker, R.; Rottoli, M.; Schreyer, F.; Bauer, N.; Baumstark, L.; et al. Impact of Declining Renewable Energy Costs on Electrification in Low-Emission Scenarios. *Nat. Energy* **2022**, *7*, 32−42.

(8) Campos-Martin, J. M.; Blanco-Brieva, G.; Fierro, J. L. G. Hydrogen Peroxide Synthesis: An Outlook beyond the Anthraquinone Process. *Angew. Chemie Int. Ed.* **2006**, *45*, 6962−6984.

(9) Capdevila-Cortada, M. Electrifying the Haber-Bosch. *Nat. Catal.* **2019**, *2*, 1055.

(10) Van Hook, J. P. Methane-Steam Reforming. *Catal. Rev. Eng.* **1980**, *21*, 1−51.

(11) MacFarlane, D. R.; Cherepanov, P. V.; Choi, J.; Suryanto, B. H. R.; Hodgetts, R. Y.; Bakker, J. M.; Ferrero Vallana, F. M.; Simonov, A. N. A Roadmap to the Ammonia Economy. *Joule* **2020**, *4*, 1186−1205.

(12) Ursua, A.; Gandia, L. M.; Sanchis, P. Hydrogen Production from Water Electrolysis: Current Status and Future Trends. *Proc. IEEE* **2012**, *100*, 410−426.

(13) Roger, I.; Shipman, M. A.; Symes, M. D. Earth-Abundant Catalysts for Electrochemical and Photoelectrochemical Water Splitting. *Nat. Rev. Chem.* **2017**, *1*, 0003.

(14) Du, L.; Prabhakaran, V.; Xie, X.; Park, S.; Wang, Y.; Shao, Y. Low-PGM and PGM-Free Catalysts for Proton Exchange Membrane Fuel Cells: Stability Challenges and Material Solutions. *Adv. Mater.* **2021**, *33*, 1908232.

(15) Zhang, S.; Fan, Q.; Xia, R.; Meyer, T. J. CO2 Reduction: From Homogeneous to Heterogeneous Electrocatalysis. *Acc. Chem. Res.* **2020**, *53*, 255−264.

(16) Voiry, D.; Shin, H. S.; Loh, K. P.; Chhowalla, M. Low-Dimensional Catalysts for Hydrogen Evolution and CO_2 Reduction. *Nat. Rev. Chem.* **2018**, *2*, 0105.

(17) Verdaguer-Casadevall, A.; Deiana, D.; Karamad, M.; Siahrostami, S.; Malacrida, P.; Hansen, T. W.; Rossmeisl, J.; Chorkendorff, I.; Stephens, I. E. L. Trends in the Electrochemical Synthesis of H 2 O 2 : Enhancing Activity and Selectivity by Electrocatalytic Site Engineering. *Nano Lett.* **2014**, *14*, 1603−1608.

(18) Iriawan, H.; Andersen, S. Z.; Zhang, X.; Comer, B. M.; Barrio, J.; Chen, P.; Medford, A. J.; Stephens, I. E. L.; Chorkendorff, I.; Shao-Horn, Y. Methods for Nitrogen Activation by Reduction and Oxidation. *Nat. Rev. Methods Prim.* **2021**, *1*, 56.

(19) Andersen, S. Z.; Čolić, V.; Yang, S.; Schwalbe, J. A.; Nielander, A. C.; McEnaney, J. M.; Enemark-Rasmussen, K.; Baker, J. G.; Singh, A. R.; Rohr, B. A.; et al. A Rigorous Electrochemical Ammonia Synthesis Protocol with Quantitative Isotope Measurements. *Nature* **2019**, *570*, 504−508.

(20) Li, K.; Andersen, S. Z.; Statt, M. J.; Saccoccio, M.; Bukas, V. J.; Krempl, K.; Sazinas, R.; Pedersen, J. B.; Shadravan, V.; Zhou, Y.; et al. Enhancement of Lithium-Mediated Ammonia Synthesis by Addition of Oxygen. *Science* **2021**, *374*, 1593−1597.

(21) Jiao, L.; Li, J.; Richard, L. L.; Sun, Q.; Stracensky, T.; Liu, E.; Sougrati, M. T.; Zhao, Z.; Yang, F.; Zhong, S.; et al. Chemical Vapour Deposition of Fe-N-C Oxygen Reduction Catalysts with Full Utilization of Dense Fe-N4 Sites. *Nat. Mater.* **2021**, *20*, 1385−1391.

(22) García de Arquer, F. P.; Dinh, C.-T.; Ozden, A.; Wicks, J.; McCallum, C.; Kirmani, A. R.; Nam, D.-H.; Gabardo, C.; Seifitokaldani, A.; Wang, X.; et al. CO_2 Electrolysis to Multicarbon Products at Activities Greater than 1 A cm^{-2}. *Science* **2020**, *367*, 661−666.

(23) Stephens, I. E. L.; Bondarenko, A. S.; Grønbjerg, U.; Rossmeisl, J.; Chorkendorff, I. Understanding the Electrocatalysis of Oxygen Reduction on Platinum and Its Alloys. *Energy Environ. Sci.* **2012**, *5*, 6744−6762.

(24) Hansen, J. N.; Prats, H.; Toudahl, K. K.; Mørch Secher, N.; Chan, K.; Kibsgaard, J.; Chorkendorff, I. Is There Anything Better than Pt for HER? *ACS Energy Lett.* **2021**, *6*, 1175−1180.

(25) Malinovic, M.; Ledendecker, M. Whittling Iridium down to Size. *Nat. Energy* **2022**, *7*, 7−8.

(26) Lim, J.; Park, D.; Jeon, S. S.; Roh, C.-W.; Choi, J.; Yoon, D.; Park, M.; Jung, H.; Lee, H. Ultrathin IrO2 Nanoneedles for Electrochemical Water Oxidation. *Adv. Funct. Mater.* **2018**, *28*, 1704796.

(27) Keersemaker, M. *Critical Raw Materials.* **2020**, 69−82.

(28) Minke, C.; Suermann, M.; Bensmann, B.; Hanke-Rauschenbach, R. Is Iridium Demand a Potential Bottleneck in the Realization of Large-Scale PEM Water Electrolysis? *Int. J. Hydrogen Energy* **2021**, *46*, 23581−23590.

(29) Hubert, M. A.; King, L. A.; Jaramillo, T. F. Evaluating the Case for Reduced Precious Metal Catalysts in Proton Exchange Membrane Electrolyzers. *ACS Energy Lett.* **2022**, *7*, 17−23.

(30) Azadi, M.; Northey, S. A.; Ali, S. H.; Edraki, M. Transparency on Greenhouse Gas Emissions from Mining to Enable Climate Change Mitigation. *Nat. Geosci.* **2020**, *13*, 100−104.

(31) White, R. J.; Antonietti, M.; Titirici, M.-M. Naturally Inspired Nitrogen Doped Porous Carbon. *J. Mater. Chem.* **2009**, *19*, 8645.

(32) Li, Y.; Liu, W.; Zhang, Z.; Du, X.; Yu, L.; Deng, Y. A Self-Powered Electrolytic Process for Glucose to Hydrogen Conversion. *Commun. Chem.* **2019**, *2*, 67.

(33) Field, C. B.; Behrenfeld, M. J.; Randerson, J. T.; Falkowski, P. Primary Production of the Biosphere: Integrating Terrestrial and Oceanic Components. *Science* **1998**, *281*, 237−240.

(34) Zhang, Y.; Chen, X.; Wu, Y.; Shuai, C.; Shen, L. The Environmental Kuznets Curve of CO2 Emissions in the Manufacturing and Construction Industries: A Global Empirical Analysis. *Environ. Impact Assess. Rev.* **2019**, *79*, 106303.

https://doi.org/10.1021/acs.chemrev.2c00429
Chem. Rev. 2023, 123, 2311−2348

(35) Liu, H.; Xu, Z.; Guo, Z.; Feng, J.; Li, H.; Qiu, T.; Titirici, M. A Life Cycle Assessment of Hard Carbon Anodes for Sodium-Ion Batteries. *Philos. Trans. R. Soc. A* **2021**, *379*, 20200340.
(36) Nicolae, S. A.; Au, H.; Modugno, P.; Luo, H.; Szego, A. E.; Qiao, M.; Li, L.; Yin, W.; Heeres, H. J.; Berge, N.; et al. Recent Advances in Hydrothermal Carbonisation: From Tailored Carbon Materials and Biochemicals to Applications and Bioenergy. *Green Chem.* **2020**, *22*, 4747−4800.
(37) Yuan, H.; Liu, T.; Liu, Y.; Nai, J.; Wang, Y.; Zhang, W.; Tao, X. A Review of Biomass Materials for Advanced Lithium-Sulfur Batteries. *Chem. Sci.* **2019**, *10*, 7484−7495.
(38) Yadav, M.; Goel, G.; Hatton, F. L.; Bhagat, M.; Mehta, S. K.; Mishra, R. K.; Bhojak, N. A Review on Biomass-Derived Materials and Their Applications as Corrosion Inhibitors, Catalysts, Food and Drug Delivery Agents. *Curr. Res. Green Sustain. Chem.* **2021**, *4*, 100153.
(39) Thompson, M.; Xia, Q.; Hu, Z.; Zhao, X. S. A Review on Biomass-Derived Hard Carbon Materials for Sodium-Ion Batteries. *Mater. Adv.* **2021**, *2*, 5881−5905.
(40) Ning, P.; Yang, G.; Hu, L.; Sun, J.; Shi, L.; Zhou, Y.; Wang, Z.; Yang, J. Recent Advances in the Valorization of Plant Biomass. *Biotechnol. Biofuels* **2021**, *14*, 102.
(41) Kubo, S.; White, R. J.; Yoshizawa, N.; Antonietti, M.; Titirici, M.-M. Ordered Carbohydrate-Derived Porous Carbons. *Chem. Mater.* **2011**, *23*, 4882−4885.
(42) Wu, Z.-Y.; Liang, H.-W.; Chen, L.-F.; Hu, B.-C.; Yu, S.-H. Bacterial Cellulose: A Robust Platform for Design of Three Dimensional Carbon-Based Functional Nanomaterials. *Acc. Chem. Res.* **2016**, *49*, 96−105.
(43) Meng, W.; Bai, X.; Wang, B.; Liu, Z.; Lu, S.; Yang, B. Biomass-Derived Carbon Dots and Their Applications. *ENERGY Environ. Mater.* **2019**, *2*, 172−192.
(44) Wareing, T. C.; Gentile, P.; Phan, A. N. Biomass-Based Carbon Dots: Current Development and Future Perspectives. *ACS Nano* **2021**, *15*, 15471−15501.
(45) Borghei, M.; Lehtonen, J.; Liu, L.; Rojas, O. J. Advanced Biomass-Derived Electrocatalysts for the Oxygen Reduction Reaction. *Adv. Mater.* **2018**, *30*, 1703691.
(46) Hu, B.; Yu, S.-H.; Wang, K.; Liu, L.; Xu, X.-W. Functional Carbonaceous Materials from Hydrothermal Carbonization of Biomass: An Effective Chemical Process. *Dalt. Trans.* **2008**, No. 40, 5414−5423.
(47) Falco, C.; Perez Caballero, F.; Babonneau, F.; Gervais, C.; Laurent, G.; Titirici, M.-M.; Baccile, N. Hydrothermal Carbon from Biomass: Structural Differences between Hydrothermal and Pyrolyzed Carbons via 13C Solid State NMR. *Langmuir* **2011**, *27*, 14460−14471.
(48) Chambon, C. L.; Fitriyanti, V.; Verdía, P.; Yang, S. M.; Hérou, S.; Titirici, M.-M.; Brandt-Talbot, A.; Fennell, P. S.; Hallett, J. P. Fractionation by Sequential Antisolvent Precipitation of Grass, Softwood, and Hardwood Lignins Isolated Using Low-Cost Ionic Liquids and Water. *ACS Sustain. Chem. Eng.* **2020**, *8*, 3751−3761.
(49) Schlee, P.; Hosseinaei, O.; O'Keefe, C. A.; Mostazo-López, M. J.; Cazorla-Amorós, D.; Herou, S.; Tomani, P.; Grey, C. P.; Titirici, M.-M. Hardwood *versus* Softwood Kraft Lignin - Precursor-Product Relationships in the Manufacture of Porous Carbon Nanofibers for Supercapacitors. *J. Mater. Chem. A* **2020**, *8*, 23543−23554.
(50) Tomani, P. The Lignoboost Process. *Cellul. Chem. Technol.* **2010**, *44*, 53−58.
(51) Ortíz, I.; Quintero, R.Chapter 4 - Recent Advancements in Pretreatment Technologies of Biomass to Produce Bioenergy. In *Bioenergy Research: Advances and Applications*; Gupta, V. K., Tuohy, M. G., Kubicek, C. P., Saddler, J., Xu, F., Eds.; Elsevier: Amsterdam, The NEtherlands, 2014; pp 57−69.
(52) Brandt, A.; Gräsvik, J.; Hallett, J. P.; Welton, T. Deconstruction of Lignocellulosic Biomass with Ionic Liquids. *Green Chem.* **2013**, *15*, 550−583.
(53) George, A.; Brandt, A.; Tran, K.; Zahari, S. M. S. N. S.; Klein-Marcuschamer, D.; Sun, N.; Sathitsuksanoh, N.; Shi, J.; Stavila, V.; Parthasarathi, R.; et al. Design of Low-Cost Ionic Liquids for Lignocellulosic Biomass Pretreatment. *Green Chem.* **2015**, *17*, 1728−1734.
(54) Chen, M.; Malaret, F.; Firth, A. E. J.; Verdía, P.; Abouelela, A. R.; Chen, Y.; Hallett, J. P. Design of a Combined Ionosolv-Organosolv Biomass Fractionation Process for Biofuel Production and High Value-Added Lignin Valorisation. *Green Chem.* **2020**, *22*, 5161−5178.
(55) Chen, Q.-X.; Liu, Y.-H.; He, Z.; Wang, J.-L.; Liu, J.-W.; Jiang, H.-J.; Huang, W.-R.; Gao, G.-Y.; Hou, Z.-H.; Yu, S.-H. Microchemical Engineering in a 3D Ordered Channel Enhances Electrocatalysis. *J. Am. Chem. Soc.* **2021**, *143*, 12600−12608.
(56) Tang, Z.; Pei, Z.; Wang, Z.; Li, H.; Zeng, J.; Ruan, Z.; Huang, Y.; Zhu, M.; Xue, Q.; Yu, J.; Zhi, C. Highly Anisotropic, Multichannel Wood Carbon with Optimized Heteroatom Doping for Supercapacitor and Oxygen Reduction Reaction. *Carbon N. Y.* **2018**, *130*, 532−543.
(57) Chen, C.; Zhang, Y.; Li, Y.; Dai, J.; Song, J.; Yao, Y.; Gong, Y.; Kierzewski, I.; Xie, J.; Hu, L. All-Wood, Low Tortuosity, Aqueous, Biodegradable Supercapacitors with Ultra-High Capacitance. *Energy Environ. Sci.* **2017**, *10*, 538−545.
(58) Liu, D.; Yu, S.; Shen, Y.; Chen, H.; Shen, Z.; Zhao, S.; Fu, S.; Yu, Y.; Bao, B. Polyaniline Coated Boron Doped Biomass Derived Porous Carbon Composites for Supercapacitor Electrode Materials. *Ind. Eng. Chem. Res.* **2015**, *54*, 12570−12579.
(59) Peng, X.; Zhang, L.; Chen, Z.; Zhong, L.; Zhao, D.; Chi, X.; Zhao, X.; Li, L.; Lu, X.; Leng, K.; et al. Hierarchically Porous Carbon Plates Derived from Wood as Bifunctional ORR/OER Electrodes. *Adv. Mater.* **2019**, *31*, 1900341.
(60) Zan, Y.; Zhang, Z.; Liu, H.; Dou, M.; Wang, F. Nitrogen and Phosphorus Co-Doped Hierarchically Porous Carbons Derived from Cattle Bones as Efficient Metal-Free Electrocatalysts for the Oxygen Reduction Reaction. *J. Mater. Chem. A* **2017**, *5*, 24329−24334.
(61) Guan, J.; Zhang, Z.; Ji, J.; Dou, M.; Wang, F. Hydrothermal Synthesis of Highly Dispersed Co3O4 Nanoparticles on Biomass-Derived Nitrogen-Doped Hierarchically Porous Carbon Networks as an Efficient Bifunctional Electrocatalyst for Oxygen Reduction and Evolution Reactions. *ACS Appl. Mater. Interfaces* **2017**, *9*, 30662−30669.
(62) Liu, H.; Cao, Y.; Wang, F.; Zhang, W.; Huang, Y. Pig Bone Derived Hierarchical Porous Carbon-Supported Platinum Nanoparticles with Superior Electrocatalytic Activity Towards Oxygen Reduction Reaction. *Electroanalysis* **2014**, *26*, 1831−1839.
(63) Li, S.; Xu, R.; Wang, H.; Brett, D. J. L.; Ji, S.; Pollet, B. G.; Wang, R. Ultra-High Surface Area and Mesoporous N-Doped Carbon Derived from Sheep Bones with High Electrocatalytic Performance toward the Oxygen Reduction Reaction. *J. Solid State Electrochem.* **2017**, *21*, 2947−2954.
(64) Huang, X.; Shen, T.; Zhang, T.; Qiu, H.; Gu, X.; Ali, Z.; Hou, Y. Efficient Oxygen Reduction Catalysts of Porous Carbon Nanostructures Decorated with Transition Metal Species. *Adv. Energy Mater.* **2020**, *10*, 1900375.
(65) Nagy, L.; Burger, K.; Kürti, J.; Mostafa, M. A.; Korecz, L.; Kiricsi, I. Iron(III) Complexes of Sugar-Type Ligands. *Inorg. Chim. Acta* **1986**, *124*, 55−59.
(66) Liu, X.; Amiinu, I. S.; Liu, S.; Cheng, K.; Mu, S. Transition Metal/Nitrogen Dual-Doped Mesoporous Graphene-like Carbon Nanosheets for the Oxygen Reduction and Evolution Reactions. *Nanoscale* **2016**, *8*, 13311−13320.
(67) Proppe, A. H.; Li, Y. C.; Aspuru-Guzik, A.; Berlinguette, C. P.; Chang, C. J.; Cogdell, R.; Doyle, A. G.; Flick, J.; Gabor, N. M.; van Grondelle, R.; et al. Bioinspiration in Light Harvesting and Catalysis. *Nat. Rev. Mater.* **2020**, *5*, 828−846.
(68) Bullock, R. M.; Chen, J. G.; Gagliardi, L.; Chirik, P. J.; Farha, O. K.; Hendon, C. H.; Jones, C. W.; Keith, J. A.; Klosin, J.; Minteer, S. D.; et al. Using Nature's Blueprint to Expand Catalysis with Earth-Abundant Metals. *Science* **2020**, *369*, No. eabc3183.
(69) Lee, C. C.; Hu, Y.; Ribbe, M. W. Vanadium Nitrogenase Reduces CO. *Science* **2010**, *329*, 642−642.
(70) Jia, H. P.; Quadrelli, E. A. Mechanistic Aspects of Dinitrogen Cleavage and Hydrogenation to Produce Ammonia in Catalysis and

https://doi.org/10.1021/acs.chemrev.2c00429
Chem. Rev. 2023, 123, 2311−2348

Organometallic Chemistry: Relevance of Metal Hydride Bonds and Dihydrogen. *Chem. Soc. Rev.* **2014**, *43*, 547−564.
(71) Milton, R. D.; Abdellaoui, S.; Khadka, N.; Dean, D. R.; Leech, D.; Seefeldt, L. C.; Minteer, S. D. Nitrogenase Bioelectrocatalysis: Heterogeneous Ammonia and Hydrogen Production by MoFe Protein. *Energy Environ. Sci.* **2016**, *9*, 2550−2554.
(72) Le, J. M.; Bren, K. L. Engineered Enzymes and Bioinspired Catalysts for Energy Conversion. *ACS Energy Lett.* **2019**, *4*, 2168−2180.
(73) Wakerley, D.; Lamaison, S.; Ozanam, F.; Menguy, N.; Mercier, D.; Marcus, P.; Fontecave, M.; Mougel, V. Bio-Inspired Hydrophobicity Promotes CO2 Reduction on a Cu Surface. *Nat. Mater.* **2019**, *18*, 1222−1227.
(74) Zhang, C.; Mcadams II, D. A.; Grunlan, J. C. Nano/Micro-Manufacturing of Bioinspired Materials: A Review of Methods to Mimic Natural Structures. *Adv. Mater.* **2016**, *28*, 6292−6321.
(75) Li, J.; Zhu, Y.; Chen, W.; Lu, Z.; Xu, J.; Pei, A.; Peng, Y.; Zheng, X.; Zhang, Z.; Chu, S.; et al. Breathing-Mimicking Electrocatalysis for Oxygen Evolution and Reduction. *Joule* **2019**, *3*, 557−569.
(76) Xia, Z.; Wang, S.; Jiang, L.; Sun, H.; Liu, S.; Fu, X.; Zhang, B.; Su, D. S.; Wang, J.; Sun, G. Bio-Inspired Construction of Advanced Fuel Cell Cathode with Pt Anchored in Ordered Hybrid Polymer Matrix. *Sci. Rep.* **2015**, *5*, 16100.
(77) Fourmond, V.; Léger, C. Dinitrogen Reduction: Interfacing the Enzyme Nitrogenase with Electrodes. *Angew. Chemie Int. Ed.* **2017**, *56*, 4388−4390.
(78) Maruyama, J.; Okamura, J.; Miyazaki, K.; Abe, I. Two-Step Carbonization as a Method of Enhancing Catalytic Properties of Hemoglobin at the Fuel Cell Cathode. *J. Phys. Chem. C* **2007**, *111*, 6597−6600.
(79) Guo, C.; Liao, W.; Li, Z.; Chen, C. Exploration of the Catalytically Active Site Structures of Animal Biomass-Modified on Cheap Carbon Nanospheres for Oxygen Reduction Reaction with High Activity, Stability and Methanol-Tolerant Performance in Alkaline Medium. *Carbon* **2015**, *85*, 279−288.
(80) Fratzl, P.; Weinkamer, R. Nature's Hierarchical Materials. *Prog. Mater. Sci.* **2007**, *52*, 1263−1334.
(81) Trogadas, P.; Ramani, V.; Strasser, P.; Fuller, T. F.; Coppens, M.-O. Hierarchically Structured Nanomaterials for Electrochemical Energy Conversion. *Angew. Chemie Int. Ed.* **2016**, *55*, 122−148.
(82) Trogadas, P.; Cho, J. I. S.; Neville, T. P.; Marquis, J.; Wu, B.; Brett, D. J. L.; Coppens, M. O. A Lung-Inspired Approach to Scalable and Robust Fuel Cell Design. *Energy Environ. Sci.* **2018**, *11*, 136−143.
(83) Liu, M.; Zhao, Z.; Duan, X.; Huang, Y. Nanoscale Structure Design for High-Performance Pt-Based ORR Catalysts. *Adv. Mater.* **2019**, *31*, 1802234.
(84) Meng, Z.; Cai, S.; Tu, W.; Tang, H. Hierarchical Nanostructured Electrocatalysts for Oxygen Reduction Reaction. *J. Nanosci. Nanotechnol.* **2020**, *20*, 1085−1097.
(85) Yang, X.-Y.; Chen, L.-H.; Li, Y.; Rooke, J. C.; Sanchez, C.; Su, B.-L. Hierarchically Porous Materials: Synthesis Strategies and Structure Design. *Chem. Soc. Rev.* **2017**, *46*, 481−558.
(86) Zhang, D.; Zhang, W.; Gu, J.; Zhu, S.; Su, H.; Liu, Q.; Fan, T.; Ding, J.; Guo, Q. Bio-Inspired Functional Materials Templated from Nature Materials. *kona powder Part. J.* **2010**, *28*, 116−130.
(87) Ayers, K.; Danilovic, N.; Ouimet, R.; Carmo, M.; Pivovar, B.; Bornstein, M. Perspectives on Low-Temperature Electrolysis and Potential for Renewable Hydrogen at Scale. *Ann. Rev. Chem. Biomol. Eng.* **2019**, *10*, 219−239.
(88) Schalenbach, M.; Zeradjanin, A. R.; Kasian, O.; Cherevko, S.; Mayrhofer, K. J. J. A Perspective on Low-Temperature Water Electrolysis-Challenges in Alkaline and Acidic Technology. *Int. J. Electrochem. Sci.* **2018**, *13*, 1173−1226.
(89) Man, I. C.; Su, H. Y.; Calle-Vallejo, F.; Hansen, H. A.; Martínez, J. I.; Inoglu, N. G.; Kitchin, J.; Jaramillo, T. F.; Nørskov, J. K.; Rossmeisl, J. Universality in Oxygen Evolution Electrocatalysis on Oxide Surfaces. *ChemCatChem.* **2011**, *3*, 1159−1165.
(90) Rossmeisl, J.; Logadottir, A.; Nørskov, J. K. Electrolysis of Water on (Oxidized) Metal Surfaces. *Chem. Phys.* **2005**, *319*, 178−184.
(91) Huang, J.; Scott, S. B.; Chorkendorff, I.; Wen, Z. Online Electrochemistry-Mass Spectrometry Evaluation of the Acidic Oxygen Evolution Reaction at Supported Catalysts. *ACS Catal.* **2021**, *11*, 12745−12753.
(92) Chen, N.; Paek, S. Y.; Lee, J. Y.; Park, J. H.; Lee, S. Y.; Lee, Y. M. High-Performance Anion Exchange Membrane Water Electrolyzers with a Current Density of 7.68 A Cm-2 and a Durability of 1000 h. *Energy Environ. Sci.* **2021**, *14*, 6338−6348.
(93) Liu, Z.; Sajjad, S. D.; Gao, Y.; Yang, H.; Kaczur, J. J.; Masel, R. I. The Effect of Membrane on an Alkaline Water Electrolyzer. *Int. J. Hydrogen Energy* **2017**, *42*, 29661−29665.
(94) Schalenbach, M.; Tjarks, G.; Carmo, M.; Lueke, W.; Mueller, M.; Stolten, D. Acidic or Alkaline? Towards a New Perspective on the Efficiency of Water Electrolysis. *J. Electrochem. Soc.* **2016**, *163*, F3197−F3208.
(95) Kucernak, A. R.; Zalitis, C. General Models for the Electrochemical Hydrogen Oxidation and Hydrogen Evolution Reactions: Theoretical Derivation and Experimental Results under Near Mass-Transport Free Conditions. *J. Phys. Chem. C* **2016**, *120*, 10721−10745.
(96) Debe, M. K.; Hendricks, S. M.; Vernstrom, G. D.; Meyers, M.; Brostrom, M.; Stephens, M.; Chan, Q.; Willey, J.; Hamden, M.; Mittelsteadt, C. K.; et al. Initial Performance and Durability of Ultra-Low Loaded NSTF Electrodes for PEM Electrolyzers. *J. Electrochem. Soc.* **2012**, *159*, K165−K176.
(97) Rao, R. R.; Corby, S.; Bucci, A.; García-Tecedor, M.; Mesa, C. A.; Rossmeisl, J.; Giménez, S.; Lloret-Fillol, J.; Stephens, I. E. L.; Durrant, J. R. Spectroelectrochemical Analysis of the Water Oxidation Mechanism on Doped Nickel Oxides. *J. Am. Chem. Soc.* **2022**, *144*, 7622−7633.
(98) Fabbri, E.; Schmidt, T. J. Oxygen Evolution Reaction—The Enigma in Water Electrolysis. *ACS Catal.* **2018**, *8*, 9765−9774.
(99) Huang, Z.-F.; Song, J.; Du, Y.; Xi, S.; Dou, S.; Nsanzimana, J. M. V.; Wang, C.; Xu, Z. J.; Wang, X. Chemical and Structural Origin of Lattice Oxygen Oxidation in Co-Zn Oxyhydroxide Oxygen Evolution Electrocatalysts. *Nat. Energy* **2019**, *4*, 329−338.
(100) Yoo, J. S.; Rong, X.; Liu, Y.; Kolpak, A. M. Role of Lattice Oxygen Participation in Understanding Trends in the Oxygen Evolution Reaction on Perovskites. *ACS Catal.* **2018**, *8*, 4628−4636.
(101) Zagalskaya, A.; Evazzade, I.; Alexandrov, V. Ab Initio Thermodynamics and Kinetics of the Lattice Oxygen Evolution Reaction in Iridium Oxides. *ACS Energy Lett.* **2021**, *6*, 1124−1133.
(102) Gao, R.; Dai, Q.; Du, F.; Yan, D.; Dai, L. C60-Adsorbed Single-Walled Carbon Nanotubes as Metal-Free, PH-Universal, and Multifunctional Catalysts for Oxygen Reduction, Oxygen Evolution, and Hydrogen Evolution. *J. Am. Chem. Soc.* **2019**, *141*, 11658−11666.
(103) Kweon, D. H.; Baek, J.-B. Edge-Functionalized Graphene Nanoplatelets as Metal-Free Electrocatalysts for Dye-Sensitized Solar Cells. *Adv. Mater.* **2019**, *31*, 1804440.
(104) Paul, R.; Dai, Q.; Hu, C.; Dai, L. Ten Years of Carbon-based Metal-free Electrocatalysts. *Carbon Energy* **2019**, *1*, 19−31.
(105) Huang, Y.; Wu, D.; Cao, D.; Cheng, D. Facile Preparation of Biomass-Derived Bifunctional Electrocatalysts for Oxygen Reduction and Evolution Reactions. *Int. J. Hydrogen Energy* **2018**, *43*, 8611−8622.
(106) Wang, G.; Deng, Y.; Yu, J.; Zheng, L.; Du, L.; Song, H.; Liao, S. From Chlorella to Nestlike Framework Constructed with Doped Carbon Nanotubes: A Biomass-Derived, High-Performance, Bifunctional Oxygen Reduction/Evolution Catalyst. *ACS Appl. Mater. Interfaces* **2017**, *9*, 32168−32178.
(107) Wu, H.; Geng, J.; Ge, H.; Guo, Z.; Wang, Y.; Zheng, G. Egg-Derived Mesoporous Carbon Microspheres as Bifunctional Oxygen Evolution and Oxygen Reduction Electrocatalysts. *Adv. Energy Mater.* **2016**, *6*, 1600794.
(108) Hu, C.; Dai, L. Multifunctional Carbon-Based Metal-Free Electrocatalysts for Simultaneous Oxygen Reduction, Oxygen Evolution, and Hydrogen Evolution. *Adv. Mater.* **2017**, *29*, 1604942.
(109) Xiao, Z.; Huang, X.; Xu, L.; Yan, D.; Huo, J.; Wang, S. Edge-Selectively Phosphorus-Doped Few-Layer Graphene as an Efficient Metal-Free Electrocatalyst for the Oxygen Evolution Reaction. *Chem. Commun.* **2016**, *52*, 13008−13011.

https://doi.org/10.1021/acs.chemrev.2c00429
Chem. Rev. 2023, 123, 2311−2348

(110) Chen, S.; Duan, J.; Ran, J.; Qiao, S.-Z. Paper-Based N-Doped Carbon Films for Enhanced Oxygen Evolution Electrocatalysis. *Adv. Sci.* **2015**, *2*, 1400015.
(111) Bayazit, M. K.; Moniz, S. J. A.; Coleman, K. S. Gram-Scale Production of Nitrogen Doped Graphene Using a 1,3-Dipolar Organic Precursor and Its Utilisation as a Stable, Metal Free Oxygen Evolution Reaction Catalyst. *Chem. Commun.* **2017**, *53*, 7748−7751.
(112) Li, O. L.; Pham, N. N. T.; Kim, J.; Choi, H.; Lee, D. H.; Yang, Y.; Yao, W.; Cho, Y.-R.; Lee, S. G. Insights on Boosting Oxygen Evolution Reaction Performance via Boron Incorporation into Nitrogen-Doped Carbon Electrocatalysts. *Appl. Surf. Sci.* **2020**, *528*, 146979.
(113) Li, J.-C.; Hou, P.-X.; Zhao, S.-Y.; Liu, C.; Tang, D.-M.; Cheng, M.; Zhang, F.; Cheng, H.-M. A 3D Bi-Functional Porous N-Doped Carbon Microtube Sponge Electrocatalyst for Oxygen Reduction and Oxygen Evolution Reactions. *Energy Environ. Sci.* **2016**, *9*, 3079−3084.
(114) He, D.; Xiong, Y.; Yang, J.; Chen, X.; Deng, Z.; Pan, M.; Li, Y.; Mu, S. Nanocarbon-Intercalated and Fe-N-Codoped Graphene as a Highly Active Noble-Metal-Free Bifunctional Electrocatalyst for Oxygen Reduction and Evolution. *J. Mater. Chem. A* **2017**, *5*, 1930−1934.
(115) Hoang, V. C.; Gomes, V. G.; Dinh, K. N. Ni- and P-Doped Carbon from Waste Biomass: A Sustainable Multifunctional Electrode for Oxygen Reduction, Oxygen Evolution and Hydrogen Evolution Reactions. *Electrochim. Acta* **2019**, *314*, 49−60.
(116) Niu, J.; Shao, R.; Liu, M.; Zan, Y.; Dou, M.; Liu, J.; Zhang, Z.; Huang, Y.; Wang, F. Porous Carbons Derived from Collagen-Enriched Biomass: Tailored Design, Synthesis, and Application in Electrochemical Energy Storage and Conversion. *Adv. Funct. Mater.* **2019**, *29*, 1905095.
(117) Jin, H.; Guo, C.; Liu, X.; Liu, J.; Vasileff, A.; Jiao, Y.; Zheng, Y.; Qiao, S.-Z. Emerging Two-Dimensional Nanomaterials for Electrocatalysis. *Chem. Rev.* **2018**, *118*, 6337−6408.
(118) Zuliani, A.; Cano, M.; Calsolaro, F.; Puente Santiago, A. R.; Giner-Casares, J. J.; Rodríguez-Castellón, E.; Berlier, G.; Cravotto, G.; Martina, K.; Luque, R. Improving the Electrocatalytic Performance of Sustainable Co/Carbon Materials for the Oxygen Evolution Reaction by Ultrasound and Microwave Assisted Synthesis. *Sustain. Energy Fuels* **2021**, *5*, 720−731.
(119) Yang, Z.; Yan, C.; Xiang, M.; Shi, Y.; Ding, M.; Hui, J. Biomass Carbon Dual-doped with Iron and Nitrogen for High-performance Electrocatalyst in Water Splitting. *Int. J. Energy Res.* **2021**, *45*, 8474−8483.
(120) Tzadikov, J.; Amsellem, M.; Amlani, H.; Barrio, J.; Azoulay, A.; Volokh, M.; Kozuch, S.; Shalom, M. Coordination-Directed Growth of Transition-Metal-Crystalline-Carbon Composites with Controllable Metal Composition. *Angew. Chemie Int. Ed.* **2019**, *58*, 14964−14968.
(121) Ma, N.; Jia, Y.; Yang, X.; She, X.; Zhang, L.; Peng, Z.; Yao, X.; Yang, D. Seaweed Biomass Derived (Ni,Co)/CNT Nanoaerogels: Efficient Bifunctional Electrocatalysts for Oxygen Evolution and Reduction Reactions. *J. Mater. Chem. A* **2016**, *4*, 6376−6384.
(122) Murdachaew, G.; Laasonen, K. Oxygen Evolution Reaction on Nitrogen-Doped Defective Carbon Nanotubes and Graphene. *J. Phys. Chem. C* **2018**, *122*, 25882−25892.
(123) Wang, X.; Vasileff, A.; Jiao, Y.; Zheng, Y.; Qiao, S.-Z. Electronic and Structural Engineering of Carbon-Based Metal-Free Electrocatalysts for Water Splitting. *Adv. Mater.* **2019**, *31*, 1803625.
(124) Lei, C.; Zheng, Q.; Cheng, F.; Hou, Y.; Yang, B.; Li, Z.; Wen, Z.; Lei, L.; Chai, G.; Feng, X. High-Performance Metal-Free Nanosheets Array Electrocatalyst for Oxygen Evolution Reaction in Acid. *Adv. Funct. Mater.* **2020**, *30*, 2003000.
(125) Zhang, J.; Ren, M.; Wang, L.; Li, Y.; Yakobson, B. I.; Tour, J. M. Oxidized Laser-Induced Graphene for Efficient Oxygen Electrocatalysis. *Adv. Mater.* **2018**, *30*, 1707319.
(126) Kiciński, W.; Dyjak, S. Transition Metal Impurities in Carbon-Based Materials: Pitfalls, Artifacts and Deleterious Effects. *Carbon* **2020**, *168*, 748−845.
(127) Stuart, E. J. E.; Pumera, M. Electrochemistry of a Whole Group of Compounds Affected by Metallic Impurities within Carbon Nanotubes. *J. Phys. Chem. C* **2010**, *114*, 21296−21298.
(128) Tzadikov, J.; Geva, R.; Azoulay, A.; Shalom, M. Facile Synthesis of Carbon-Sulfur Scaffold with Transition-Metal Sulfides and Oxides as Efficient Electrocatalysts for Oxygen Evolution Reaction. *ChemCatChem.* **2021**, *13*, 3749−3753.
(129) Barber, J. Crystal Structure of the Oxygen-Evolving Complex of Photosystem II. *Inorg. Chem.* **2008**, *47*, 1700−1710.
(130) McEvoy, J. P.; Brudvig, G. W. Water-Splitting Chemistry of Photosystem II. *Chem. Rev.* **2006**, *106*, 4455−4483.
(131) Zhang, L.; Paakkarinen, V.; van Wijk, K. J.; Aro, E.-M. Co-Translational Assembly of the D1 Protein into Photosystem II*. *J. Biol. Chem.* **1999**, *274*, 16062−16067.
(132) Schweinar, K.; Gault, B.; Mouton, I.; Kasian, O. Lattice Oxygen Exchange in Rutile IrO2 during the Oxygen Evolution Reaction. *J. Phys. Chem. Lett.* **2020**, *11*, 5008−5014.
(133) Barber, J. A Mechanism for Water Splitting and Oxygen Production in Photosynthesis. *Nat. Plants* **2017**, *3*, 17041.
(134) Cox, N.; Pantazis, D. A.; Neese, F.; Lubitz, W. Artificial Photosynthesis: Understanding Water Splitting in Nature. *Interface Focus* **2015**, *5*, 20150009.
(135) Capone, M.; Narzi, D.; Guidoni, L. Mechanism of Oxygen Evolution and Mn4CaO5 Cluster Restoration in the Natural Water-Oxidizing Catalyst. *Biochemistry* **2021**, *60*, 2341−2348.
(136) Umena, Y.; Kawakami, K.; Shen, J.-R.; Kamiya, N. Crystal Structure of Oxygen-Evolving Photosystem II at a Resolution of 1.9 Å. *Nature* **2011**, *473*, 55−60.
(137) Siegbahn, P. E. M. A Structure-Consistent Mechanism for Dioxygen Formation in Photosystem II. *Chem. -Eur. J.* **2008**, *14*, 8290−8302.
(138) Siegbahn, P. E. M. Structures and Energetics for O2 Formation in Photosystem II. *Acc. Chem. Res.* **2009**, *42*, 1871−1880.
(139) Sun, L. A Closer Mimic of the Oxygen Evolution Complex of Photosystem II. *Science* **2015**, *348*, 635−636.
(140) Zhang, C.; Chen, C.; Dong, H.; Shen, J.-R.; Dau, H.; Zhao, J. A Synthetic Mn_4Ca-Cluster Mimicking the Oxygen-Evolving Center of Photosynthesis. *Science* **2015**, *348*, 690−693.
(141) Dismukes, G. C.; Brimblecombe, R.; Felton, G. A. N.; Pryadun, R. S.; Sheats, J. E.; Spiccia, L.; Swiegers, G. F. Development of Bioinspired Mn4O4-Cubane Water Oxidation Catalysts: Lessons from Photosynthesis. *Acc. Chem. Res.* **2009**, *42*, 1935−1943.
(142) Nocera, D. G. The Artificial Leaf. *Acc. Chem. Res.* **2012**, *45*, 767−776.
(143) Suseno, S.; McCrory, C. C. L.; Tran, R.; Gul, S.; Yano, J.; Agapie, T. Molecular Mixed-Metal Manganese Oxido Cubanes as Precursors to Heterogeneous Oxygen Evolution Catalysts. *Chem. - A Eur. J.* **2015**, *21*, 13420−13430.
(144) Zhou, T.; Wang, D.; Chun-Kiat Goh, S.; Hong, J.; Han, J.; Mao, J.; Xu, R. Bio-Inspired Organic Cobalt(Ii) Phosphonates toward Water Oxidation. *Energy Environ. Sci.* **2015**, *8*, 526−534.
(145) Jiang, X.; Li, J.; Yang, B.; Wei, X.-Z.; Dong, B.-W.; Kao, Y.; Huang, M.-Y.; Tung, C.-H.; Wu, L.-Z. A Bio-Inspired Cu4O4 Cubane: Effective Molecular Catalysts for Electrocatalytic Water Oxidation in Aqueous Solution. *Angew. Chemie Int. Ed.* **2018**, *57*, 7850−7854.
(146) Lin, J.; Liang, X.; Cao, X.; Wei, N.; Ding, Y. An Octanuclear Cu(Ii) Cluster with a Bio-Inspired Cu4O4 Cubic Fragment for Efficient Photocatalytic Water Oxidation. *Chem. Commun.* **2018**, *54*, 12515−12518.
(147) Li, W.; Li, F.; Yang, H.; Wu, X.; Zhang, P.; Shan, Y.; Sun, L. A Bio-Inspired Coordination Polymer as Outstanding Water Oxidation Catalyst via Second Coordination Sphere Engineering. *Nat. Commun.* **2019**, *10*, 5074.
(148) Wilson, A. D.; Newell, R. H.; McNevin, M. J.; Muckerman, J. T.; DuBois, M. R.; DuBois, D. L. Hydrogen Oxidation and Production Using Nickel-Based Molecular Catalysts with Positioned Proton Relays. *J. Am. Chem. Soc.* **2006**, *128*, 358−366.
(149) Zhao, Y.; Swierk, J. R.; Megiatto, J. D.; Sherman, B.; Youngblood, W. J.; Qin, D.; Lentz, D. M.; Moore, A. L.; Moore, T. A.; Gust, D.; et al. Improving the Efficiency of Water Splitting in Dye-Sensitized Solar Cells by Using a Biomimetic Electron Transfer Mediator. *Proc. Natl. Acad. Sci. U.S.A.* **2012**, *109*, 15612−15616.

https://doi.org/10.1021/acs.chemrev.2c00429
Chem. Rev. 2023, 123, 2311−2348

(150) Na, Y.; Miao, S.; Zhou, L.; Wei, P.; Cao, Y. Bio-Inspired Model of Photosystem II: Supramolecular Assembly of an Electron Mediator into an SnO2 Photoanode Co-Sensitized by a Porphyrin Photosensitizer and Ruthenium Molecular Catalyst. *Sustain. Energy Fuels* **2018**, *2*, 545−548.
(151) Ferreira, K. N.; Iverson, T. M.; Maghlaoui, K.; Barber, J.; Iwata, S. Architecture of the Photosynthetic Oxygen-Evolving Center. *Science* **2004**, *303*, 1831−1838.
(152) Nørskov, J. K.; Bligaard, T.; Logadottir, A.; Kitchin, J. R.; Chen, J. G.; Pandelov, S.; Stimming, U. Trends in the Exchange Current for Hydrogen Evolution. *J. Electrochem. Soc.* **2005**, *152*, J23−J26.
(153) Zhao, G.; Rui, K.; Dou, S. X.; Sun, W. Heterostructures for Electrochemical Hydrogen Evolution Reaction: A Review. *Adv. Funct. Mater.* **2018**, *28*, 1803291.
(154) Subbaraman, R.; Tripkovic, D.; Strmcnik, D.; Chang, K.-C.; Uchimura, M.; Paulikas, A. P.; Stamenkovic, V.; Markovic, N. M. Enhancing Hydrogen Evolution Activity in Water Splitting by Tailoring Li^+-Ni$(OH)_2$-Pt Interfaces. *Science* **2011**, *334*, 1256−1260.
(155) Geva, R.; Levy, N. R.; Tzadikov, J.; Cohen, R.; Weitman, M.; Xing, L.; Abisdris, L.; Barrio, J.; Xia, J.; Volokh, M.; et al. Molten State Synthesis of Nickel Phosphides: Mechanism and Composition-Activity Correlation for Electrochemical Applications. *J. Mater. Chem. A* **2021**, *9*, 27629−27638.
(156) Ledendecker, M.; Krick Calderón, S.; Papp, C.; Steinrück, H.-P.; Antonietti, M.; Shalom, M. The Synthesis of Nanostructured Ni5P4 Films and Their Use as a Non-Noble Bifunctional Electrocatalyst for Full Water Splitting. *Angew. Chemie Int. Ed.* **2015**, *54*, 12361−12365.
(157) Benck, J. D.; Hellstern, T. R.; Kibsgaard, J.; Chakthranont, P.; Jaramillo, T. F. Catalyzing the Hydrogen Evolution Reaction (HER) with Molybdenum Sulfide Nanomaterials. *ACS Catal.* **2014**, *4*, 3957−3971.
(158) Popczun, E. J.; Read, C. G.; Roske, C. W.; Lewis, N. S.; Schaak, R. E. Highly Active Electrocatalysis of the Hydrogen Evolution Reaction by Cobalt Phosphide Nanoparticles. *Angew. Chemie, Int. Ed.* **2014**, *53*, 5427−5430.
(159) Shalom, M.; Ressnig, D.; Yang, X.; Clavel, G.; Fellinger, T. P.; Antonietti, M. Nickel Nitride as an Efficient Electrocatalyst for Water Splitting. *J. Mater. Chem. A* **2015**, *3*, 8171−8177.
(160) Sokolikova, M. S.; Sherrell, P. C.; Palczynski, P.; Bemmer, V. L.; Mattevi, C. Direct Solution-Phase Synthesis of 1T' WSe_2 Nanosheets. *Nat. Commun.* **2019**, *10*, 712.
(161) Zheng, Y.; Jiao, Y.; Li, L. H.; Xing, T.; Chen, Y.; Jaroniec, M.; Qiao, S. Z. Toward Design of Synergistically Active Carbon-Based Catalysts for Electrocatalytic Hydrogen Evolution. *ACS Nano* **2014**, *8*, 5290−5296.
(162) Deng, J.; Li, M.; Wang, Y. Biomass-Derived Carbon: Synthesis and Applications in Energy Storage and Conversion. *Green Chem.* **2016**, *18*, 4824−4854.
(163) Zhang, J.; Li, Y.; Zhu, T.; Wang, Y.; Cui, J.; Wu, J.; Xu, H.; Shu, X.; Qin, Y.; Zheng, H.; Ajayan, P. M.; Zhang, Y.; Wu, Y. 3D Coral-Like Ni3S2 on Ni Foam as a Bifunctional Electrocatalyst for Overall Water Splitting. *ACS Appl. Mater. Interfaces* **2018**, *10*, 31330−31339.
(164) Wang, Y.; Ma, J.; Wang, J.; Chen, S.; Wang, H.; Zhang, J. Interfacial Scaffolding Preparation of Hierarchical PBA-Based Derivative Electrocatalysts for Efficient Water Splitting. *Adv. Energy Mater.* **2019**, *9*, 1802939.
(165) Wang, Y.-N.; Yang, Z.-J.; Yang, D.-H.; Zhao, L.; Shi, X.-R.; Yang, G.; Han, B.-H. FeCoP2 Nanoparticles Embedded in N and P Co-Doped Hierarchically Porous Carbon for Efficient Electrocatalytic Water Splitting. *ACS Appl. Mater. Interfaces* **2021**, *13*, 8832−8843.
(166) Tran, P. D.; Artero, V.; Fontecave, M. Water Electrolysis and Photoelectrolysis on Electrodes Engineered Using Biological and Bio-Inspired Molecular Systems. *Energy Environ. Sci.* **2010**, *3*, 727−747.
(167) Artero, V.; Berggren, G.; Atta, M.; Caserta, G.; Roy, S.; Pecqueur, L.; Fontecave, M. From Enzyme Maturation to Synthetic Chemistry: The Case of Hydrogenases. *Acc. Chem. Res.* **2015**, *48*, 2380−2387.
(168) Dubois, D. L. Development of Molecular Electrocatalysts for Energy Storage. *Inorg. Chem.* **2014**, *53*, 3935−3960.
(169) Zou, X.; Silva, R.; Goswami, A.; Asefa, T. Cu-Doped Carbon Nitride: Bio-Inspired Synthesis of H2-Evolving Electrocatalysts Using Graphitic Carbon Nitride (g-C3N4) as a Host Material. *Appl. Surf. Sci.* **2015**, *357*, 221−228.
(170) Simmons, T. R.; Berggren, G.; Bacchi, M.; Fontecave, M.; Artero, V. Mimicking Hydrogenases: From Biomimetics to Artificial Enzymes. *Coord. Chem. Rev.* **2014**, *270*−*271*, 127−150.
(171) Cabrera-García, A.; Blay, V.; Blay-Roger, R.; Ravelo, Á. G.; González-Platas, J.; Arévalo, M. C.; Sanchiz, J.; Martín-Zarza, P. Bio-Inspired Ni Dinuclear Complexes as Heterogeneous Catalysts for Hydrogen Evolution. *Chem. Eng. J.* **2021**, *420*, 130342.
(172) Gennari, M.; Duboc, C. Bio-Inspired, Multifunctional Metal-Thiolate Motif: From Electron Transfer to Sulfur Reactivity and Small-Molecule Activation. *Acc. Chem. Res.* **2020**, *53*, 2753−2761.
(173) Kaeffer, N.; Morozan, A.; Fize, J.; Martinez, E.; Guetaz, L.; Artero, V. The Dark Side of Molecular Catalysis: Diimine-Dioxime Cobalt Complexes Are Not the Actual Hydrogen Evolution Electrocatalyst in Acidic Aqueous Solutions. *ACS Catal.* **2016**, *6*, 3727−3737.
(174) Dutta, A.; Du Bois, D. L.; Roberts, J. A. S.; Shaw, W. J. Amino Acid Modified Ni Catalyst Exhibits Reversible H2 Oxidation/Production over a Broad PH Range at Elevated Temperatures. *Proc. Natl. Acad. Sci. U. S. A.* **2014**, *111*, 16286−16291.
(175) Huan, T. N.; Jane, R. T.; Benayad, A.; Guetaz, L.; Tran, P. D.; Artero, V. Bio-Inspired Noble Metal-Free Nanomaterials Approaching Platinum Performances for H2 Evolution and Uptake. *Energy Environ. Sci.* **2016**, *9*, 940−947.
(176) Zheng, X.; Yao, Y.; Ye, W.; Gao, P.; Liu, Y. Building up Bimetallic Active Sites for Electrocatalyzing Hydrogen Evolution Reaction under Acidic and Alkaline Conditions. *Chem. Eng. J.* **2021**, *413*, 128027.
(177) Chen, Y.; Ji, S.; Chen, C.; Peng, Q.; Wang, D.; Li, Y. Single-Atom Catalysts: Synthetic Strategies and Electrochemical Applications. *Joule* **2018**, *2*, 1242−1264.
(178) Gusmão, R.; Veselý, M.; Sofer, Z. Recent Developments on the Single Atom Supported at 2D Materials beyond Graphene as Catalysts. *ACS Catal.* **2020**, *10*, 9634−9648.
(179) Zhang, Q.; Guan, J. Single-Atom Catalysts for Electrocatalytic Applications. *Adv. Funct. Mater.* **2020**, *30*, 2000768.
(180) Yang, J.; Li, W.; Wang, D.; Li, Y. Electronic Metal-Support Interaction of Single-Atom Catalysts and Applications in Electrocatalysis. *Adv. Mater.* **2020**, *32*, 2003300.
(181) Wang, Y.; Wang, D.; Li, Y. Rational Design of Single-Atom Site Electrocatalysts: From Theoretical Understandings to Practical Applications. *Adv. Mater.* **2021**, *33*, 2008151.
(182) Pu, Z.; Amiinu, I. S.; Cheng, R.; Wang, P.; Zhang, C.; Mu, S.; Zhao, W.; Su, F.; Zhang, G.; Liao, S.; et al. Single-Atom Catalysts for Electrochemical Hydrogen Evolution Reaction: Recent Advances and Future Perspectives. *Nano-Micro Lett.* **2020**, *12*, 21.
(183) Wu, D.; He, B.; Wang, Yu.; Lv, P.; Ma, D.; Jia, Y. Double-Atom Catalysts for Energy-Related Electrocatalysis Applications: A Theoretical Perspective. *J. Phys. D. Appl. Phys.* **2022**, *55*, 203001.
(184) Pedersen, A.; Barrio, J.; Li, A.; Jervis, R.; Brett, D. J. L.; Titirici, M. M.; Stephens, I. E. L. Dual-Metal Atom Electrocatalysts: Theory, Synthesis, Characterization, and Applications. *Adv. Energy Mater.* **2022**, *12*, 2102715.
(185) Xu, H.; Cheng, D.; Cao, D.; Zeng, X. C. A Universal Principle for a Rational Design of Single-Atom Electrocatalysts. *Nat. Catal.* **2018**, *1*, 339−348.
(186) Hinnemann, B.; Moses, P. G.; Bonde, J.; Jørgensen, K. P.; Nielsen, J. H.; Horch, S.; Chorkendorff, I.; Nørskov, J. K. Biomimetic Hydrogen Evolution: MoS2 Nanoparticles as Catalyst for Hydrogen Evolution. *J. Am. Chem. Soc.* **2005**, *127*, 5308−5309.
(187) Casalongue, H. G. S.; Benck, J. D.; Tsai, C.; Karlsson, R. K. B.; Kaya, S.; Ng, M. L.; Pettersson, L. G. M.; Abild-Pedersen, F.; Nørskov, J. K.; Ogasawara, H.; et al. Operando Characterization of an Amorphous Molybdenum Sulfide Nanoparticle Catalyst during the Hydrogen Evolution Reaction. *J. Phys. Chem. C* **2014**, *118*, 29252−29259.

https://doi.org/10.1021/acs.chemrev.2c00429
Chem. Rev. 2023, 123, 2311−2348

(188) Wroblowa, H. S.; Yen-Chi-Pan; Razumney, G. Electroreduction of Oxygen: A New Mechanistic Criterion. *J. Electroanal. Chem. Interfacial Electrochem.* **1976**, *69*, 195−201.
(189) Ramaswamy, N.; Mukerjee, S. Alkaline Anion-Exchange Membrane Fuel Cells: Challenges in Electrocatalysis and Interfacial Charge Transfer. *Chem. Rev.* **2019**, *119*, 11945−11979.
(190) Wang, X.; Li, Z.; Qu, Y.; Yuan, T.; Wang, W.; Wu, Y.; Li, Y. Review of Metal Catalysts for Oxygen Reduction Reaction: From Nanoscale Engineering to Atomic Design. *Chem.* **2019**, *5*, 1486−1511.
(191) Calle-Vallejo, F.; Martínez, J. I.; Rossmeisl, J. Density Functional Studies of Functionalized Graphitic Materials with Late Transition Metals for Oxygen Reduction Reactions. *Phys. Chem. Chem. Phys.* **2011**, *13*, 15639−15643.
(192) Koper, M. T. M. Thermodynamic Theory of Multi-Electron Transfer Reactions: Implications for Electrocatalysis. *J. Electroanal. Chem.* **2011**, *660*, 254−260.
(193) Busch, M.; Halck, N. B.; Kramm, U. I.; Siahrostami, S.; Krtil, P.; Rossmeisl, J. Beyond the Top of the Volcano? - A Unified Approach to Electrocatalytic Oxygen Reduction and Oxygen Evolution. *Nano Energy* **2016**, *29*, 126−135.
(194) Staszak-Jirkovský, J.; Subbaraman, R.; Strmcnik, D.; Harrison, K. L.; Diesendruck, C. E.; Assary, R.; Frank, O.; Kobr, L.; Wiberg, G. K. H.; Genorio, B.; et al. Water as a Promoter and Catalyst for Dioxygen Electrochemistry in Aqueous and Organic Media. *ACS Catal.* **2015**, *5*, 6600−6607.
(195) Kjaergaard, C. H.; Rossmeisl, J.; Nørskov, J. K. Enzymatic versus Inorganic Oxygen Reduction Catalysts: Comparison of the Energy Levels in a Free-Energy Scheme. *Inorg. Chem.* **2010**, *49*, 3567−3572.
(196) Kaukonen, M. Calculated Reaction Cycle of Cytochrome c Oxidase. *J. Phys. Chem. B* **2007**, *111*, 12543−12550.
(197) Fuel Cells and Hydrogen Joint Undertaking. *Value Added of the Hydrogen and Fuel Cell Sector in Europe : Supporting European Growth and Competitiveness : Study on Value Chain and Manufacturing Competitiveness Analysis for Hydrogen and Fuel Cells Technologies : Summary Report*; Publications Office of the European Union: Luxembourg, 2019.
(198) James, B. D.; Huya-Kouadio, J. M.; Houchins, C.; DeSantis, D. A.Fuel Cell Vehicle Cost Analysis. In *FY 2017 Progress Report for the DOE Hydrogen and Fuell Cells Program*; U.S. Department of Energy: Washington, D.C., 2017.
(199) U.S. Geological Survey. *Mineral Commodity Summaries 2022*; U.S. Geological Survey: Reston, VA, 2022.
(200) Laursen, A. B.; Sehested, J.; Chorkendorff, I.; Vesborg, P. C. K. Availability of Elements for Heterogeneous Catalysis: Predicting the Industrial Viability of Novel Catalysts. *Chin. J. Catal.* **2018**, *39*, 16−26.
(201) Whiston, M. M.; Azevedo, I. L.; Litster, S.; Whitefoot, K. S.; Samaras, C.; Whitacre, J. F. Expert Assessments of the Cost and Expected Future Performance of Proton Exchange Membrane Fuel Cells for Vehicles. *Proc. Natl. Acad. Sci. U. S. A.* **2019**, *116*, 4899−4904.
(202) Ma, Z.; Cano, Z. P.; Yu, A.; Chen, Z.; Jiang, G.; Fu, X.; Yang, L.; Wu, T.; Bai, Z.; Lu, J. Enhancing Oxygen Reduction Activity of Pt-Based Electrocatalysts: From Theoretical Mechanisms to Practical Methods. *Angew. Chemie Int. Ed.* **2020**, *59*, 18334−18348.
(203) Jorge, A. B.; Jervis, R.; Periasamy, A. P.; Qiao, M.; Feng, J.; Tran, L. N.; Titirici, M.-M. 3D Carbon Materials for Efficient Oxygen and Hydrogen Electrocatalysis. *Adv. Energy Mater.* **2020**, *10*, 1902494.
(204) Wan, X.; Liu, X.; Li, Y.; Yu, R.; Zheng, L.; Yan, W.; Wang, H.; Xu, M.; Shui, J. Fe-N-C Electrocatalyst with Dense Active Sites and Efficient Mass Transport for High-Performance Proton Exchange Membrane Fuel Cells. *Nat. Catal.* **2019**, *2*, 259−268.
(205) Li, Y.; Zhang, Q.; Zhang, J.; Jin, L.; Zhao, X.; Xu, T. A Top-Down Approach for Fabricating Free-Standing Bio-Carbon Supercapacitor Electrodes with a Hierarchical Structure. *Sci. Rep.* **2015**, *5*, 14155.
(206) Zhu, G.; Ma, L.; Lv, H.; Hu, Y.; Chen, T.; Chen, R.; Liang, J.; Wang, X.; Wang, Y.; Yan, C.; et al. Pine Needle-Derived Microporous Nitrogen-Doped Carbon Frameworks Exhibit High Performances in Electrocatalytic Hydrogen Evolution Reaction and Supercapacitors. *Nanoscale* **2017**, *9*, 1237−1243.
(207) Teo, E. Y. L.; Muniandy, L.; Ng, E. P.; Adam, F.; Mohamed, A. R.; Jose, R.; Chong, K. F. High Surface Area Activated Carbon from Rice Husk as a High Performance Supercapacitor Electrode. *Electrochim. Acta* **2016**, *192*, 110−119.
(208) Tian, W.; Gao, Q.; Tan, Y.; Yang, K.; Zhu, L.; Yang, C.; Zhang, H. Bio-Inspired Beehive-like Hierarchical Nanoporous Carbon Derived from Bamboo-Based Industrial by-Product as a High Performance Supercapacitor Electrode Material. *J. Mater. Chem. A* **2015**, *3*, 5656−5664.
(209) Luan, Y.; Wang, L.; Guo, S.; Jiang, B.; Zhao, D.; Yan, H.; Tian, C.; Fu, H. A Hierarchical Porous Carbon Material from a Loofah Sponge Network for High Performance Supercapacitors. *RSC Adv.* **2015**, *5*, 42430−42437.
(210) Ren, Y.; Zhang, J.; Xu, Q.; Chen, Z.; Yang, D.; Wang, B.; Jiang, Z. Biomass-Derived Three-Dimensional Porous N-Doped Carbonaceous Aerogel for Efficient Supercapacitor Electrodes. *RSC Adv.* **2014**, *4*, 23412−23419.
(211) Liang, Q.; Ye, L.; Huang, Z. H.; Xu, Q.; Bai, Y.; Kang, F.; Yang, Q. H. A Honeycomb-like Porous Carbon Derived from Pomelo Peel for Use in High-Performance Supercapacitors. *Nanoscale* **2014**, *6*, 13831−13837.
(212) Sun, W.; Lipka, S. M.; Swartz, C.; Williams, D.; Yang, F. Hemp-Derived Activated Carbons for Supercapacitors. *Carbon* **2016**, *103*, 181−192.
(213) Zhang, C.; Shu, J.; Shi, S.; Nie, J.; Ma, G. Hemp Derived N-Doped Highly Porous Carbon Containing Co Nanoparticles as Electrocatalyst for Oxygen Reduction Reaction. *J. Colloid Interface Sci.* **2020**, *559*, 21−28.
(214) Ma, G.; Zhang, Z.; Sun, K.; Peng, H.; Yang, Q.; Ran, F.; Lei, Z. White Clover Based Nitrogen-Doped Porous Carbon for a High Energy Density Supercapacitor Electrode. *RSC Adv.* **2015**, *5*, 107707−107715.
(215) Wang, H.; Yu, W.; Shi, J.; Mao, N.; Chen, S.; Liu, W. Biomass Derived Hierarchical Porous Carbons as High-Performance Anodes for Sodium-Ion Batteries. *Electrochim. Acta* **2016**, *188*, 103−110.
(216) You, X.-l.; Liu, L.-j.; Zhang, M.-y.; Walle, M. D.; Li, Y.; Liu, Y.-N. Novel Biomass Derived Hierarchical Porous Carbon for Lithium Sulfur Batteries. *Mater. Lett.* **2018**, *217*, 167−170.
(217) Alonso-Lemus, I. L.; Escobar-Morales, B.; Rodríguez-Varela, F. J.; González-Quijano, D.; Lardizabal, D.; Pacheco-Saucedo, K.; de la Torre Saenz, L. Synthesis of Metal-Free Electrocatalyst Obtained from Different Biomass Sources with High Performance for Oxygen Reduction Reaction in Fuel Cells. *ECS Trans.* **2016**, *75*, 1035−1040.
(218) Yang, W.; Du, Z.; Ma, Z.; Wang, G.; Bai, H.; Shao, G. Facile Synthesis of Nitrogen-Doped Hierarchical Porous Lamellar Carbon for High-Performance Supercapacitors. *RSC Adv.* **2016**, *6*, 3942−3950.
(219) Luo, J.; Li, L.; Liu, X.A kind of method for preparing efficient oxygen reduction catalyst as substrate with insect wing. CN 106848332 A, 2017
(220) Feng, J.; Cai, R.; Magliocca, E.; Luo, H.; Higgins, L.; Romario, G. L. F.; Liang, X.; Pedersen, A.; Xu, Z.; Guo, Z.; et al. Iron, Nitrogen Co-Doped Carbon Spheres as Low Cost, Scalable Electrocatalysts for the Oxygen Reduction Reaction. *Adv. Funct. Mater.* **2021**, *31*, 2102974.
(221) Titirici, M. Defects Win over Pyridinic Sites. *Nat. Catal.* **2019**, *2*, 642−643.
(222) Jiao, Y.; Zheng, Y.; Jaroniec, M.; Qiao, S. Z. Origin of the Electrocatalytic Oxygen Reduction Activity of Graphene-Based Catalysts: A Roadmap to Achieve the Best Performance. *J. Am. Chem. Soc.* **2014**, *136*, 4394−4403.
(223) Yang, L.; Shui, J.; Du, L.; Shao, Y.; Liu, J.; Dai, L.; Hu, Z. Carbon-Based Metal-Free ORR Electrocatalysts for Fuel Cells: Past, Present, and Future. *Adv. Mater.* **2019**, *31*, 1804799.
(224) Fellinger, T.-P.; Hasché, F.; Strasser, P.; Antonietti, M. Mesoporous Nitrogen-Doped Carbon for the Electrocatalytic Synthesis of Hydrogen Peroxide. *J. Am. Chem. Soc.* **2012**, *134*, 4072−4075.
(225) Patel, M. A.; Luo, F.; Khoshi, M. R.; Rabie, E.; Zhang, Q.; Flach, C. R.; Mendelsohn, R.; Garfunkel, E.; Szostak, M.; He, H. P-Doped

https://doi.org/10.1021/acs.chemrev.2c00429
Chem. Rev. 2023, 123, 2311−2348

Porous Carbon as Metal Free Catalysts for Selective Aerobic Oxidation with an Unexpected Mechanism. *ACS Nano* **2016**, *10*, 2305−2315.
(226) Sun, Y.; Li, S.; Paul, B.; Han, L.; Strasser, P. Highly Efficient Electrochemical Production of Hydrogen Peroxide over Nitrogen and Phosphorus Dual-Doped Carbon Nanosheet in Alkaline Medium. *J. Electroanal. Chem.* **2021**, *896*, 115197.
(227) Melchionna, M.; Fornasiero, P.; Prato, M. The Rise of Hydrogen Peroxide as the Main Product by Metal-Free Catalysis in Oxygen Reductions. *Adv. Mater.* **2019**, *31*, 1802920.
(228) Vassilev, S. V.; Baxter, D.; Andersen, L. K.; Vassileva, C. G. An Overview of the Chemical Composition of Biomass. *Fuel* **2010**, *89*, 913−933.
(229) Zhao, L.; Zhang, Y.; Huang, L.-B.; Liu, X.-Z.; Zhang, Q.-H.; He, C.; Wu, Z.-Y.; Zhang, L.-J.; Wu, J.; Yang, W.; et al. Cascade Anchoring Strategy for General Mass Production of High-Loading Single-Atomic Metal-Nitrogen Catalysts. *Nat. Commun.* **2019**, *10*, 1278.
(230) Du, L.; Zhang, G.; Liu, X.; Hassanpour, A.; Dubois, M.; Tavares, A. C.; Sun, S. Biomass-Derived Nonprecious Metal Catalysts for Oxygen Reduction Reaction: The Demand-Oriented Engineering of Active Sites and Structures. *Carbon Energy* **2020**, *2*, 561−581.
(231) Ou, H.; Wang, D.; Li, Y. How to Select Effective Electrocatalysts: Nano or Single Atom? *Nano Sel.* **2021**, *2*, 492−511.
(232) Leonard, N. D.; Wagner, S.; Luo, F.; Steinberg, J.; Ju, W.; Weidler, N.; Wang, H.; Kramm, U. I.; Strasser, P. Deconvolution of Utilization, Site Density, and Turnover Frequency of Fe-Nitrogen-Carbon Oxygen Reduction Reaction Catalysts Prepared with Secondary N-Precursors. *ACS Catal.* **2018**, *8*, 1640−1647.
(233) Lu, Z.; Wang, B.; Hu, Y.; Liu, W.; Zhao, Y.; Yang, R.; Li, Z.; Luo, J.; Chi, B.; Jiang, Z.; et al. An Isolated Zinc-Cobalt Atomic Pair for Highly Active and Durable Oxygen Reduction. *Angew. Chem., Int. Ed.* **2019**, *58*, 2622−2626.
(234) James, B. D.; Huya-Kouadio, J. M.; Houchins, C.; DeSantis, D. A.Mass Production Cost Estimation of Direct H2 PEM Fuel Cell Systems for Transportation Applications: 2018 Update; Strategic Analysis Inc.: Arlington, VA, **2018**.
(235) Liu, S.; Li, C.; Zachman, M. J.; Zeng, Y.; Yu, H.; Li, B.; Wang, M.; Braaten, J.; Liu, J.; Meyer, H. M.; et al. Atomically Dispersed Iron Sites with a Nitrogen-Carbon Coating as Highly Active and Durable Oxygen Reduction Catalysts for Fuel Cells. *Nat. Energy* **2022**, *7*, 652−663.
(236) Ali, G.; Sharma, M.; Salama, E.-S.; Ling, Z.; Li, X. Applications of Chitin and Chitosan as Natural Biopolymer: Potential Sources, Pretreatments, and Degradation Pathways. *Biomass Convers. Biorefin.* **2022**, DOI: 10.1007/s13399-022-02684-x.
(237) Bonecco, M. B.; Martínez Sáenz, M. G.; Buffa, L. M.Chitosan, From Residue to Industry. In *Advances in Physicochemical Properties of Biopolymers*, Part 2; Masuelli, M., Renard, D., Eds.; Bentham Science Publishers: Sharjah, UAE, 2017; pp 224−256.
(238) Yan, N.; Chen, X. Sustainability: Don't Waste Seafood Waste. *Nature* **2015**, *524*, 155−157.
(239) Zagal, J. H.; Koper, M. T. M. Reactivity Descriptors for the Activity of Molecular MN4 Catalysts for the Oxygen Reduction Reaction. *Angew. Chem., Int. Ed.* **2016**, *55*, 14510−14521.
(240) Kumar, A.; Ibraheem, S.; Anh Nguyen, T.; Gupta, R. K.; Maiyalagan, T.; Yasin, G. Molecular-MN4 vs Atomically Dispersed M-N4-C Electrocatalysts for Oxygen Reduction Reaction. *Coord. Chem. Rev.* **2021**, *446*, 214122.
(241) Titirici, M.-M.; Antonietti, M.; Thomas, A. A Generalized Synthesis of Metal Oxide Hollow Spheres Using a Hydrothermal Approach. *Chem. Mater.* **2006**, *18*, 3808−3812.
(242) Wei, J.; Liang, Y.; Hu, Y.; Kong, B.; Simon, G. P.; Zhang, J.; Jiang, S. P.; Wang, H. A Versatile Iron-Tannin-Framework Ink Coating Strategy to Fabricate Biomass-Derived Iron Carbide/Fe-N-Carbon Catalysts for Efficient Oxygen Reduction. *Angew. Chem., Int. Ed.* **2016**, *55*, 1355−1359.
(243) Mehmood, A.; Pampel, J.; Ali, G.; Ha, H. Y.; Ruiz-Zepeda, F.; Fellinger, T.-P. Facile Metal Coordination of Active Site Imprinted Nitrogen Doped Carbons for the Conservative Preparation of Non-Noble Metal Oxygen Reduction Electrocatalysts. *Adv. Energy Mater.* **2018**, *8*, 1701771.
(244) Menga, D.; Ruiz-Zepeda, F.; Moriau, L.; Šala, M.; Wagner, F.; Koyutürk, B.; Bele, M.; Petek, U.; Hodnik, N.; Gaberšček, M.; Fellinger, T. Active-Site Imprinting: Preparation of Fe-N-C Catalysts from Zinc Ion-Templated Ionothermal Nitrogen-Doped Carbons. *Adv. Energy Mater.* **2019**, *9*, 1902412.
(245) Menga, D.; Low, J. L.; Li, Y.-S.; Arčon, I.; Koyutürk, B.; Wagner, F.; Ruiz-Zepeda, F.; Gaberšček, M.; Paulus, B.; Fellinger, T.-P. Resolving the Dilemma of Fe-N-C Catalysts by the Selective Synthesis of Tetrapyrrolic Active Sites via an Imprinting Strategy. *J. Am. Chem. Soc.* **2021**, *143*, 18010−18019.
(246) Barrio, J.; Pedersen, A.; Feng, J.; Sarma, S. C.; Wang, M.; Li, A. Y.; Yadegari, H.; Luo, H.; Ryan, M. P.; Titirici, M.-M.; et al. Metal Coordination in C 2 N-like Materials towards Dual Atom Catalysts for Oxygen Reduction. *J. Mater. Chem. A* **2022**, *10*, 6023−6030.
(247) Fei, H.; Dong, J.; Feng, Y.; Allen, C. S.; Wan, C.; Volosskiy, B.; Li, M.; Zhao, Z.; Wang, Y.; Sun, H.; et al. General Synthesis and Definitive Structural Identification of MN4C4 Single-Atom Catalysts with Tunable Electrocatalytic Activities. *Nat. Catal.* **2018**, *1*, 63−72.
(248) Li, J.; Jiao, L.; Wegener, E.; Richard, L. L.; Liu, E.; Zitolo, A.; Sougrati, M. T.; Mukerjee, S.; Zhao, Z.; Huang, Y. Evolution Pathway from Iron Compounds to $Fe_1(II)$-N_4 Sites through Gas-Phase Iron during Pyrolysis. *J. Am. Chem. Soc.* **2020**, *142*, 1417−1423.
(249) Li, J.; Sougrati, M. T.; Zitolo, A.; Ablett, J. M.; Oğuz, I. C.; Mineva, T.; Matanovic, I.; Atanassov, P.; Huang, Y.; Zenyuk, I.; et al. Identification of Durable and Non-Durable FeNx Sites in Fe-N-C Materials for Proton Exchange Membrane Fuel Cells. *Nat. Catal.* **2021**, *4*, 10−19.
(250) Mao, K.; Yang, L.; Wang, X.; Wu, Q.; Hu, Z. Identifying Iron-Nitrogen/Carbon Active Structures for Oxygen Reduction Reaction under the Effect of Electrode Potential. *J. Phys. Chem. Lett.* **2020**, *11*, 2896−2901.
(251) Zalitis, C. M.; Sharman, J.; Wright, E.; Kucernak, A. R. Properties of the Hydrogen Oxidation Reaction on Pt/C Catalysts at Optimised High Mass Transport Conditions and Its Relevance to the Anode Reaction in PEFCs and Cathode Reactions in Electrolysers. *Electrochim. Acta* **2015**, *176*, 763−776.
(252) Zalitis, C. M.; Kramer, D.; Kucernak, A. R. Electrocatalytic Performance of Fuel Cell Reactions at Low Catalyst Loading and High Mass Transport. *Phys. Chem. Chem. Phys.* **2013**, *15*, 4329−4340.
(253) Jaouen, F.; Jones, D.; Coutard, N.; Artero, V.; Strasser, P.; Kucernak, A. Toward Platinum Group Metal-Free Catalysts for Hydrogen/Air Proton-Exchange Membrane Fuel Cells. *Johnson Matthey Technol. Rev.* **2018**, *62*, 231−255.
(254) Tran, P. D.; Le Goff, A.; Heidkamp, J.; Jousselme, B.; Guillet, N.; Palacin, S.; Dau, H.; Fontecave, M.; Artero, V. Noncovalent Modification of Carbon Nanotubes with Pyrene-Functionalized Nickel Complexes: Carbon Monoxide Tolerant Catalysts for Hydrogen Evolution and Uptake. *Angew. Chem., Int. Ed.* **2011**, *50*, 1371−1374.
(255) Gentil, S.; Lalaoui, N.; Dutta, A.; Nedellec, Y.; Cosnier, S.; Shaw, W. J.; Artero, V.; Le Goff, A. Carbon-Nanotube-Supported Bio-Inspired Nickel Catalyst and Its Integration in Hybrid Hydrogen/Air Fuel Cells. *Angew. Chem., Int. Ed.* **2017**, *56*, 1845−1849.
(256) Schild, J.; Reuillard, B.; Morozan, A.; Chenevier, P.; Gravel, E.; Doris, E.; Artero, V. Approaching Industrially Relevant Current Densities for Hydrogen Oxidation with a Bioinspired Molecular Catalytic Material. *J. Am. Chem. Soc.* **2021**, *143*, 18150−18158.
(257) Davydova, E. S.; Mukerjee, S.; Jaouen, F.; Dekel, D. R. Electrocatalysts for Hydrogen Oxidation Reaction in Alkaline Electrolytes. *ACS Catal.* **2018**, *8*, 6665−6690.
(258) Jaouen, F.; Proietti, E.; Lefèvre, M.; Chenitz, R.; Dodelet, J.-P.; Wu, G.; Chung, H. T.; Johnston, C. M.; Zelenay, P. Recent Advances in Non-Precious Metal Catalysis for Oxygen-Reduction Reaction in Polymer Electrolyte Fuel Cells. *Energy Environ. Sci.* **2011**, *4*, 114−130.
(259) Wikström, M.; Krab, K.; Sharma, V. Oxygen Activation and Energy Conservation by Cytochrome c Oxidase. *Chem. Rev.* **2018**, *118*, 2469−2490.

(260) Dey, S.; Mondal, B.; Chatterjee, S.; Rana, A.; Amanullah, S.; Dey, A. Molecular Electrocatalysts for the Oxygen Reduction Reaction. *Nat. Rev. Chem.* **2017**, *1*, 0098.
(261) Kato, M.; Yagi, I. Electrocatalytic Oxygen Reduction at Multinuclear Metal Active Sites Inspired by Metalloenzymes. *e-Journal Surf. Sci. Nanotechnol.* **2020**, *18*, 81−93.
(262) Hayashi, T.Iron: Heme Proteins & Dioxygen Transport & Storage. In *Encyclopedia of Inorganic and Bioinorganic Chemistry*; Wiley2011.
(263) Cheon, J. Y.; Kim, T.; Choi, Y.; Jeong, H. Y.; Kim, M. G.; Sa, Y. J.; Kim, J.; Lee, Z.; Yang, T.-H.; Kwon, K.; et al. Ordered Mesoporous Porphyrinic Carbons with Very High Electrocatalytic Activity for the Oxygen Reduction Reaction. *Sci. Rep.* **2013**, *3*, 2715.
(264) Zhang, Z.; Yang, S.; Dou, M.; Liu, H.; Gu, L.; Wang, F. Systematic Study of Transition-Metal (Fe, Co, Ni, Cu) Phthalocyanines as Electrocatalysts for Oxygen Reduction and Their Evaluation by DFT. *RSC Adv.* **2016**, *6*, 67049−67056.
(265) Mihara, N.; Yamada, Y.; Takaya, H.; Kitagawa, Y.; Aoyama, S.; Igawa, K.; Tomooka, K.; Tanaka, K. Oxygen Reduction to Water by a Cofacial Dimer of Iron(III)-Porphyrin and Iron(III)-Phthalocyanine Linked through a Highly Flexible Fourfold Rotaxane. *Chem. -Eur. J.* **2017**, *23*, 7508−7514.
(266) Collman, J. P.; Denisevich, P.; Konai, Y.; Marrocco, M.; Koval, C.; Anson, F. C. Electrode Catalysis of the Four-Electron Reduction of Oxygen to Water by Dicobalt Face-to-Face Porphyrins. *J. Am. Chem. Soc.* **1980**, *102*, 6027−6036.
(267) Sun, Y.; Silvioli, L.; Sahraie, N. R.; Ju, W.; Li, J.; Zitolo, A.; Li, S.; Bagger, A.; Arnarson, L.; Wang, X.; et al. Activity-Selectivity Trends in the Electrochemical Production of Hydrogen Peroxide over Single-Site Metal-Nitrogen-Carbon Catalysts. *J. Am. Chem. Soc.* **2019**, *141*, 12372−12381.
(268) Venegas, R.; Recio, F. J.; Zuñiga, C.; Viera, M.; Oyarzún, M.-P.; Silva, N.; Neira, K.; Marco, J. F.; Zagal, J. H.; Tasca, F. Comparison of the Catalytic Activity for O2 Reduction of Fe and Co MN4 Adsorbed on Graphite Electrodes and on Carbon Nanotubes. *Phys. Chem. Chem. Phys.* **2017**, *19*, 20441−20450.
(269) Marshall-Roth, T.; Libretto, N. J.; Wrobel, A. T.; Anderton, K. J.; Pegis, M. L.; Ricke, N. D.; Van Voorhis, T.; Miller, J. T.; Surendranath, Y. A Pyridinic Fe-N_4 Macrocycle Models the Active Sites in Fe/N-Doped Carbon Electrocatalysts. *Nat. Commun.* **2020**, *11*, 5283.
(270) Abarca, G.; Viera, M.; Aliaga, C.; Marco, J. F.; Orellana, W.; Zagal, J. H.; Tasca, F. In Search of the Most Active MN4 Catalyst for the Oxygen Reduction Reaction. The Case of Perfluorinated Fe Phthalocyanine. *J. Mater. Chem. A* **2019**, *7*, 24776−24783.
(271) Riquelme, J.; Neira, K.; Marco, J. F.; Hermosilla-Ibáñez, P.; Orellana, W.; Zagal, J. H.; Tasca, F. Biomimicking Vitamin B12. A Co Phthalocyanine Pyridine Axial Ligand Coordinated Catalyst for the Oxygen Reduction Reaction. *Electrochim. Acta* **2018**, *265*, 547−555.
(272) Chen, K.; Liu, K.; An, P.; Li, H.; Lin, Y.; Hu, J.; Jia, C.; Fu, J.; Li, H.; Liu, H.; et al. Iron Phthalocyanine with Coordination Induced Electronic Localization to Boost Oxygen Reduction Reaction. *Nat. Commun.* **2020**, *11*, 4173.
(273) Cao, R.; Thapa, R.; Kim, H.; Xu, X.; Gyu Kim, M.; Li, Q.; Park, N.; Liu, M.; Cho, J. Promotion of Oxygen Reduction by a Bio-Inspired Tethered Iron Phthalocyanine Carbon Nanotube-Based Catalyst. *Nat. Commun.* **2013**, *4*, 2076.
(274) Venegas, R.; Recio, F. J.; Riquelme, J.; Neira, K.; Marco, J. F.; Ponce, I.; Zagal, J. H.; Tasca, F. Biomimetic Reduction of O2 in an Acid Medium on Iron Phthalocyanines Axially Coordinated to Pyridine Anchored on Carbon Nanotubes. *J. Mater. Chem. A* **2017**, *5*, 12054−12059.
(275) Govan, J.; Orellana, W.; Zagal, J. H.; Tasca, F. Penta-Coordinated Transition Metal Macrocycles as Electrocatalysts for the Oxygen Reduction Reaction. *J. Solid State Electrochem.* **2021**, *25*, 15−31.
(276) Meng, Y.; Yin, C.; Li, K.; Tang, H.; Wang, Y.; Wu, Z. Improved Oxygen Reduction Activity in Heteronuclear FeCo-Codoped Graphene: A Theoretical Study. *ACS Sustain. Chem. Eng.* **2019**, *7*, 17273−17281.
(277) Yoshikawa, S.; Shinzawa-Itoh, K.; Nakashima, R.; Yaono, R.; Yamashita, E.; Inoue, N.; Yao, M.; Fei, M. J.; Libeu, C. P.; Mizushima, T.; et al. Redox-Coupled Crystal Structural Changes in Bovine Heart Cytochrome c Oxidase. *Science* **1998**, *280*, 1723−1729.
(278) Tsukihara, T.; Aoyama, H.; Yamashita, E.; Tomizaki, T.; Yamaguchi, H.; Shinzawa-Itoh, K.; Nakashima, R.; Yaono, R.; Yoshikawa, S. The Whole Structure of the 13-Subunit Oxidized Cytochrome c Oxidase at 2.8 Å. *Science* **1996**, *272*, 1136−1144. PDB ID 1OCC.
(279) Titirici, M.; Baird, S. G.; Sparks, T. D.; Yang, S. M.; Brandt-Talbot, A.; Hosseinaei, O.; Harper, D. P.; Parker, R. M.; Vignolini, S.; Berglund, L. A.; et al. The Sustainable Materials Roadmap. *J. Phys. Mater.* **2022**, *5*, 032001.
(280) Gasteiger, H. A.; Marković, N. M. Just a Dream—or Future Reality? *Science* **2009**, *324*, 48−49.
(281) Gasteiger, H. A.; Kocha, S. S.; Sompalli, B.; Wagner, F. T. Activity Benchmarks and Requirements for Pt, Pt-Alloy, and Non-Pt Oxygen Reduction Catalysts for PEMFCs. *Appl. Catal. B Environ.* **2005**, *56*, 9−35.
(282) Vojvodic, A.; Nørskov, J. K. New Design Paradigm for Heterogeneous Catalysts. *Natl. Sci. Rev.* **2015**, *2*, 140−143.
(283) Peljo, P.; Murtomäki, L.; Kallio, T.; Xu, H.-J.; Meyer, M.; Gros, C. P.; Barbe, J.-M.; Girault, H. H.; Laasonen, K.; Kontturi, K. Biomimetic Oxygen Reduction by Cofacial Porphyrins at a Liquid-Liquid Interface. *J. Am. Chem. Soc.* **2012**, *134*, 5974−5984.
(284) Collman, J. P.; Marrocco, M.; Denisevich, P.; Koval, C.; Anson, F. C. Potent Catalysis of the Electroreduction of Oxygen to Water by Dicobalt Porphyrin Dimers Adsorbed on Graphite Electrodes. *J. Electroanal. Chem.* **1979**, *101*, 117−122.
(285) Wan, H.; Østergaard, T. M.; Arnarson, L.; Rossmeisl, J. Climbing the 3D Volcano for the Oxygen Reduction Reaction Using Porphyrin Motifs. *ACS Sustain. Chem. Eng.* **2019**, *7*, 611−617.
(286) Cichocka, M. O.; Liang, Z.; Feng, D.; Back, S.; Siahrostami, S.; Wang, X.; Samperisi, L.; Sun, Y.; Xu, H.; Hedin, N.; et al. A Porphyrinic Zirconium Metal-Organic Framework for Oxygen Reduction Reaction: Tailoring the Spacing between Active-Sites through Chain-Based Inorganic Building Units. *J. Am. Chem. Soc.* **2020**, *142*, 15386−15395.
(287) Sours, T.; Patel, A.; Nørskov, J.; Siahrostami, S.; Kulkarni, A. Circumventing Scaling Relations in Oxygen Electrochemistry Using Metal-Organic Frameworks. *J. Phys. Chem. Lett.* **2020**, *11*, 10029−10036.
(288) Yoshii, T.; Chida, K.; Nishihara, H.; Tani, F. Ordered Carbonaceous Frameworks: A New Class of Carbon Materials with Molecular-Level Design. *Chem. Commun.* **2022**, *58*, 3578−3590.
(289) Nishihara, H.; Hirota, T.; Matsuura, K.; Ohwada, M.; Hoshino, N.; Akutagawa, T.; Higuchi, T.; Jinnai, H.; Koseki, Y.; Kasai, H.; et al. Synthesis of Ordered Carbonaceous Frameworks from Organic Crystals. *Nat. Commun.* **2017**, *8*, 109.
(290) Svane, K. L.; Hansen, H. A.; Vegge, T. A Comparison of Single and Double Co Sites Incorporated in N-Doped Graphene for the Oxygen Reduction Reaction. *J. Catal.* **2021**, *393*, 230−237.
(291) Xiao, M.; Zhang, H.; Chen, Y.; Zhu, J.; Gao, L.; Jin, Z.; Ge, J.; Jiang, Z.; Chen, S.; Liu, C.; Xing, W. Identification of Binuclear Co2N5 Active Sites for Oxygen Reduction Reaction with More than One Magnitude Higher Activity than Single Atom CoN4 Site. *Nano Energy* **2018**, *46*, 396−403.
(292) Wang, J.; Liu, W.; Luo, G.; Li, Z.; Zhao, C. C.; Zhang, H.; Zhu, M.; Xu, Q.; Wang, X.; Zhao, C. C.; et al. Synergistic Effect of Well-Defined Dual Sites Boosting the Oxygen Reduction Reaction. *Energy Environ. Sci.* **2018**, *11*, 3375−3379.
(293) Xiao, M.; Chen, Y.; Zhu, J.; Zhang, H.; Zhao, X.; Gao, L.; Wang, X.; Zhao, J.; Ge, J.; Jiang, Z.; et al. Climbing the Apex of the ORR Volcano Plot via Binuclear Site Construction: Electronic and Geometric Engineering. *J. Am. Chem. Soc.* **2019**, *141*, 17763−17770.
(294) Wang, J.; Huang, Z.; Liu, W.; Chang, C.; Tang, H.; Li, Z.; Chen, W.; Jia, C.; Yao, T.; Wei, S.; et al. Design of N-Coordinated Dual-Metal

Sites: A Stable and Active Pt-Free Catalyst for Acidic Oxygen Reduction Reaction. *J. Am. Chem. Soc.* **2017**, *139*, 17281−17284.
(295) Liu, D.; Wang, B.; Li, H.; Huang, S.; Liu, M.; Wang, J.; Wang, Q.; Zhang, J.; Zhao, Y. Distinguished Zn,Co-Nx-C-Sy Active Sites Confined in Dentric Carbon for Highly Efficient Oxygen Reduction Reaction and Flexible Zn-Air Batteries. *Nano Energy* **2019**, *58*, 277−283.
(296) Ye, W.; Chen, S.; Lin, Y.; Yang, L.; Chen, S.; Zheng, X.; Qi, Z.; Wang, C.; Long, R.; Chen, M.; et al. Precisely Tuning the Number of Fe Atoms in Clusters on N-Doped Carbon toward Acidic Oxygen Reduction Reaction. *Chem.* **2019**, *5*, 2865−2878.
(297) Smits, N. W. G.; Rademaker, D.; Konovalov, A. I.; Siegler, M. A.; Hetterscheid, D. G. H. Influence of the Spatial Distribution of Copper Sites on the Selectivity of the Oxygen Reduction Reaction. *Dalt. Trans.* **2022**, *51*, 1206−1215.
(298) Xi, Y. T.; Wei, P. J.; Wang, R. C.; Liu, J. G. Bio-Inspired Multinuclear Copper Complexes Covalently Immobilized on Reduced Graphene Oxide as Efficient Electrocatalysts for the Oxygen Reduction Reaction. *Chem. Commun.* **2015**, *51*, 7455−7458.
(299) Mukherjee, S.; Mukherjee, A.; Bhagi-Damodaran, A.; Mukherjee, M.; Lu, Y.; Dey, A. A Biosynthetic Model of Cytochrome c Oxidase as an Electrocatalyst for Oxygen Reduction. *Nat. Commun.* **2015**, *6*, 8467.
(300) Mano, N.; Soukharev, V.; Heller, A. A Laccase-Wiring Redox Hydrogel for Efficient Catalysis of O2 Electroreduction. *J. Phys. Chem. B* **2006**, *110*, 11180−11187.
(301) Xiao, X.; Xia, H.; Wu, R.; Bai, L.; Yan, L.; Magner, E.; Cosnier, S.; Lojou, E.; Zhu, Z.; Liu, A. Tackling the Challenges of Enzymatic (Bio)Fuel Cells. *Chem. Rev.* **2019**, *119*, 9509−9558.
(302) Gonzalez-Solino, C.; Lorenzo, M. Enzymatic Fuel Cells: Towards Self-Powered Implantable and Wearable Diagnostics. *Biosensors* **2018**, *8*, 11.
(303) Jeon, W.-Y.; Lee, J.-H.; Dashnyam, K.; Choi, Y.-B.; Kim, T.-H.; Lee, H.-H.; Kim, H.-W.; Kim, H.-H. Performance of a Glucose-Reactive Enzyme-Based Biofuel Cell System for Biomedical Applications. *Sci. Rep.* **2019**, *9*, 10872.
(304) Primbs, M.; Sun, Y.; Roy, A.; Malko, D.; Mehmood, A.; Sougrati, M.-T.; Blanchard, P.-Y.; Granozzi, G.; Kosmala, T.; Daniel, G.; et al. Establishing Reactivity Descriptors for Platinum Group Metal (PGM)-Free Fe-N-C Catalysts for PEM Fuel Cells. *Energy Environ. Sci.* **2020**, *13*, 2480−2500.
(305) Malko, D.; Kucernak, A.; Lopes, T. In Situ Electrochemical Quantification of Active Sites in Fe-N/C Non-Precious Metal Catalysts. *Nat. Commun.* **2016**, *7*, 13285.
(306) Luo, F.; Choi, C. H.; Primbs, M. J. M.; Ju, W.; Li, S.; Leonard, N. D.; Thomas, A.; Jaouen, F.; Strasser, P. Accurate Evaluation of Active-Site Density (SD) and Turnover Frequency (TOF) of PGM-Free Metal-Nitrogen-Doped Carbon (MNC) Electrocatalysts Using CO Cryo Adsorption. *ACS Catal.* **2019**, *9*, 4841−4852.
(307) Bae, G.; Kim, H.; Choi, H.; Jeong, P.; Kim, D. H.; Kwon, H. C.; Lee, K.-S.; Choi, M.; Oh, H.-S.; Jaouen, F.; et al. Quantification of Active Site Density and Turnover Frequency: From Single-Atom Metal to Nanoparticle Electrocatalysts. *JACS Au* **2021**, *1*, 586−597.
(308) Thompson, S. T.; Wilson, A. R.; Zelenay, P.; Myers, D. J.; More, K. L.; Neyerlin, K. C.; Papageorgopoulos, D. ElectroCat: DOE's Approach to PGM-Free Catalyst and Electrode R&D. *Solid State Ionics* **2018**, *319*, 68−76.
(309) US Department of Energy. *ElectroCat Consortium*. https://www.electrocat.org/.
(310) *Critical Raw material ElectrocatalystS replacement ENabling Designed pOst-2020 PEMFC*. European Commission. DOI: 10.3030/779366.
(311) *PEMFC based on platinum Group metAl free StrUctured cathodeS*. European Commission. DOI: 10.3030/779550.
(312) Office of Energy Efficiency and Renewable Energy. 3.4 Fuel Cells, 2016. In *Fuel Cell Technologies Office: Multi-Year Research, Development, and Demonstration Plan*; U.S. Department of Energy: Washington, D.C., 2016.
(313) Banham, D.; Kishimoto, T.; Zhou, Y.; Sato, T.; Bai, K.; Ozaki, J.; Imashiro, Y.; Ye, S. Critical Advancements in Achieving High Power and Stable Nonprecious Metal Catalyst-Based MEAs for Real-World Proton Exchange Membrane Fuel Cell Applications. *Sci. Adv.* **2018**, *4*, No. eaar7180.
(314) Ehelebe, K.; Ashraf, T.; Hager, S.; Seeberger, D.; Thiele, S.; Cherevko, S. Fuel Cell Catalyst Layer Evaluation Using a Gas Diffusion Electrode Half-Cell: Oxygen Reduction Reaction on Fe-N-C in Alkaline Media. *Electrochem. commun.* **2020**, *116*, 106761.
(315) Yang, N.; Peng, L.; Li, L.; Li, J.; Liao, Q.; Shao, M.; Wei, Z. Theoretically Probing the Possible Degradation Mechanisms of an FeNC Catalyst during the Oxygen Reduction Reaction. *Chem. Sci.* **2021**, *12*, 12476−12484.
(316) Xia, D.; Yu, C.; Zhao, Y.; Wei, Y.; Wu, H.; Kang, Y.; Li, J.; Gan, L.; Kang, F. Degradation and Regeneration of Fe-N x Active Sites for the Oxygen Reduction Reaction: The Role of Surface Oxidation, Fe Demetallation and Local Carbon Microporosity. *Chem. Sci.* **2021**, *12*, 11576−11584.
(317) Boldrin, P.; Malko, D.; Mehmood, A.; Kramm, U. I.; Wagner, S.; Paul, S.; Weidler, N.; Kucernak, A. Deactivation, Reactivation and Super-Activation of Fe-N/C Oxygen Reduction Electrocatalysts: Gas Sorption, Physical and Electrochemical Investigation Using NO and O2. *Appl. Catal. B Environ.* **2021**, *292*, 120169.
(318) Messerschmidt, A.; Luecke, H.; Huber, R. X-Ray Structures and Mechanistic Implications of Three Functional Derivatives of Ascorbate Oxidase from Zucchini. *J. Mol. Biol.* **1993**, *230*, 997−1014.
(319) Lee, S. K.; George, S. D. B.; Antholine, W. E.; Hedman, B.; Hodgson, K. O.; Solomon, E. I. Nature of the Intermediate Formed in the Reduction of O2 to H2O at the Trinuclear Copper Cluster Active Site in Native Laccase. *J. Am. Chem. Soc.* **2002**, *124*, 6180−6193.
(320) U.S. Department of State*Leaders Summit on Climate: Day 1*; U.S. Department of State: Washington, D.C., 2021.
(321) Fernández, J. R.; Garcia, S.; Sanz-Pérez, E. S. CO2 Capture and Utilization Editorial. *Ind. Eng. Chem. Res.* **2020**, *59*, 6767−6772.
(322) Leonzio, G.; Foscolo, P. U.; Zondervan, E.; Bogle, I. D. L. Scenario Analysis of Carbon Capture, Utilization (Particularly Producing Methane and Methanol), and Storage (CCUS) Systems. *Ind. Eng. Chem. Res.* **2020**, *59*, 6961−6976.
(323) Kuhl, K. P.; Cave, E. R.; Abram, D. N.; Jaramillo, T. F. New Insights into the Electrochemical Reduction of Carbon Dioxide on Metallic Copper Surfaces. *Energy Environ. Sci.* **2012**, *5*, 7050−7059.
(324) Hori, Y.; Murata, A.; Takahashi, R. Formation of Hydrocarbons in the Electrochemical Reduction of Carbon Dioxide at a Copper Electrode in Aqueous Solution. *J. Chem. Soc. Faraday Trans. 1 Phys. Chem. Condens. Phases* **1989**, *85*, 2309−2326.
(325) Fan, L.; Xia, C.; Yang, F.; Wang, J.; Wang, H.; Lu, Y. Strategies in Catalysts and Electrolyzer Design for Electrochemical CO_2 Reduction toward C_{2+} Products. *Sci. Adv.* **2020**, *6*, No. eaay3111.
(326) Mezzavilla, S.; Horch, S.; Stephens, I. E. L.; Seger, B.; Chorkendorff, I. Structure Sensitivity in the Electrocatalytic Reduction of CO2 with Gold Catalysts. *Angew. Chemie Int. Ed.* **2019**, *58*, 3774−3778.
(327) Kim, C.; Eom, T.; Jee, M. S.; Jung, H.; Kim, H.; Min, B. K.; Hwang, Y. J. Insight into Electrochemical CO 2 Reduction on Surface-Molecule-Mediated Ag Nanoparticles. *ACS Catal.* **2017**, *7*, 779−785.
(328) Zhao, K.; Quan, X. Carbon-Based Materials for Electrochemical Reduction of CO 2 to C 2+ Oxygenates: Recent Progress and Remaining Challenges. *ACS Catal.* **2021**, *11*, 2076−2097.
(329) Jia, C.; Dastafkan, K.; Ren, W.; Yang, W.; Zhao, C. Carbon-Based Catalysts for Electrochemical CO2 Reduction. *Sustain. Energy Fuels* **2019**, *3*, 2890−2906.
(330) Cui, H.; Guo, Y.; Guo, L.; Wang, L.; Zhou, Z.; Peng, Z. Heteroatom-Doped Carbon Materials and Their Composites as Electrocatalysts for CO2 Reduction. *J. Mater. Chem. A* **2018**, *6*, 18782−18793.
(331) Barrio, J.; Volokh, M.; Shalom, M. Polymeric Carbon Nitrides and Related Metal-Free Materials for Energy and Environmental Applications. *J. Mater. Chem. A* **2020**, *8*, 11075−11116.

(332) Paraknowitsch, J. P.; Thomas, A. Doping Carbons beyond Nitrogen: An Overview of Advanced Heteroatom Doped Carbons with Boron, Sulphur and Phosphorus for Energy Applications. *Energy Environ. Sci.* **2013**, *6*, 2839−2855.
(333) Oates, R. P.; Murawski, J.; Hor, C.; Shen, X.; Weber, D. J.; Oezaslan, M.; Shaffer, M. S. P.; Stephens, I. E. L. How to Minimise Hydrogen Evolution on Carbon Based Materials? *J. Electrochem. Soc.* **2022**, *169*, 054516.
(334) Song, Y.; Wang, S.; Chen, W.; Li, S.; Feng, G.; Wei, W.; Sun, Y. Enhanced Ethanol Production from CO2 Electroreduction at Micropores in Nitrogen-Doped Mesoporous Carbon. *ChemSusChem* **2020**, *13*, 293−297.
(335) Nitopi, S.; Bertheussen, E.; Scott, S. B.; Liu, X.; Engstfeld, A. K.; Horch, S.; Seger, B.; Stephens, I. E. L.; Chan, K.; Hahn, C.; et al. Progress and Perspectives of Electrochemical CO 2 Reduction on Copper in Aqueous Electrolyte. *Chem. Rev.* **2019**, *119*, 7610−7672.
(336) Lum, Y.; Ager, J. W. Evidence for Product-Specific Active Sites on Oxide-Derived Cu Catalysts for Electrochemical CO2 Reduction. *Nat. Catal.* **2019**, *2*, 86−93.
(337) Fan, L.; Xia, C.; Zhu, P.; Lu, Y.; Wang, H. Electrochemical CO_2 Reduction to High-Concentration Pure Formic Acid Solutions in an All-Solid-State Reactor. *Nat. Commun.* **2020**, *11*, 3633.
(338) Zhu, P.; Wang, H. High-Purity and High-Concentration Liquid Fuels through CO2 Electroreduction. *Nat. Catal.* **2021**, *4*, 943−951.
(339) Mougel, V. Bio-Inspired Molecules and Materials: CO 2 Reduction as a Case Study. *Chim. Int. J. Chem.* **2020**, *74*, 710−715.
(340) Raaijmakers, H. C. A.; Romão, M. J. Formate-Reduced *E. coli* Formate Dehydrogenase H: The Reinterpretation of the Crystal Structure Suggests a New Reaction Mechanism. *JBIC J. Biol. Inorg. Chem.* **2006**, *11*, 849−854.
(341) Li, Y.; Gomez-Mingot, M.; Fogeron, T.; Fontecave, M. Carbon Dioxide Reduction: A Bioinspired Catalysis Approach. *Acc. Chem. Res.* **2021**, *54*, 4250−4261.
(342) Dobbek, H.; Gremer, L.; Kiefersauer, R.; Huber, R.; Meyer, O. Catalysis at a Dinuclear [CuSMo(O)OH] Cluster in a CO Dehydrogenase Resolved at 1.1-Å Resolution. *Proc. Natl. Acad. Sci. U. S. A.* **2002**, *99*, 15971−15976.
(343) Jeoung, J.-H.; Dobbek, H. Carbon Dioxide Activation at the Ni,Fe-Cluster of Anaerobic Carbon Monoxide Dehydrogenase. *Science* **2007**, *318*, 1461−1464.
(344) Mouchfiq, A.; Todorova, T. K.; Dey, S.; Fontecave, M.; Mougel, V. A Bioinspired Molybdenum-Copper Molecular Catalyst for CO2 Electroreduction. *Chem. Sci.* **2020**, *11*, 5503−5510.
(345) Gao, Y.; Zhao, F.; Wang, Q.; Zhang, Y.; Xu, B. Small Peptide Nanofibers as the Matrices of Molecular Hydrogels for Mimicking Enzymes and Enhancing the Activity of Enzymes. *Chem. Soc. Rev.* **2010**, *39*, 3425−3433.
(346) Ahmed, M. E.; Adam, S.; Saha, D.; Fize, J.; Artero, V.; Dey, A.; Duboc, C. Repurposing a Bio-Inspired NiFe Hydrogenase Model for CO2 Reduction with Selective Production of Methane as the Unique C-Based Product. *ACS Energy Lett.* **2020**, *5*, 3837−3842.
(347) Savéant, J.-M. Molecular Catalysis of Electrochemical Reactions. Mechanistic Aspects. *Chem. Rev.* **2008**, *108*, 2348−2378.
(348) Francke, R.; Schille, B.; Roemelt, M. Homogeneously Catalyzed Electroreduction of Carbon Dioxide—Methods, Mechanisms, and Catalysts. *Chem. Rev.* **2018**, *118*, 4631−4701.
(349) Varela, A. S.; Ranjbar Sahraie, N.; Steinberg, J.; Ju, W.; Oh, H.-S.; Strasser, P. Metal-Doped Nitrogenated Carbon as an Efficient Catalyst for Direct CO 2 Electroreduction to CO and Hydrocarbons. *Angew. Chem., Int. Ed.* **2015**, *54*, 10758−10762.
(350) Varela, A. S.; Ju, W.; Bagger, A.; Franco, P.; Rossmeisl, J.; Strasser, P. Electrochemical Reduction of CO 2 on Metal-Nitrogen-Doped Carbon Catalysts. *ACS Catal.* **2019**, *9*, 7270−7284.
(351) González-Cervantes, E.; Crisóstomo, A. A.; Gutiérrez-Alejandre, A.; Varela, A. S. Optimizing FeNC Materials as Electrocatalysts for the CO2 Reduction Reaction: Heat-Treatment Temperature, Structure and Performance Correlations. *ChemCatChem.* **2019**, *11*, 4854−4861.
(352) Varela, A. S.; Ju, W.; Strasser, P. Molecular Nitrogen-Carbon Catalysts, Solid Metal Organic Framework Catalysts, and Solid Metal/Nitrogen-Doped Carbon (MNC) Catalysts for the Electrochemical CO2 Reduction. *Adv. Energy Mater.* **2018**, *8*, 1703614.
(353) Schreier, M.; Yoon, Y.; Jackson, M. N.; Surendranath, Y. Competition between H and CO for Active Sites Governs Copper-Mediated Electrosynthesis of Hydrocarbon Fuels. *Angew. Chem., Int. Ed.* **2018**, *57*, 10221−10225.
(354) Song, Y.; Peng, R.; Hensley, D. K.; Bonnesen, P. V.; Liang, L.; Wu, Z.; Meyer, H. M., III; Chi, M.; Ma, C.; Sumpter, B. G.; et al. High-Selectivity Electrochemical Conversion of CO2 to Ethanol Using a Copper Nanoparticle/N-Doped Graphene Electrode. *ChemistrySelect* **2016**, *1*, 6055−6061.
(355) Cheng, Y.-S.; Chu, X.-P.; Ling, M.; Li, N.; Wu, K.-L.; Wu, F.-H.; Li, H.; Yuan, G.; Wei, X.-W. An MOF-Derived Copper@nitrogen-Doped Carbon Composite: The Synergistic Effects of N-Types and Copper on Selective CO2 Electroreduction. *Catal. Sci. Technol.* **2019**, *9*, 5668−5675.
(356) Karapinar, D.; Huan, N. T.; Ranjbar Sahraie, N.; Li, J.; Wakerley, D.; Touati, N.; Zanna, S.; Taverna, D.; Galvão Tizei, L. H.; Zitolo, A.; et al. Electroreduction of CO2 on Single-Site Copper-Nitrogen-Doped Carbon Material: Selective Formation of Ethanol and Reversible Restructuration of the Metal Sites. *Angew. Chem., Int. Ed.* **2019**, *58*, 15098−15103.
(357) Zhao, K.; Nie, X.; Wang, H.; Chen, S.; Quan, X.; Yu, H.; Choi, W.; Zhang, G.; Kim, B.; Chen, J. G. Selective Electroreduction of CO_2 to Acetone by Single Copper Atoms Anchored on N-Doped Porous Carbon. *Nat. Commun.* **2020**, *11*, 2455.
(358) Hansen, H. A.; Varley, J. B.; Peterson, A. A.; Nørskov, J. K. Understanding Trends in the Electrocatalytic Activity of Metals and Enzymes for CO_2 Reduction to CO. *J. Phys. Chem. Lett.* **2013**, *4*, 388−392.
(359) Wan, H.; Jiao, Y.; Bagger, A.; Rossmeisl, J. Three-Dimensional Carbon Electrocatalysts for CO2 or CO Reduction. *ACS Catal.* **2021**, *11*, 533−541.
(360) Zhao, J.; Zhao, J.; Li, F.; Chen, Z. Copper Dimer Supported on a C 2 N Layer as an Efficient Electrocatalyst for CO 2 Reduction Reaction: A Computational Study. *J. Phys. Chem. C* **2018**, *122*, 19712−19721.
(361) Gu, J.; Hsu, C.-S.; Bai, L.; Chen, H. M.; Hu, X. Atomically dispersed Fe 3+ sites catalyze efficient CO 2 electroreduction to CO. *Science* **2019**, *364*, 1091−1094.
(362) Ouyang, Y.; Shi, L.; Bai, X.; Li, Q.; Wang, J. Breaking Scaling Relations for Efficient CO 2 Electrochemical Reduction through Dual-Atom Catalysts. *Chem. Sci.* **2020**, *11*, 1807−1813.
(363) Bagger, A.; Wan, H.; Stephens, I. E. L.; Rossmeisl, J. Role of Catalyst in Controlling N 2 Reduction Selectivity: A Unified View of Nitrogenase and Solid Electrodes. *ACS Catal.* **2021**, *11*, 6596−6601.
(364) Karmodak, N.; Vijay, S.; Kastlunger, G.; Chan, K. Computational Screening of Single and Di-Atom Catalysts for Electrochemical CO2 Reduction. *ACS Catal.* **2022**, *12*, 4818−4824.
(365) Chen, M.; Wang, S.; Zhang, H.; Zhang, P.; Tian, Z.; Lu, M.; Xie, X.; Huang, L.; Huang, W. Intrinsic Defects in Biomass-Derived Carbons Facilitate Electroreduction of CO2. *Nano Res.* **2020**, *13*, 729−735.
(366) Ginovska-Pangovska, B.; Dutta, A.; Reback, M. L.; Linehan, J. C.; Shaw, W. J. Beyond the Active Site: The Impact of the Outer Coordination Sphere on Electrocatalysts for Hydrogen Production and Oxidation. *Acc. Chem. Res.* **2014**, *47*, 2621−2630.
(367) Li, Q.; He, T.; Zhang, Y.-Q.; Wu, H.; Liu, J.; Qi, Y.; Lei, Y.; Chen, H.; Sun, Z.; Peng, C.; Yi, L.; Zhang, Y. Biomass Waste-Derived 3D Metal-Free Porous Carbon as a Bifunctional Electrocatalyst for Rechargeable Zinc-Air Batteries. *ACS Sustain. Chem. Eng.* **2019**, *7*, 17039−17046.
(368) Guan, J.; Zhang, Z.; Ji, J.; Dou, M.; Wang, F. Hydrothermal Synthesis of Highly Dispersed Co3O4 Nanoparticles on Biomass-Derived Nitrogen-Doped Hierarchically Porous Carbon Networks as an Efficient Bifunctional Electrocatalyst for Oxygen Reduction and

https://doi.org/10.1021/acs.chemrev.2c00429
Chem. Rev. 2023, 123, 2311−2348

Evolution Reactions. *ACS Appl. Mater. Interfaces* **2017**, *9*, 30662−30669.
(369) Shen, J.; Wu, H.; Sun, W.; Wu, Q.; Zhen, S.; Wang, Z.; Sun, K. Biomass-Derived Hierarchically Porous Carbon Skeletons with in Situ Decorated IrCo Nanoparticles as High-Performance Cathode Catalysts for Li-O2 Batteries. *J. Mater. Chem. A* **2019**, *7*, 10662−10671.
(370) Tao, X.; Luo, S.; Tian, C.; Qing, Y.; Lu, X.; Yan, N.; Wu, Y. Ni@Ni2P Encapsulation in Interconnected N-Doped Carbonized Cellulose Nanofibril Network for Efficient Oxygen Evolution Reaction. *ACS Sustain. Chem. Eng.* **2020**, *8*, 1859−1867.
(371) Tiwari, J. N.; Dang, N. K.; Sultan, S.; Thangavel, P.; Jeong, H. Y.; Kim, K. S. Multi-Heteroatom-Doped Carbon from Waste-Yeast Biomass for Sustained Water Splitting. *Nat. Sustain.* **2020**, *3*, 556−563.
(372) Niu, Y.; Teng, X.; Gong, S.; Chen, Z. A Bimetallic Alloy Anchored on Biomass-Derived Porous N-Doped Carbon Fibers as a Self-Supporting Bifunctional Oxygen Electrocatalyst for Flexible Zn-Air Batteries. *J. Mater. Chem. A* **2020**, *8*, 13725−13734.
(373) Li, D.; Wang, Q.; Yao, Y.; Wu, F.; Yu, Y.; Zhang, C. New Application of Waste Citrus Maxima Peel-Derived Carbon as an Oxygen Electrode Material for Lithium Oxygen Batteries. *ACS Appl. Mater. Interfaces* **2018**, *10*, 32058−32066.
(374) Liu, X.; Zhou, Y.; Zhou, W.; Li, L.; Huang, S.; Chen, S. Biomass-Derived Nitrogen Self-Doped Porous Carbon as Effective Metal-Free Catalysts for Oxygen Reduction Reaction. *Nanoscale* **2015**, *7*, 6136−6142.
(375) Wang, T.; Yang, R.; Shi, N.; Yang, J.; Yan, H.; Wang, J.; Ding, Z.; Huang, W.; Luo, Q.; Lin, Y.; et al. Cu,N-Codoped Carbon Nanodisks with Biomimic Stomata-Like Interconnected Hierarchical Porous Topology as Efficient Electrocatalyst for Oxygen Reduction Reaction. *Small* **2019**, *15*, 1902410.
(376) Lee, S. H.; Kim, J.; Chung, D. Y.; Yoo, J. M.; Lee, H. S.; Kim, M. J.; Mun, B. S.; Kwon, S. G.; Sung, Y.-E.; Hyeon, T. Design Principle of Fe-N-C Electrocatalysts: How to Optimize Multimodal Porous Structures? *J. Am. Chem. Soc.* **2019**, *141*, 2035−2045.
(377) Zhao, Y.; Li, X.; Jia, X.; Gao, S. Why and How to Tailor the Vertical Coordinate of Pore Size Distribution to Construct ORR-Active Carbon Materials? *Nano Energy* **2019**, *58*, 384−391.
(378) Murray, C. D. THE PHYSIOLOGICAL PRINCIPLE OF MINIMUM WORK APPLIED TO THE ANGLE OF BRANCHING OF ARTERIES. *J. Gen. Physiol.* **1926**, *9*, 835−841.
(379) Sherman, T. F. On Connecting Large Vessels to Small. *J. Gen. Physiol.* **1981**, *78*, 431−453.
(380) Joshi, A.; Kaur, S.; Dharamvir, K.; Nayyar, H.; Verma, G. Multi-Walled Carbon Nanotubes Applied through Seed-Priming Influence Early Germination, Root Hair, Growth and Yield of Bread Wheat (*Triticum aestivum* L.). *J. Sci. Food Agric.* **2018**, *98*, 3148−3160.
(381) Wasserthal, L. T. Flight-Motor-Driven Respiratory Air Flow in the Hawkmoth Manduca Sexta. *J. Exp. Biol.* **2001**, *204*, 2209−2220.
(382) Zheng, X.; Shen, G.; Wang, C.; Li, Y.; Dunphy, D.; Hasan, T.; Brinker, C. J.; Su, B. L. Bio-Inspired Murray Materials for Mass Transfer and Activity. *Nat. Commun.* **2017**, *8*, 14921.
(383) Deng, C.; Wu, K. H.; Scott, J.; Zhu, S.; Zheng, X.; Amal, R.; Wang, D. W. Spherical Murray-Type Assembly of Co-N-C Nanoparticles as a High-Performance Trifunctional Electrocatalyst. *ACS Appl. Mater. Interfaces* **2019**, *11*, 9925−9933.
(384) Peng, Z.; Chen, L. H.; Sun, M. H.; Zhao, H.; Wang, Z.; Li, Y.; Li, L. Y.; Zhou, J.; Liu, Z. C.; Su, B. L. A Hierarchical Zeolitic Murray Material with a Mass Transfer Advantage Promotes Catalytic Efficiency Improvement. *Inorg. Chem. Front.* **2018**, *5*, 2829−2835.
(385) Deng, C.; Wu, K.-H.; Scott, J.; Zhu, S.; Zheng, X.; Amal, R.; Wang, D.-W. Spherical Murray-Type Assembly of Co-N-C Nanoparticles as a High-Performance Trifunctional Electrocatalyst. *ACS Appl. Mater. Interfaces* **2019**, *11*, 9925−9933.
(386) Parthasarathy, M.; Kannan, R.; Sreekumar, K.; Pillai, V. K. Bio-Inspired Catalyst Compositions for Enhanced Oxygen Reduction Using Nanostructured Pt Electrocatalysts in Polymer Electrolyte Fuel Cells. *J. Mater. Chem.* **2010**, *20*, 9651−9657.
(387) Dogutan, D. K.; Bediako, D. K.; Teets, T. S.; Schwalbe, M.; Nocera, D. G. Efficient Synthesis of Hangman Porphyrins. *Org. Lett.* **2010**, *12*, 1036−1039.
(388) McGuire Jr, R.; Dogutan, D. K.; Teets, T. S.; Suntivich, J.; Shao-Horn, Y.; Nocera, D. G. Oxygen Reduction Reactivity of Cobalt(Ii) Hangman Porphyrins. *Chem. Sci.* **2010**, *1*, 411−414.
(389) Passard, G.; Dogutan, D. K.; Qiu, M.; Costentin, C.; Nocera, D. G. Oxygen Reduction Reaction Promoted by Manganese Porphyrins. *ACS Catal.* **2018**, *8*, 8671−8679.
(390) Mukherjee, S.; Nayek, A.; Bhunia, S.; Dey, S. G.; Dey, A. A Single Iron Porphyrin Shows pH Dependent Switch between "Push" and "Pull" Effects in Electrochemical Oxygen Reduction. *Inorg. Chem.* **2020**, *59*, 14564−14576.
(391) Bhunia, S.; Rana, A.; Roy, P.; Martin, D. J.; Pegis, M. L.; Roy, B.; Dey, A. Rational Design of Mononuclear Iron Porphyrins for Facile and Selective $4e^-/4H^+$ O_2 Reduction: Activation of O-O Bond by 2nd Sphere Hydrogen Bonding. *J. Am. Chem. Soc.* **2018**, *140*, 9444−9457.
(392) Yu, C.; Zhang, P.; Wang, J.; Jiang, L. Superwettability of Gas Bubbles and Its Application: From Bioinspiration to Advanced Materials. *Adv. Mater.* **2017**, *29*, 1703053.
(393) Zhang, F.; Guo, Z. Bioinspired Materials for Water-Harvesting: Focusing on Microstructure Designs and the Improvement of Sustainability. *Mater. Adv.* **2020**, *1*, 2592−2613.
(394) Si, Y.; Dong, Z.; Jiang, L. Bioinspired Designs of Superhydrophobic and Superhydrophilic Materials. *ACS Cent. Sci.* **2018**, *4*, 1102−1112.
(395) Ahmad, I.; Kan, C. A Review on Development and Applications of Bio-Inspired Superhydrophobic Textiles. *Materials* **2016**, *9*, 892.
(396) Wang, J.; Zheng, Y.; Nie, F.-Q.; Zhai, J.; Jiang, L. Air Bubble Bursting Effect of Lotus Leaf. *Langmuir* **2009**, *25*, 14129−14134.
(397) Barthlott, W.; Schimmel, T.; Wiersch, S.; Koch, K.; Brede, M.; Barczewski, M.; Walheim, S.; Weis, A.; Kaltenmaier, A.; Leder, A.; et al. The Salvinia Paradox: Superhydrophobic Surfaces with Hydrophilic Pins for Air Retention Under Water. *Adv. Mater.* **2010**, *22*, 2325−2328.
(398) Yong, J.; Chen, F.; Fang, Y.; Huo, J.; Yang, Q.; Zhang, J.; Bian, H.; Hou, X. Bioinspired Design of Underwater Superaerophobic and Superaerophilic Surfaces by Femtosecond Laser Ablation for Anti- or Capturing Bubbles. *ACS Appl. Mater. Interfaces* **2017**, *9*, 39863−39871.
(399) Xu, W.; Lu, Z.; Wan, P.; Kuang, Y.; Sun, X. High-Performance Water Electrolysis System with Double Nanostructured Superaerophobic Electrodes. *Small* **2016**, *12*, 2492−2498.
(400) Lu, Z.; Xu, W.; Ma, J.; Li, Y.; Sun, X.; Jiang, L. Superaerophilic Carbon-Nanotube-Array Electrode for High-Performance Oxygen Reduction Reaction. *Adv. Mater.* **2016**, *28*, 7155−7161.
(401) Neumann, D.; Woermann, D. Stability of the Volume of Air Trapped on the Abdomen of the Water Spider *Argyroneta aquatica*. *SpringerPlus* **2013**, *2*, 694.
(402) Seymour, R. S.; Hetz, S. K. The Diving Bell and the Spider: The Physical Gill of Argyroneta Aquatica. *J. Exp. Biol.* **2011**, *214*, 2175−2181.
(403) Kim, B. K.; Kim, M. J.; Kim, J. J. Impact of Surface Hydrophilicity on Electrochemical Water Splitting. *ACS Appl. Mater. Interfaces* **2021**, *13*, 11940−11947.
(404) Li, Y.; Zhang, H.; Xu, T.; Lu, Z.; Wu, X.; Wan, P.; Sun, X.; Jiang, L. Under-Water Superaerophobic Pine-Shaped Pt Nanoarray Electrode for Ultrahigh-Performance Hydrogen Evolution. *Adv. Funct. Mater.* **2015**, *25*, 1737−1744.
(405) Lu, Z.; Zhang, H.; Zhu, W.; Yu, X.; Kuang, Y.; Chang, Z.; Lei, X.; Sun, X. In Situ Fabrication of Porous MoS2 Thin-Films as High-Performance Catalysts for Electrochemical Hydrogen Evolution. *Chem. Commun.* **2013**, *49*, 7516−7518.
(406) Hao, J.; Yang, W.; Huang, Z.; Zhang, C. Superhydrophilic and Superaerophobic Copper Phosphide Microsheets for Efficient Electrocatalytic Hydrogen and Oxygen Evolution. *Adv. Mater. Interfaces* **2016**, *3*, 1600236.
(407) Yang, Q.; Li, T.; Lu, Z.; Sun, X.; Liu, J. Hierarchical Construction of an Ultrathin Layered Double Hydroxide Nanoarray for Highly-Efficient Oxygen Evolution Reaction. *Nanoscale* **2014**, *6*, 11789−11794.

https://doi.org/10.1021/acs.chemrev.2c00429
Chem. Rev. 2023, 123, 2311−2348

(408) Xie, Q.; Zhou, D.; Li, P.; Cai, Z.; Xie, T.; Gao, T.; Chen, R.; Kuang, Y.; Sun, X. Enhancing Oxygen Evolution Reaction by Cationic Surfactants. *Nano Res.* **2019**, *12*, 2302−2306.
(409) Wang, P.; Hayashi, T.; Meng, Q.; Wang, Q.; Liu, H.; Hashimoto, K.; Jiang, L. Highly Boosted Oxygen Reduction Reaction Activity by Tuning the Underwater Wetting State of the Superhydrophobic Electrode. *Small* **2017**, *13*, 1601250.
(410) Hoshi, N.; Nakamura, M. Enhancement of the Activity for the Oxygen Reduction Reaction on Well-Defined Single Crystal Electrodes of Pt by Hydrophobic Species. *Chem. Lett.* **2021**, *50*, 72−79.
(411) He, J.; Yang, C.; Yang, X.; Liu, L.; Li, J.; Liu, Q.; Peng, L.; Liu, X.; Qu, M. Hydrophobic Electrocatalyst for the Enhanced Activity of Oxygen Reduction Reaction through Controllable Liquid/Gas/Solid Interface. *Appl. Surf. Sci.* **2020**, *532*, 147357.
(412) Favero, S.; Stephens, I. E. L.; Titirici, M. M. Engineering the Electrochemical Interface of Oxygen Reduction Electrocatalysts with Ionic Liquids: A Review. *Adv. Energy Sustain. Res.* **2021**, *2*, 2000062.
(413) Hansen, K. U.; Jiao, F. Hydrophobicity of CO2 Gas Diffusion Electrodes. *Joule* **2021**, *5*, 754−757.
(414) Budd, P. M.; Msayib, K. J.; Tattershall, C. E.; Ghanem, B. S.; Reynolds, K. J.; McKeown, N. B.; Fritsch, D. Gas Separation Membranes from Polymers of Intrinsic Microporosity. *J. Membr. Sci.* **2005**, *251*, 263−269.
(415) Xing, Z.; Hu, L.; Ripatti, D. S.; Hu, X.; Feng, X. Enhancing Carbon Dioxide Gas-Diffusion Electrolysis by Creating a Hydrophobic Catalyst Microenvironment. *Nat. Commun.* **2021**, *12*, 136.
(416) Sung, J. H.; Esch, M. B.; Prot, J.-M.; Long, C. J.; Smith, A.; Hickman, J. J.; Shuler, M. L. Microfabricated Mammalian Organ Systems and Their Integration into Models of Whole Animals and Humans. *Lab Chip* **2013**, *13*, 1201−1212.
(417) Zhang, H.; Shen, P. K. Recent Development of Polymer Electrolyte Membranes for Fuel Cells. *Chem. Rev.* **2012**, *112*, 2780−2832.
(418) Dhanapal; Xiao; Wang; Meng. A Review on Sulfonated Polymer Composite/Organic-Inorganic Hybrid Membranes to Address Methanol Barrier Issue for Methanol Fuel Cells. *Nanomaterials* **2019**, *9*, 668.
(419) Rosli, N. A. H.; Loh, K. S.; Wong, W. Y.; Yunus, R. M.; Lee, T. K.; Ahmad, A.; Chong, S. T. Review of Chitosan-Based Polymers as Proton Exchange Membranes and Roles of Chitosan-Supported Ionic Liquids. *Int. J. Mol. Sci.* **2020**, *21*, 632.
(420) Honma, I.; Yamada, M. Bio-Inspired Membranes for Advanced Polymer Electrolyte Fuel Cells. Anhydrous Proton-Conducting Membrane via Molecular Self-Assembly. *Bull. Chem. Soc. Jpn.* **2007**, *80*, 2110−2123.
(421) Lupatini, K. N.; Schaffer, J. V.; Machado, B.; Silva, E. S.; Ellendersen, L. S. N.; Muniz, G. I. B.; Ferracin, R. J.; Alves, H. J. Development of Chitosan Membranes as a Potential PEMFC Electrolyte. *J. Polym. Environ.* **2018**, *26*, 2964−2972.
(422) Smitha, B.; Devi, D. A.; Sridhar, S. Proton-Conducting Composite Membranes of Chitosan and Sulfonated Polysulfone for Fuel Cell Application. *Int. J. Hydrogen Energy* **2008**, *33*, 4138−4146.
(423) Pecoraro, C. M.; Santamaria, M.; Bocchetta, P.; Di Quarto, F. Influence of Synthesis Conditions on the Performance of Chitosan-Heteropolyacid Complexes as Membranes for Low Temperature H2-O2 Fuel Cell. *Int. J. Hydrogen Energy* **2015**, *40*, 14616−14626.
(424) Permana, D.; Purwanto, M.; Ramadhan, L. O. A.; Atmaja, L. Synthesis and Characterization of Chitosan/Phosphotungstic Acid-Montmorillonite Modified by Silane for DMFC Membrane. *Indones. J. Chem.* **2015**, *15*, 218−225.
(425) Cui, Z.; Xing, W.; Liu, C.; Liao, J.; Zhang, H. Chitosan/Heteropolyacid Composite Membranes for Direct Methanol Fuel Cell. *J. Power Sources* **2009**, *188*, 24−29.
(426) Wang, J.; Zheng, X.; Wu, H.; Zheng, B.; Jiang, Z.; Hao, X.; Wang, B. Effect of Zeolites on Chitosan/Zeolite Hybrid Membranes for Direct Methanol Fuel Cell. *J. Power Sources* **2008**, *178*, 9−19.
(427) Kalaiselvimary, J.; Prabhu, M. R. Influence of Sulfonated GO/Sulfonated Biopolymer as Polymer Electrolyte Membrane for Fuel Cell Application. *J. Mater. Sci. Mater. Electron.* **2018**, *29*, 5525−5535.
(428) Santamaria, M.; Pecoraro, C. M.; Di Quarto, F.; Bocchetta, P. Chitosan-Phosphotungstic Acid Complex as Membranes for Low Temperature H2-O2 Fuel Cell. *J. Power Sources* **2015**, *276*, 189−194.
(429) V, V.; Khastgir, D. Fabrication and Comprehensive Investigation of Physicochemical and Electrochemical Properties of Chitosan-Silica Supported Silicotungstic Acid Nanocomposite Membranes for Fuel Cell Applications. *Energy* **2018**, *142*, 313−330.
(430) Schaffer, J. V.; Lupatini, K. N.; Machado, B.; Silva, E. S.; Ferracin, R. J.; Alves, H. J. Parameters Effect on Proton Conductivity to Obtain Chitosan Membranes for Use as Electrolytes in PEMFC. *Int. J. Energy Res.* **2018**, *42*, 1381−1385.
(431) Rayung, M.; Aung, M. M.; Azhar, S. C.; Abdullah, L. C.; Su'ait, M. S.; Ahmad, A.; Jamil, S. N. A. M. Bio-Based Polymer Electrolytes for Electrochemical Devices: Insight into the Ionic Conductivity Performance. *Materials (Basel).* **2020**, *13*, 838.
(432) Koh, J. C. H.; Ahmad, Z. A.; Mohamad, A. A. Bacto Agar-Based Gel Polymer Electrolyte. *Ionics* **2012**, *18*, 359−364.
(433) Moon, W. G.; Kim, G.-P.; Lee, M.; Song, H. D.; Yi, J. A Biodegradable Gel Electrolyte for Use in High-Performance Flexible Supercapacitors. *ACS Appl. Mater. Interfaces* **2015**, *7*, 3503−3511.
(434) Singh, R.; Jadhav, N. A.; Majumder, S.; Bhattacharya, B.; Singh, P. K. Novel Biopolymer Gel Electrolyte for Dye-Sensitized Solar Cell Application. *Carbohydr. Polym.* **2013**, *91*, 682−685.
(435) Boopathi, G.; Pugalendhi, S.; Selvasekarapandian, S.; Premalatha, M.; Monisha, S.; Aristatil, G. Development of Proton Conducting Biopolymer Membrane Based on Agar-Agar for Fuel Cell. *Ionics* **2017**, *23*, 2781−2790.
(436) Raphael, E.; Avellaneda, C. O.; Manzolli, B.; Pawlicka, A. Agar-Based Films for Application as Polymer Electrolytes. *Electrochim. Acta* **2010**, *55*, 1455−1459.
(437) Gurunathan, B.; Pugalendhi, S.; Subramanian, P.; Jesudas, D. M.; Subramanian, K. S. Performance Evaluation of Single PEM Fuel Cell (PEMFC) with Novel Bio-Degradable Polymer Membrane Based on Agar-Agar. *Environ. Ecol.* **2019**, *37*, 198−203.
(438) Yabu, H.; Matsui, J.; Hara, M.; Nagano, S.; Matsuo, Y.; Nagao, Y. Proton Conductivities of Lamellae-Forming Bioinspired Block Copolymer Thin Films Containing Silver Nanoparticles. *Langmuir* **2016**, *32*, 9484−9491.
(439) He, Y.; Wang, J.; Zhang, H.; Zhang, T.; Zhang, B.; Cao, S.; Liu, J. Polydopamine-Modified Graphene Oxide Nanocomposite Membrane for Proton Exchange Membrane Fuel Cell under Anhydrous Conditions. *J. Mater. Chem. A* **2014**, *2*, 9548−9558.
(440) Wang, J.; Bai, H.; Zhang, H.; Zhao, L.; Chen, H.; Li, Y. Anhydrous Proton Exchange Membrane of Sulfonated Poly(Ether Ether Ketone) Enabled by Polydopamine-Modified Silica Nanoparticles. *Electrochim. Acta* **2015**, *152*, 443−455.
(441) D'Amato, R.; Donnadio, A.; Battocchio, C.; Sassi, P.; Pica, M.; Carbone, A.; Gatto, I.; Casciola, M. Polydopamine Coated CeO2 as Radical Scavenger Filler for Aquivion Membranes with High Proton Conductivity. *Materials* **2021**, *14*, 5280.
(442) Rao, Z.; Lan, M.; Wang, Z.; Wan, H.; Li, G.; Zhu, J.; Tang, B.; Liu, H. Effectively Facilitating the Proton Conduction of Proton Exchange Membrane by Polydopamine Modified Hollow Metal-organic Framework. *J. Membr. Sci.* **2022**, *644*, 120098.
(443) Cai, Y. Y.; Yang, Q.; Sun, L. X.; Zhu, Z. Y.; Zhang, Q. G.; Zhu, A. M.; Liu, Q. L. Bioinspired Layered Proton-Exchange Membranes with High Strength and Proton Conductivity. *Int. J. Hydrogen Energy* **2021**, *46*, 4087−4099.
(444) Zhao, G.; Zhao, H.; Zhuang, X.; Shi, L.; Cheng, B.; Xu, X.; Yin, Y. Nanofiber Hybrid Membranes: Progress and Application in Proton Exchange Membranes. *J. Mater. Chem. A* **2021**, *9*, 3729−3766.
(445) Wang, S.; Luo, H.; Li, X.; Shi, L.; Cheng, B.; Zhuang, X.; Li, Z. Amino Acid-Functionalized Metal Organic Framework with Excellent Proton Conductivity for Proton Exchange Membranes. *Int. J. Hydrogen Energy* **2021**, *46*, 1163−1173.
(446) Xu, X.; Zhao, G.; Wang, H.; Li, X.; Feng, X.; Cheng, B.; Shi, L.; Kang, W.; Zhuang, X.; Yin, Y. Bio-Inspired Amino-Acid-Functionalized Cellulose Whiskers Incorporated into Sulfonated Polysulfone for Proton Exchange Membrane. *J. Power Sources* **2019**, *409*, 123−131.

https://doi.org/10.1021/acs.chemrev.2c00429
Chem. Rev. 2023, 123, 2311−2348

(447) Wang, S.; Shi, L.; Zhang, S.; Wang, H.; Cheng, B.; Zhuang, X.; Li, Z. Proton-Conducting Amino Acid-Modified Chitosan Nanofibers for Nanocomposite Proton Exchange Membranes. *Eur. Polym. J.* **2019**, *119*, 327−334.
(448) Zhao, G.; Xu, X.; Di, Y.; Wang, H.; Cheng, B.; Shi, L.; Zhu, Y.; Zhuang, X.; Yin, Y. Amino Acid Clusters Supported by Cellulose Nanofibers for Proton Exchange Membranes. *J. Power Sources* **2019**, *438*, 227035.
(449) Arvay, A.; French, J.; Wang, J.-C.; Peng, X.-H.; Kannan, A. M. Nature Inspired Flow Field Designs for Proton Exchange Membrane Fuel Cell. *Int. J. Hydrogen Energy* **2013**, *38*, 3717−3726.
(450) Iranzo, A.; Arredondo, C. H.; Kannan, A. M.; Rosa, F. Biomimetic Flow Fields for Proton Exchange Membrane Fuel Cells: A Review of Design Trends. *Energy* **2020**, *190*, 116435.
(451) Kloess, J. P.; Wang, X.; Liu, J.; Shi, Z.; Guessous, L. Investigation of Bio-Inspired Flow Channel Designs for Bipolar Plates in Proton Exchange Membrane Fuel Cells. *J. Power Sources* **2009**, *188*, 132−140.
(452) Ramos-Alvarado, B.; Hernandez-Guerrero, A.; Elizalde-Blancas, F.; Ellis, M. W. Constructal Flow Distributor as a Bipolar Plate for Proton Exchange Membrane Fuel Cells. *Int. J. Hydrogen Energy* **2011**, *36*, 12965−12976.
(453) Roshandel, R.; Arbabi, F.; Moghaddam, G. K. Simulation of an Innovative Flow-Field Design Based on a Bio Inspired Pattern for PEM Fuel Cells. *Renew. Energy* **2012**, *41*, 86−95.
(454) Cheng, S. J.; Miao, J. M.; Tai, C. H. Numerical Simulation Applied to Study the Effects of Fractal Tree-Liked Network Channel Designs on PEMFC Performance. *Adv. Mater. Res.* **2012**, *488*, 1219−1223.
(455) Kjelstrup, S.; Coppens, M. O.; Pharoah, J. G.; Pfeifer, P. Nature-Inspired Energy-and Material-Efficient Design of a Polymer Electrolyte Membrane Fuel Cell. *Energy Fuels* **2010**, *24*, 5097−5108.
(456) Tüber, K.; Oedegaard, A.; Hermann, M.; Hebling, C. Investigation of Fractal Flow-Fields in Portable Proton Exchange Membrane and Direct Methanol Fuel Cells. *J. Power Sources* **2004**, *131*, 175−181.
(457) Ouellette, D.; Ozden, A.; Ercelik, M.; Colpan, C. O.; Ganjehsarabi, H.; Li, X.; Hamdullahpur, F. Assessment of Different Bio-Inspired Flow Fields for Direct Methanol Fuel Cells through 3D Modeling and Experimental Studies. *Int. J. Hydrogen Energy* **2018**, *43*, 1152−1170.
(458) Ozden, A.; Ercelik, M.; Ouellette, D.; Colpan, C. O.; Ganjehsarabi, H.; Hamdullahpur, F. Designing, Modeling and Performance Investigation of Bio-Inspired Flow Field Based DMFCs. *Int. J. Hydrogen Energy* **2017**, *42*, 21546−21558.
(459) Liu, S.; Chen, T.; Xie, Y.; Zhang, J.; Wu, C. Numerical Simulation and Experimental Study on the Effect of Symmetric and Asymmetric Bionic Flow Channels on PEMFC Performance under Gravity. *Int. J. Hydrogen Energy* **2019**, *44*, 29618−29630.
(460) Cho, J. I. S.; Neville, T. P.; Trogadas, P.; Meyer, Q.; Wu, Y.; Ziesche, R.; Boillat, P.; Cochet, M.; Manzi-Orezzoli, V.; Shearing, P.; et al. Visualization of Liquid Water in a Lung-Inspired Flow-Field Based Polymer Electrolyte Membrane Fuel Cell via Neutron Radiography. *Energy* **2019**, *170*, 14−21.
(461) Trogadas, P.; Coppens, M. O. Nature-Inspired Electrocatalysts and Devices for Energy Conversion. *Chem. Soc. Rev.* **2020**, *49*, 3107−3141.
(462) Zhang, S.; Xu, H.; Qu, Z.; Liu, S.; Talkhoncheh, F. K. Bio-Inspired Flow Channel Designs for Proton Exchange Membrane Fuel Cells: A Review. *J. Power Sources* **2022**, *522*, 231003.
(463) Kumar, H.; Kumar, K.; Bhardwaj, H. K. Review of Recent Advancements Made In Flexible Energy Storage Devices. *IOP Conf. Ser. Mater. Sci. Eng.* **2021**, *1104*, 012040.
(464) Lin, L.; Ning, H.; Song, S.; Xu, C.; Hu, N. Flexible Electrochemical Energy Storage: The Role of Composite Materials. *Compos. Sci. Technol.* **2020**, *192*, 108102.
(465) Song, W. J.; Lee, S.; Song, G.; Son, H. B.; Han, D. Y.; Jeong, I.; Bang, Y.; Park, S. Recent Progress in Aqueous Based Flexible Energy Storage Devices. *Energy Storage Mater.* **2020**, *30*, 260−286.
(466) Dubal, D. P.; Chodankar, N. R.; Kim, D. H.; Gomez-Romero, P. Towards Flexible Solid-State Supercapacitors for Smart and Wearable Electronics. *Chem. Soc. Rev.* **2018**, *47*, 2065−2129.
(467) Nguyen, T. H.; Fraiwan, A.; Choi, S. Paper-Based Batteries: A Review. *Biosens. Bioelectron.* **2014**, *54*, 640−649.
(468) Yang, Y.; Zhu, X.; Wang, Q.; Ye, D.; Chen, R.; Liao, Q. Towards Flexible Fuel Cells: Development, Challenge and Prospect. *Appl. Therm. Eng.* **2022**, *203*, 117937.
(469) Wang, Y.; Kwok, H.; Zhang, Y.; Pan, W.; Leung, D. Y. C. Flexible Hydrogen Fuel Cell Fabricated on Paper with Embedded Aluminium Foil. *E3S Web Conf.* **2019**, *83*, 01004.
(470) Wang, Y.; Kwok, H. Y. H.; Zhang, Y.; Pan, W.; Zhang, H.; Lu, X.; Leung, D. Y. C. A Flexible Paper-Based Hydrogen Fuel Cell for Small Power Applications. *Int. J. Hydrogen Energy* **2019**, *44*, 29680−29691.
(471) Dector, A.; Galindo-de-la-Rosa, J.; Amaya-Cruz, D. M.; Ortíz-Verdín, A.; Guerra-Balcázar, M.; Olivares-Ramírez, J. M.; Arriaga, L. G.; Ledesma-García, J. Towards Autonomous Lateral Flow Assays: Paper-Based Microfluidic Fuel Cell inside an HIV-Test Using a Blood Sample as Fuel. *Int. J. Hydrogen Energy* **2017**, *42*, 27979−27986.
(472) Mousavi Ehteshami, S. M.; Asadnia, M.; Tan, S. N.; Chan, S. H. Paper-Based Membraneless Hydrogen Peroxide Fuel Cell Prepared by Micro-Fabrication. *J. Power Sources* **2016**, *301*, 392−395.
(473) Luo, S.; Wang, Y.; Kong, T. C.; Pan, W.; Zhao, X.; Leung, D. Y. C. Flexible Direct Formate Paper Fuel Cells with High Performance and Great Durability. *J. Power Sources* **2021**, *490*, 229526.
(474) Copenhaver, T. S.; Purohit, K. H.; Domalaon, K.; Pham, L.; Burgess, B. J.; Manorothkul, N.; Galvan, V.; Sotez, S.; Gomez, F. A.; Haan, J. L. A Microfluidic Direct Formate Fuel Cell on Paper. *Electrophoresis* **2015**, *36*, 1825−1829.
(475) Zhang, B.; Jiang, Y.; Han, J. A Flexible Nanocomposite Membrane Based on Traditional Cotton Fabric to Enhance Performance of Microbial Fuel Cell. *Fibers Polym.* **2017**, *18*, 1296−1303.
(476) Tseng, P.; Perotto, G.; Napier, B.; Riahi, P.; Li, W.; Shirman, E.; Kaplan, D. L.; Zenyuk, I. V.; Omenetto, F. G. Silk Fibroin-Carbon Nanotube Composite Electrodes for Flexible Biocatalytic Fuel Cells. *Adv. Electron. Mater.* **2016**, *2*, 1600190.
(477) Qian, G.; Zhu, B.; Liao, X.; Zhai, H.; Srinivasan, A.; Fritz, N. J.; Cheng, Q.; Ning, M.; Qie, B.; Li, Y.; et al. Bioinspired, Spine-Like, Flexible, Rechargeable Lithium-Ion Batteries with High Energy Density. *Adv. Mater.* **2018**, *30*, 1704947.
(478) Kim, M.-H.; Nam, S.; Oh, M.; Lee, H.-J.; Jang, B.; Hyun, S. Bioinspired, Shape-Morphing Scale Battery for Untethered Soft Robots. *Soft Rob.* **2022**, *9*, 486−496.
(479) Cai, C.; Zhou, W.; Fu, Y. Bioinspired MXene Nacre with Mechanical Robustness for Highly Flexible All-Solid-State Photo-thermo-Supercapacitor. *Chem. Eng. J.* **2021**, *418*, 129275.
(480) Fu, J.; Zhu, B.; You, W.; Jaroniec, M.; Yu, J. A Flexible Bio-Inspired H2-Production Photocatalyst. *Appl. Catal. B Environ.* **2018**, *220*, 148−160.
(481) Nguyen, D. D.; Hsiao, C. H.; Su, T. Y.; Hsieh, P. Y.; Chen, Y. L.; Chueh, Y. L.; Lee, C. Y.; Tai, N. H. Bioinspired Networks Consisting of Spongy Carbon Wrapped by Graphene Sheath for Flexible Transparent Supercapacitors. *Commun. Chem.* **2019**, *2*, 137.
(482) Meng, X.; Cai, Z.; Zhang, Y.; Hu, X.; Xing, Z.; Huang, Z.; Huang, Z.; Cui, Y.; Hu, T.; Su, M.; et al. Bio-Inspired Vertebral Design for Scalable and Flexible Perovskite Solar Cells. *Nat. Commun.* **2020**, *11*, 3016.
(483) Hu, X.; Huang, Z.; Li, F.; Su, M.; Huang, Z.; Zhao, Z.; Cai, Z.; Yang, X.; Meng, X.; Li, P.; et al. Nacre-Inspired Crystallization and Elastic "Brick-and-Mortar" Structure for a Wearable Perovskite Solar Module. *Energy Environ. Sci.* **2019**, *12*, 979−987.
(484) Huang, C.; Kang, L.; Zhang, N.; Wan, S.; Zhou, X.; Zhang, J. Bioinspired Interfacial Strengthening Flexible Supercapacitors via Hierarchically Topological Interlocking Strategy. *ACS Appl. Mater. Interfaces* **2019**, *11*, 38303−38312.
(485) Jian, M.; Xia, K.; Wang, Q.; Yin, Z.; Wang, H.; Wang, C.; Xie, H.; Zhang, M.; Zhang, Y. Flexible and Highly Sensitive Pressure

https://doi.org/10.1021/acs.chemrev.2c00429
Chem. Rev. 2023, 123, 2311−2348

Sensors Based on Bionic Hierarchical Structures. *Adv. Funct. Mater.* **2017**, *27*, 1606066.
(486) Wei, Y.; Chen, S.; Lin, Y.; Yang, Z.; Liu, L. Cu-Ag Core-Shell Nanowires for Electronic Skin with a Petal Molded Microstructure. *J. Mater. Chem. C* **2015**, *3*, 9594−9602.
(487) Nie, P.; Wang, R.; Xu, X.; Cheng, Y.; Wang, X.; Shi, L.; Sun, J. High-Performance Piezoresistive Electronic Skin with Bionic Hierarchical Microstructure and Microcracks. *ACS Appl. Mater. Interfaces* **2017**, *9*, 14911−14919.
(488) Su, B.; Gong, S.; Ma, Z.; Yap, L. W.; Cheng, W. Mimosa-Inspired Design of a Flexible Pressure Sensor with Touch Sensitivity. *Small* **2015**, *11*, 1886−1891.
(489) Wan, Y.; Qiu, Z.; Hong, Y.; Wang, Y.; Zhang, J.; Liu, Q.; Wu, Z.; Guo, C. F. A Highly Sensitive Flexible Capacitive Tactile Sensor with Sparse and High-Aspect-Ratio Microstructures. *Adv. Electron. Mater.* **2018**, *4*, 1700586.
(490) Wei, C.; Rao, R. R.; Peng, J.; Huang, B.; Stephens, I. E. L.; Risch, M.; Xu, Z. J.; Shao-Horn, Y. Recommended Practices and Benchmark Activity for Hydrogen and Oxygen Electrocatalysis in Water Splitting and Fuel Cells. *Adv. Mater.* **2019**, *31*, 1806296.
(491) Voiry, D.; Chhowalla, M.; Gogotsi, Y.; Kotov, N. A.; Li, Y.; Penner, R. M.; Schaak, R. E.; Weiss, P. S. Best Practices for Reporting Electrocatalytic Performance of Nanomaterials. *ACS Nano* **2018**, *12*, 9635−9638.
(492) Clark, E. L.; Resasco, J.; Landers, A.; Lin, J.; Chung, L.-T.; Walton, A.; Hahn, C.; Jaramillo, T. F.; Bell, A. T. Standards and Protocols for Data Acquisition and Reporting for Studies of the Electrochemical Reduction of Carbon Dioxide. *ACS Catal.* **2018**, *8*, 6560−6570.
(493) Xia, C.; Kim, J. Y.; Wang, H. Recommended Practice to Report Selectivity in Electrochemical Synthesis of H_2O_2. *Nat. Catal.* **2020**, *3*, 605−607.
(494) Akbashev, A. R. Electrocatalysis Goes Nuts. *ACS Catal.* **2022**, *12*, 4296−4301.
(495) Mehmood, A.; Gong, M.; Jaouen, F.; Roy, A.; Zitolo, A.; Khan, A.; Sougrati, M.; Primbs, M.; Bonastre, A. M.; Fongalland, D.; et al. High Loading of Single Atomic Iron Sites in Fe-NC Oxygen Reduction Catalysts for Proton Exchange Membrane Fuel Cells. *Nat. Catal.* **2022**, *5*, 311−323.
(496) Mitchell, S.; Parés, F.; Faust Akl, D.; Collins, S. M.; Kepaptsoglou, D. M.; Ramasse, Q. M.; Garcia-Gasulla, D.; Pérez-Ramírez, J.; López, N. Automated Image Analysis for Single-Atom Detection in Catalytic Materials by Transmission Electron Microscopy. *J. Am. Chem. Soc.* **2022**, *144*, 8018−8029.
(497) Snitkoff-Sol, R. Z.; Friedman, A.; Honig, H. C.; Yurko, Y.; Kozhushner, A.; Zachman, M. J.; Zelenay, P.; Bond, A. M.; Elbaz, L. Quantifying the Electrochemical Active Site Density of Precious Metal-Free Catalysts in Situ in Fuel Cells. *Nat. Catal.* **2022**, *5*, 163−170.
(498) Thorarinsdottir, A. E.; Veroneau, S. S.; Nocera, D. G. Self-Healing Oxygen Evolution Catalysts. *Nat. Commun.* **2022**, *13*, 1243.

https://doi.org/10.1021/acs.chemrev.2c00429
Chem. Rev. 2023, 123, 2311−2348